FOVEAL REFLECTION ANALYZER

On the Spectral and Directional Reflectance of the Retina

Niels Zagers

FOVEAL REFLECTION ANALYZER

On the Spectral and Directional Reflectance of the Retina

Een instrument voor analyse van de foveale reflectie

Over de spectrale en richtingsafhankelijke reflectie van het netvlies
(met een samenvatting in het Nederlands)

Proefschrift ter verkrijging van de graad van doctor aan de Universiteit Utrecht op gezag van de Rector Magnificus, Prof. dr. W. H. Gispen, ingevolge het besluit van het College voor Promoties in het openbaar te verdedigen op dinsdag 27 januari 2004 des middags te 16.15 uur.

door

Niels Petrus Antonius Zagers

geboren op 16 september 1976 te Zundert

Promotor:

Prof. dr. D. van Norren

Faculteit Geneeskunde, Universiteit Utrecht

Voor Jessica

Contents

List of Publications

Papers:

1. "Simultaneous measurement of foveal spectral reflectance and cone-photoreceptor directionality", N.P.A. Zagers, J. van de Kraats, T.T.J.M. Berendschot, and D. van Norren, Appl. Opt. **41** (2002), 4686–4696, based on Chapter 3

2. "Wavelength dependence of reflectometric cone photoreceptor directionality", N.P.A. Zagers, T.T.J.M. Berendschot, and D. van Norren, J. Opt. Soc. Am. A **20** (2003), 18–23, based on Chapter 4

3. "Absorption of the eye lens and macular pigment derived from the reflectance of cone photoreceptors", N.P.A. Zagers and D. van Norren, *Submitted*, based on Chapter 5

4. "Spectral and directional reflectance of the fovea in diabetes mellitus", N.P.A. Zagers, M.C.A. Pot, and D. van Norren, *Submitted*, based on Chapter 6

Abstracts:

1. "A new type of reflectometer: Foveal Reflection Analyzer", N.P.A. Zagers, T.T.J.M. Berendschot, J. van de Kraats, and D. van Norren, ARVO abstract NO. 3779, 2001, based on Chapter 3

2. "Photoreceptors act as spectrally flat reflectors", N.P.A. Zagers and D. van Norren, ARVO abstract NO. 2873, 2003, based on Chapter 5

3. "Foveal reflection analysis in diabetes", D. van Norren, M.C.A. Pot, and N.P.A. Zagers, ARVO abstract NO. 4008, 2003, based on Chapter 6

Chapter 1

Introduction

1.1 Aim of the Thesis

The main aim of this investigation was to develop a new instrument for measurement of light reflected from the retina in a living human eye. At the start of the project, the requirements were formulated as follows. First, the instrument should measure the spectral composition of the reflected light. Second, it should be able to measure the distribution of light in the pupil plane. This distribution exhibits the directional properties of the retinal reflectance. Third, it was desirable to have the ability to observe the pupil and the measured part of the retina. There are two fields of interest where the new instrument could play an important role. First, model analysis of spectra yields the optical densities of ocular absorbers, *e.g.*, the eye lens, melanin, and the macular pigment.[1–5] Second, the directional reflectance provides information on the integrity of the foveal cone photoreceptors.[6,7]

Models for the spectral reflectance rely on the assumption that light is reflected at a limited number of layers within the eye, and that other layers absorb light. The models are capable of handling several reflecting and absorbing layers, on the condition that the spectral properties of these layers are know. They yield the optical densities of a number of absorbing pigments in the eye.[1–3] In particular the yellow macular pigment has received substantial interest in the past years. It is predominantly present in the region used for sharp vision, the fovea, also called the yellow spot. The pigment is a collection of the carotenoids lutein and zeaxanthin.[8] It has been suggested to reduce the risk for the important retinal disease called age-related macular degeneration.[9–11] Intervention may be possible because macular pigment density has been demonstrated to increase after dietary supplementation of lutein,[12,13] and with consumption of foods rich in lutein such as spinach or corn.[14] Demonstration of

the efficacy of macular pigment awaits further supplementation studies, more extensive epidemiological research, and randomized intervention studies. On the premise that the protection hypothesis holds, a screening tool of the general population might become useful. The instrument presented in this thesis could play a role in all the mentioned fields of research on macular pigment.

The second possible application relies on measurement of the directional properties of the light reflected from the retina. These properties are inferred from the distribution of light in the pupil plane. Normally, more light is reflected near the center of the pupil compared with the edges.[15–23] This is called the optical Stiles–Crawford effect. The source of the directional reflectance resides in the cone cells. These cells are mainly known for their sensitivity to light. They have an elongated cylindrical shape. In the healthy eye, the long axes of the cells are pointed precisely toward a common location near the center of the pupil.[24] When illuminated by a narrow beam of light impinging parallel to their long axes, they act as a tiny flash-torch in the reverse direction, reflecting predominately toward the location of common alignment in the pupil. Hence, a prominent maximum in the reflection is produced. Both the amplitude of the directional reflectance and the width of the distribution provide information on the health of the foveal cone photoreceptors.[6,7] Objective information on the foveal receptors is not easily available with the present clinical tests.

It was proposed to base the new instrument on an imaging spectrograph. The first goal to be reached was a demonstration of the feasibility of this concept. In our particular application, the slit of the spectrograph will be placed over the dilated pupil of the eye, where it defines a horizontal bar. A single small spot on the retina will be illuminated with a halogen lamp. Note that such a lamp emits a continuous spectrum in the visible wavelength range. Light reflected from the center of the illuminated spot will be sampled. The spectrograph will produce a spectrum for each point along the bar-shaped exit pupil. In effect, a spectral image is produced, hence the qualification "imaging". The resulting spectral image can be looked upon in two ways: first, as spectra versus location along the horizontal bar in the pupil, and second, as images of the bar depicting a profile of the distribution of light in the pupil for each wavelength. Thus, the proposed arrangement should facilitate simultaneous measurement of both the spectral and the directional properties of the retinal reflectance. The two proclaimed applications concentrate on the fovea: the region of the retina specialized for acute vision. Therefore, the apparatus was coined the "Foveal Reflection Analyzer".
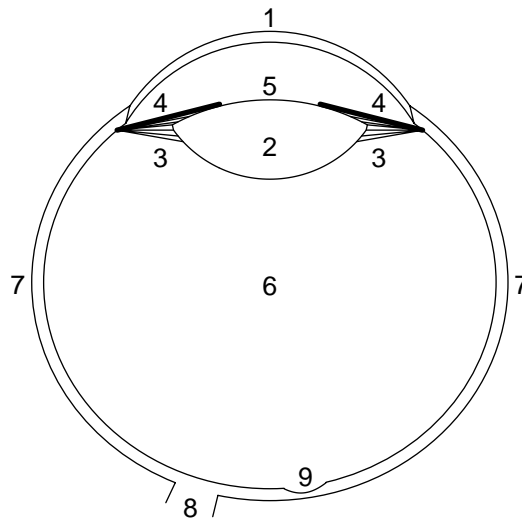
Figure 1.1: Schematic cross section of the human eye. The main components are 1, cornea; 2, lens; 3, zonules; 4, iris; 5, aqueous humor; 6, vitreous humor; 7, sclera; 8, optic nerve. The small depression at the bottom (9) is called the foveal pit. This region is shown in more detail in Fig. 1.3.

1.2 Optical Anatomy

In this Section we briefly review the optical anatomy of the eye. The purpose is to identify the structural components relevant for the optical interaction of light with the eye, a topic to be discussed in the next Section. More detailed information can be found in the books by Wyszecki and Styles,[25] by Bloom and Fawcett,[26] and by Atchison and Smith.[27] The book "*Eye and Brain*" by Richard L. Gregory could serve as an introduction to the more specialized literature, and covers many interesting aspects of vision and visual science outside the scope of the present thesis.[28]

The schematic cross section in Fig. 1.1 depicts the main components of the human eye. The cornea and the eye lens focus light on the retina, comparable to a photographic camera. At its edge, the lens is supported by the zonules. On the outside, the zonules are attached to the ciliary body. Contraction of the ciliary muscle contained therein allows the lens to become more convex, which provides accommodation on nearby objects. Relaxation of the ciliary muscle results in flattening of the lens. This brings faraway objects into focus. Near the front surface of the lens, the iris restricts the amount of light entering the eye, comparable to a diaphragm. The central opening

Figure 1.2: An example of a fundus photograph. The bright spot left of the center is the optic disk. This is where the blood vessels enter and leave the eye. At the right of the center, the slightly darker area marks the location of the macula and fovea.

in the iris forms the pupil of the eye. Its diameter depends on the lighting conditions, but on other factors as well. Between the cornea and the lens is a small space, which contains the aqueous humor. The eyeball is filled with the vitreous humor, a gelatinous mass consisting mainly of water. An opaque white tissue, the sclera, encloses the eye. Together with the intraocular fluid pressure, it serves to maintain the shape of the eyeball.

The fundus covers the larger part of the inside of the eyeball. Figure 1.2 presents an example of a fundus photograph. This photo shows the region at the back of the eye, opposite to the lens, which is called the posterior pole. The most striking features are the blood vessels. They concentrate toward the optic disk, where they enter and leave the eyeball. At the right of the center, a slightly darker area can be recognized. This is the macula, which is also called the yellow spot. Its yellow appearance is caused by the presence of the macular pigment. It is located along the axons of the nerve fibers in front of the receptors,[29, 30] and is highly concentrated towards the center of the macula.[29–32] As is apparent from Fig. 1.2, large blood vessels are absent in the macula. Embedded in the macula is the fovea. This is the most important area of the retina, because it is specialized for high visual acuity. The fovea measures approximately one degree in diameter. (Clinical terminology is used here, *c.f.*, Jalkh and Celorio.[33]) It is densely packed with cone photoreceptor cells; the rods are absent in this area.[34]
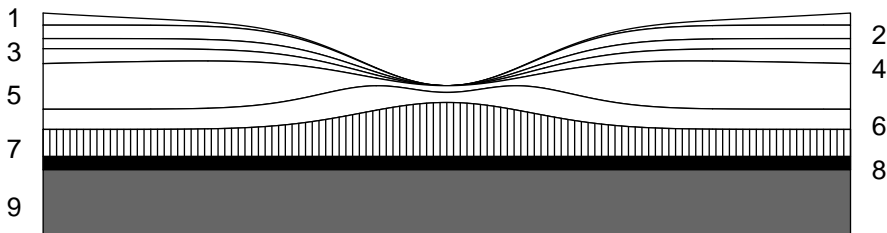
Figure 1.3: Schematic section of the fovea depicting the main layers of the retina. From top to bottom these are 1, the optic nerve fibres; 2, the ganglion cells; 3,4, the inner plexiform and nuclear layers; 5,6, the outer plexiform and nuclear layers; 7, the photoreceptors; 8, the retinal pigment epithelium; 9, the choroid. The top layers spread away from the fovea, visible as a small depression: the foveal pit. In the living eye layers 1–6 are transparent, 7 contains the visual pigments, and 8 and 9 contain the highly absorbing pigment melanin.

The fundus is a stratified tissue. The main layers are visible in the schematic section of the fovea depicted in Fig. 1.3. At the top, the inner limiting membrane forms the boundary between the vitreous humor and the retina. From top to bottom, the other layers of the retina are the layer of optic nerve fibres, the ganglion cells, the inner plexiform and nuclear layers, the outer plexiform and nuclear layers, the layer of photoreceptors, and the retinal pigment epithelium (RPE). The retina is supported by the choroid. This layer contains a large number of blood vessels and melanocytes. On the inside, it is delimited by Bruch's membrane, on the outside by the sclera. The layers in front of the photoreceptors spread away from the fovea, visible as a small depression: the foveal pit. The outer segments of the photoreceptors contain in the order of one thousand parallel membranes or disks.[25,35,36] These membranes support the visual pigments.

1.3 Optical Interaction of Light with the Eye

We are most familiar with the idea of the eye as a structure facilitating the sense of vision. The dark pupil creates the impression that light can enter the eye, but cannot escape it. This is not true. When the eye is entered with a beam of light, light is reflected and scattered back at the various layers in the eye that were introduced in the previous Section, *e.g.*, the choroid, the RPE, the photoreceptor layer, the inner limiting membrane, and the cornea. A small portion of the light escapes the eye, and can be analyzed quantitatively. The next Chapter will discuss several techniques
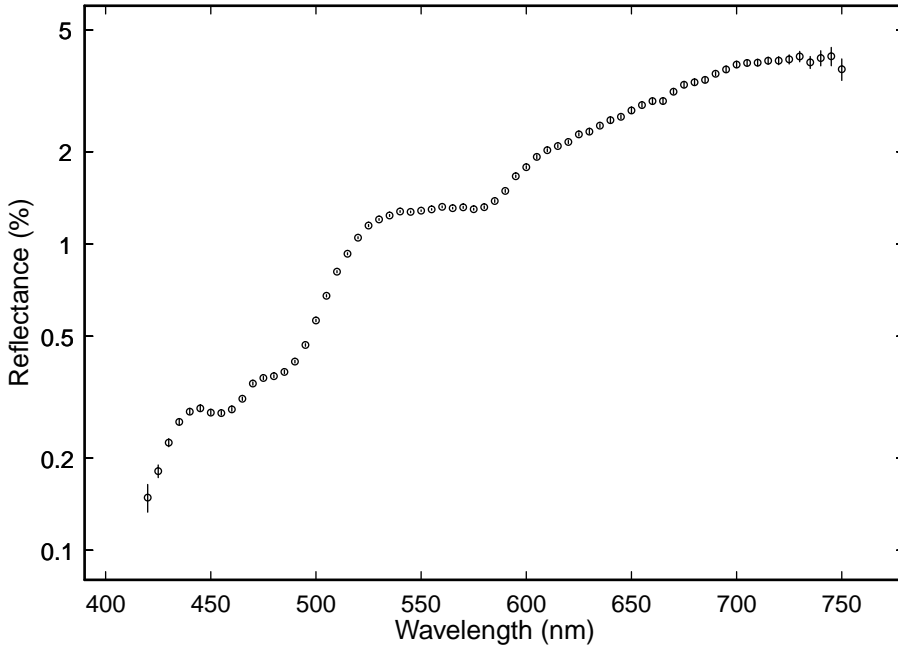
Figure 1.4: A typical reflectance spectrum for a female subject aged 20 years. The re-
flectance is expressed as a percentage relative to a white diffuse 99% reflecting surface and is
plotted on a logarithmic scale. The horizontal axis depicts the wavelength in nanometer (nm)
and roughly spans the visible wavelength range. The spectrum shows a strong decrease from
the longest wavelengths (red light) toward the shortest wavelengths (blue light).

for measuring light reflected from the eye. In this Section, the general spectral and
directional properties of light reflected from the retina are discussed. In addition, it
is described how the measurement light itself influences the reflectance.

1.3.1   Spectral Absorption and Reflection

The spectral characteristics of the light absorbing pigments in the eye dictate the
behavior of fundus reflectance with wavelength.[1–3] The reflectivity is generally ex-
pressed relative to a white diffuse 99% reflecting surface. A typical reflectance spec-
trum for a subject aged 20 years is shown in Fig. 1.4. The highest reflectance amount-
ing to 4% is obtained for wavelengths above 600 nm. In this wavelength region
melanin is the most important absorber. The spectra are dominated by light scattered
back from the choroid. Below 600 nm, the absorption by the hemoglobin in blood
sets in. Reflectance, mainly originating from the cone outer segments, the retinal
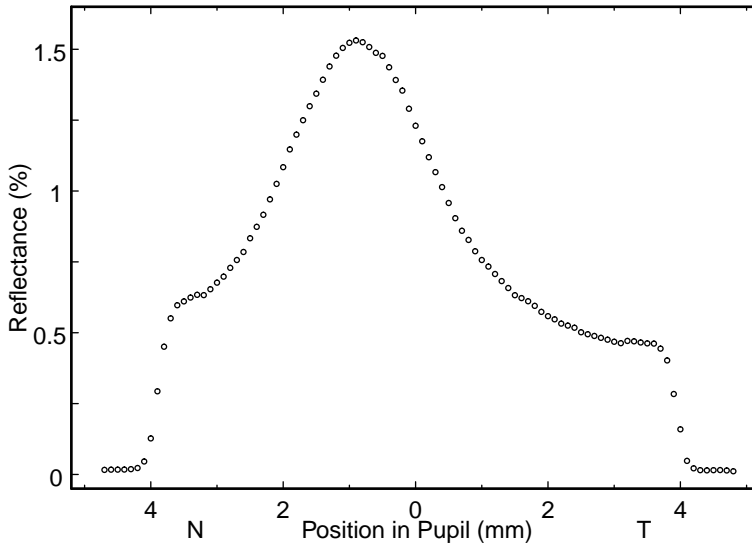
Figure 1.5: An example of an intersection through the distribution of reflectance in the pupil plane, obtained at 540 nm for the same subject as in Fig. 1.4. Again, the reflectance is expressed as a percentage reflectance. The horizontal axis depicts the horizontal location in the pupil plane in millimeters (mm); the nasal (N) and temporal (T) side are indicated. The intersection shows a peaked directional component on top of a flat background. Two sharp drops at about 4 mm nasal and temporal mark the edges of the dilated pupil. The profile has a maximum 1 mm nasal of the pupil center, which corresponds to the common point of alignment of the photoreceptors.

pigment epithelium, and the superficial choroidal layers, decreases to approximately 1.3%. For spectra obtained from the fovea, below 500 nm, macular pigment further reduces the reflectance. Below 430 nm absorption in the lens increases strongly. This causes the reflectance to drop below 0.2%. At this level, small amounts of light reflected and back scattered from the inner limiting membrane, the vitreous, and the cornea, easily dominate the light reflected from the fundus. Spectra of the periphery[2] and of the optic disk[37] decrease strongly with wavelength as well. As a consequence, seen through an ophthalmoscope, the retina has a red color. Another manifestation of this property is the appearance of "red eyes" on flashlight pictures taken in the dark.

1.3.2 Directional Reflectance

Stiles and Crawford demonstrated in 1933 that light entering near the center of the pupil is perceived brighter, compared to light entering at the edge.[38] This effect

is now called the psychophysical Stiles–Crawford effect of the first kind (SCE I).[36] The effect originates from the directional sensitivity of the photoreceptors. As stated before, they have an elongated cylindrical shape and their long axis is oriented toward a position near the center of the pupil.[24] As a result, the angle made with the receptors is small for rays entering the pupil near this point, and larger for rays entering near the pupil edge. The visual efficiency of the light decreases with the angle of incidence.

The same antenna characteristics of the photoreceptors that cause the SCE I endow the light reflected from the retina with directionality. The disks within the cone outer segments reflect light predominately along the long axis of the receptors.[3] The resulting distribution of light in the pupil plane exhibits a maximum near the point of common alignment of the photoreceptors. An example of an intersection of such a distribution for the same subject as in Fig. 1.4 is depicted in Fig. 1.5. In analogy with the psychophysical SCE I, the directional reflectance of light from the fundus is called the optical Stiles–Crawford effect (SCE).[15–23] In principle, the SCE I and SCE are purely retinal phenomena. A complicating factor is that the spectral absorption of light in the eye lens also depends on the location of entry and exit in the pupil. The light absorbing pigments are mainly present in the inner part of the lens, and to a lesser extent in the outer part, and they change with age in a different manner in these two compartments.[39, 40] Furthermore, the central and marginal path lengths are different.[41] Fortunately, because the absorption in the lens strongly decreases with increasing wavelength, these effects can be neglected for wavelengths above approximately 440 nm. For the larger part of the visible wavelength range, the distribution of light in the pupil can be considered directly related to the directionality of the retinal reflectance.

1.3.3   Retinal Illuminance and Light History

The retinal illuminance of the measuring light influences the optical density of the visual pigments in the receptors. A high illuminance will cause them to bleach to a nearly transparent state. In the dark, the visual pigments are maximally regenerated. A change in the optical density of the visual pigments has its effect on the directional and spectral properties of the reflected light. During regeneration of the visual pigments at dark adaptation, the spectral reflectance and the amplitude of the optical SCE are reduced at wavelengths where the pigments absorb.[3, 16] With bleaching, the reflectance and the amplitude of the SCE increase.

In addition to changes in the visual pigments, a second mechanism plays a role. On time scales longer than required for near complete light or dark adaptation of the retina, DeLint *et al.*[42] still observed changes in spectral and directional reflectance.
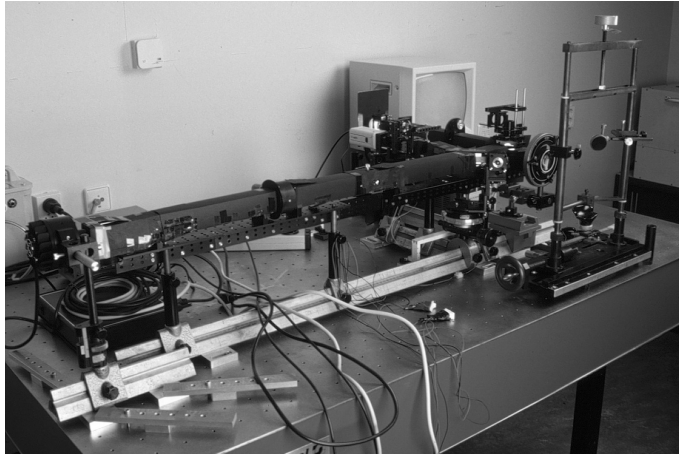
Figure 1.6: The new instrument was constructed on an optical bench. The tube running from the left to the right forms the imaging spectrograph. At the left, the black housing of the CCD camera can be recognized. The optics providing the entrance beam and the observation channel are situated at the top right. The subjects were aligned with the instrument by means of a headrest, visible at the right of the image. A detailed explanation of the instrument will be given in Chapter 3.

These slow optical changes were attributed to changes in the reflectivity of the disks in the receptor outer segments. The slow increase of reflectance after a long period in the dark was dependent on the retinal illuminance during a bleached period preceding the measurement. This indicates that the light history has an influence on the reflectance on a time scale of 10–30 minutes.

1.4   Outline of the Thesis

First, Chapter 2 briefly reviews existing techniques in quantitative fundus reflectometry. Emphasis is placed on previous instruments for measurement of the spectral and directional properties of fundus reflectance. In Chapter 3, we describe the Foveal Reflection Analyzer in detail. Figure 1.6 depicts a photograph of the experimental setup. To demonstrate the feasibility of simultaneous measurement of spectral and directional fundus reflectance, we analyze single spectra, taken at the location where the distribution of light in the pupil has a maximum, and single pupil profiles at 540 nm. These spectra and profiles are compared with earlier results described in the literature.

The model available for analysis of the spectra was developed a few years earlier in our group.[3] Unfortunately, the model cannot be applied to entire spectrograph images. As a consequence, the model analysis is restricted to single spectra and profiles. We set out to expand the model, with the aim to fit the entire two-dimensional data set simultaneously. This is first shown in Chapter 4, in which we analyze the directionality, or peakedness, of the distribution of reflectance in the pupil as a function of wavelength. Second, in Chapter 5 we obtain spectra for the amplitude of the directional reflectance, and we elaborate on the spectral reflectance of the receptors and the absorption of light in the macular pigment and in the eye lens. These results are important steps towards improvement of future models of spectral and directional fundus reflectance.

Finally, in Chapter 6, we present a pilot study on diabetic patients. The optical density of the macular pigment and the eye lens are assessed from single spectra. The integrity of the foveal cones is judged from the directional reflectance obtained at 540 nm. The results warrant initiation of clinical studies on a larger scale, parallel to the more fundamental work. For this future purpose, our group has recently developed a tabletop version of the instrument.

Chapter 2

Review of Instruments
for Fundus Reflectometry

2.1 Introduction

The cornea, the lens, and the fluids in the eye are relatively transparent in the visible wavelength region. This, of course, is crucial for clear sight, but also allows *in vivo* probing of the fundus with light. This technique is generally referred to as fundus reflectometry. The discipline dates back to the invention of the ophthalmoscope by Helmholtz in 1851.[43] His device contained a number of parallel glass plates. The function of these plates was to reflect light into the investigated eye. When looking through the plates, the observer could see the other eye's retina. Later, similar arrangements were invented, for example a mirror with a central hole. Qualitative application of Helmholtz's principle in the clinic was an enormous success. The first quantitative experiments started in the fifties of last century, and were focussed on the assessment of the optical density of the visual pigments.[44, 45] Recently, Berendschot *et al.*[45] reviewed the principles and applications of fundus reflectometry, covering both the historical and modern developments.

Important considerations for the design of an instrument for measurement of fundus reflectance are the optical configuration in the retinal plane, the optical configuration in the pupil plane, the spectral range and resolution, and the retinal illuminance of the measuring light. The interplay between the optical properties of the eye and those of the fundus reflectometer determine what is eventually measured. In this Chapter we explore several existing instrumental designs. Emphasis is placed on recent techniques, similar to those applied in the present thesis. Reviews with a broader scope were given by Knighton[46] and in the aforementioned paper by Berendschot *et al.*[45]

2.2   Single Spot Reflectometers

Van Norren and van de Kraats (1989, 1996)

Van Norren and van de Kraats originally built a single spot reflectometer for assessment of the optical density of the visual pigments,[47] but later it was applied to collect spectral reflectance data in general.[3] The measuring beam, obtained from a 30 W halogen lamp, illuminated a small spot on the retina. Available field sizes were 2.3, 3.0, 4.5 or 6.9 deg; the sampled fields measured 1.6, 2.8, 3.5 or 5.4 deg. In order to decrease the influence of imperfect imaging, the illuminated fields were in general slightly larger. An image of the filament of the lamp, focussed in the pupil plane, defined an entrance pupil of 1×0.5 mm. The exit pupil, separated by 0.25 mm from the entrance pupil, was half circular and 2.5 mm in diameter. The small size of the pupil arrangement allowed scanning of the pupil plane and made the apparatus sensitive to the directional reflectance. The measuring beam contained a rotating (14 revolutions per second) filter wheel. The wheel contained 14 interference filters in the range 410–740 nm with a bandwidth of 7 nm. As the wheel rotated, different filters lined up in the measuring beam in a repeating sequence. This method enabled consecutive measurements at different wavelengths in a fast manner. The interference filters were combined with a set of neutral density filters to keep the retinal illuminance at a low level. This allowed measurements in a dark adapted condition. With a separate illumination channel the visual pigments could be bleached to 93–97%, depending on the position of the entrance beam in the pupil plane.

Delori and Pflibsen (1989)

Delori and Pflibsen modified a Carl Zeiss fundus camera to a single spot reflectometer.[2] The measuring light was a 3 ms flash of a xenon arc lamp. The illuminated field was in the range 1–4 deg. The configuration of the entrance and exit beams in the pupil plane was not specified. It is assumed that the original configuration of a Zeiss camera was used: an annulus for the entrance beam and a concentric circular field in the center of the pupil for the exit beam. With this configuration, the directional properties of the reflectance cannot be measured. The reflected light of the polychromatic flash was resolved spectrally with a spectrograph. The spectral range was 400–912 nm, the resolution was 7.5 nm. Data of 19 different wavelengths in the range 455–805 nm were used for further analysis. Prior to the measurements, the light used for observation and alignment bleached more than 99.5% of the visual pigments.

Delori (1992, 1994)

Delori constructed an improved spectrophotometer for measurement of spectral reflectance and the intrinsic fluorescence of the fundus.[48,49] The light source was a 150 W xenon-arc lamp. For the excitation of fluorescence excitation filters with a transmission window of approximately 20 nm were inserted in the entrance beam. For fundus reflectometry, the full spectrum was passed, but the beam was attenuated with a 2.5 neutral density filter. The illuminated field size was 3.0 deg; the sampled field measured 1.3 or 2.0 deg. The pupil plane configuration was not optimized for the measurement of directional fundus reflectance. Spectral analysis of the fluorescent and reflected light was facilitated with a monochromator and a multichannel analyzer. Presumably, all spectra were obtained in a bleached condition.

2.3 Retinal Imaging Spectrograph

Hammer *et al.* (1997) equipped a Zeiss RCM 250 fundus camera with an imaging fundus spectrograph.[50] The device measured the spectral reflectance of a spatially resolved bar on the retina. The spectral reflectance versus location gave information on the distribution of absorbing pigments in the fundus. Also, it provided the spectral reflectance of detailed structures such as blood vessels or small regions with retinal pathology. A 40×1500 μm bar shaped field (0.14×5.15 deg) was illuminated with the flash of a xenon-arc flash lamp. The illuminated field on the fundus was imaged on the entrance slit of an imaging spectrograph. The spectral range was 400–710 nm, the spectral resolution was better than 2 nm. The image obtained with the CCD was usually binned to 64 rows in the spatial direction. In this case, the spatial resolution of the spectrograph achieved in practice was 23.8 μm (8.18×10^{-2} deg). The configuration of the entrance and exit beams in the pupil plane was not specified. Again, it is assumed that the pupil plane configuration of an original Zeiss camera was used: an annulus for the entrance beam and a concentric circular field in the center of the pupil for the exit beam. With this configuration, the directional properties of the reflectance cannot be measured. A tungsten halogen lamp was available for fundus observation with a 45 deg field angle. Presumably, the illuminance of this observation light was high enough to bleach the visual pigment.

2.4   Photoreceptor Alignment Reflectometers

Gorrand and Delori (1995)

Gorrand and Delori built an apparatus to measure the orientation and directionality of the photoreceptors.[18] Their aim was to study photoreceptor function in normal observers, and the abnormalities occurring with retinal pathology. The instrument, the photoreceptor alignment reflectometer (PAR), gave information similar to a psychophysical SCE test, but within less time and with higher reliability. The measuring beam was provided by a 543 nm He–Ne laser. The illuminated field sizes were 2, 3, 4, or 5 deg in diameter. The sampled fields sizes were always chosen 1 deg smaller. The PAR jointly moved a closely separated entrance and exit pupil in the pupil plane with stationary retinal fields. Thus, the retinal angle was sampled with both the entrance and the exit beam. In one 4 s measurement, five horizontal lines 1 mm apart were scanned in 7.14 μm steps. 56 horizontal steps were averaged; data points were separated 0.4 mm in the horizontal direction. The diameter of the entrance pupil was less than 0.1 mm. The exit pupil diameter was 1 mm. Their separation was 1.2 mm. At the start of a measurement, illumination for 10 s with the measuring beam bleached 95% of the visual pigment.

Burns *et al.* (1995)

Burns, Wu, Delori and Elsner modified the PAR described above.[19] Their objectives were similar: measuring orientation and directionality of the photoreceptors. The measuring beam was provided by a 543 nm He–Ne laser. The size of the illuminated field on the retina was 2 deg; the size of the sampled field was 1 deg. The entrance beam measured 28 μm in diameter in the pupil. In contrast to the earlier design, the location in the pupil plane was stationary during a single measurement. With the modified PAR the distribution of light in the pupil plane was imaged on a 512×512 pixels CCD. Usually 3×3 pixels were binned, which yielded a resolution of 0.075 mm/pixel. Typically, the integration time was 4 s. The illuminance of the measurement light could be reduced for measurements in a dark-adapted state.

2.5   Scanning Laser Ophthalmoscopes

Webb *et al.* (1980, 1987)

In 1980, Webb, Hughes and Pomerantzeff built the first scanning laser ophthalmoscope (SLO), called flying spot TV ophthalmoscope.[51] Their aim was to construct an

ophthalmoscope capable of operating at light levels far lower than used in common ophthalmoscopes and fundus cameras. This was achieved by profiting from the high throughput of the laser light source: a small entrance pupil could be used, leaving room for a large exit pupil. Webb, Hughes and Delori[52] made several changes to the SLO design resulting in a new type: the confocal SLO. In older types, the exit beam was stationary. In the confocal SLO, the exit beam was descanned. The detector was still placed at a plane conjugate to the pupil, but in the confocal SLO an aperture conjugate to the retina in front of the detector limited the region from which light was collected. This configuration increased the contrast of the images. The scanning laser ophthalmoscope proved to be a versatile instrument for imaging and fluorescein angiography, and has become common practice in many ophthalmology departments.

Van Norren and van de Kraats (1989)

Van Norren and van de Kraats[53] constructed a confocal SLO following the design by Webb *et al.*[52] It was intended for imaging retinal densitometry, an application suggested earlier by van Norren.[54] The scanning beam was provided by either a 633 nm He–Ne laser or a 514 nm Ar laser. An important difference with Webb *et al.*'s design was the configuration of the entrance and exit pupil in the pupil plane. In the designs by Webb *et al.*, the entire pupil was used to collect light from.[51,52] The pupil plane configuration in van Norren and van de Kraats' SLO was similar to the arrangement in their single spot reflectometer.[47] The circular entrance pupil measured 0.5 mm and was separated by 0.25 mm from the half circular exit pupil, measuring approximately 2 mm in diameter. The small sizes left a choice in position in the dilated pupil of the subject. DeLint *et al.* obtained retinal images with this SLO, while scanning the small entrance and exit pupil configuration along a horizontal line in the pupil plane.[20] The images showed the optical SCE versus location on the retina. A fast shutter enabled capture of single frames, each recording bleaching less than 1% of the cone or rod pigments. With a sufficiently low frame rate, images of the dark adapted retina could be obtained.

2.6   Discussion

To briefly recall the aim of this study (*c.f.*, Section 1.1): we intended to built an instrument based on an imaging spectrograph. Imaging spectroscopy on the living human eye was demonstrated before by Hammer *et al.*[50] In their instrument, the entrance slit of the spectrograph was conjugate to the retinal plane. We aimed at

Table 2.1: Indication of the performance of the apparatus on a scale good (+), moderate (±) and bad (−). The criteria were resolution in the retinal plane (R. RES.), resolution in the pupil plane (P. RES.), the ability to gather spectral information (SPEC.), and the ability to measure under dark adapted conditions (D.A.).

First author (year)	Instrument	R. RES.	P. RES.	SPEC.	D.A.
Van Norren[47] (1989), Van de Kraats[3] (1996)	densitometer	−	±	±	+
Delori[2] (1989)	reflectometer	−	−	±	−
Delori[48,49] (1992, 1994)	reflectometer	−	−	+	−
Hammer[50] (1997)	imaging spectrograph	+	−	+	−
Gorrand[18] (1995)	PAR	−	±	−	−
Burns[19] (1995)	PAR	−	+	−	+
Van Norren[53] (1989), DeLint[20] (1997)	SLO	+	±	−	+
present thesis	new instrument	−	+	+	−

placing the entrance slit of an imaging spectrograph conjugate to the pupil plane. The configuration achieves high spatial resolution in the pupil plane (along the bar) and high spectral resolution at the same time. Because only a single 1.9 deg spot on the retina will be sampled, the retinal resolution will be poor. To achieve enough signal for detection in the spectrograph, the instrument will operate at light levels that nearly fully bleach the visual pigments; dark adapted measurements will not be possible. The new instrument will be described in detail in the next Chapter. Table 2.1 gives a qualitative overview of the characteristics of the previous designs and the proposed new instrument. The review given in this Chapter demonstrates the novelty of the proposed concept. The new instrument will be discussed in relation to the existing designs more extensively in the General Discussion (Chapter 7).

Chapter 3

Simultaneous Measurement of Foveal Spectral Reflectance and Cone Photoreceptor Directionality

N.P.A. Zagers, J. van de Kraats, T.T.J.M. Berendschot, and D. van Norren

Abstract:
An instrument for simultaneous measurement of foveal spectral reflectance and cone-photoreceptor directionality is described. The key element is an imaging spectrograph (spectral range of 420–790 nm) with its entrance slit conjugate to the pupil plane of a human eye. A 1.9-deg spot on the retina is sampled in 1 s. Video observation of the retina and the pupil facilitates proper alignment. Measurements were performed on 21 healthy subjects. Model analysis of spectra provided densities of photostable ocular absorbers. As an example, macular pigment and melanin are discussed in more detail. Spatial profiles exhibited the optical Stiles–Crawford effect, reflecting cone-photoreceptor directionality.

3.1   Introduction

The transparent media of the human eye allow non invasive probing of the fundus with light. In the past decades, a large number of quantitative reflectometry techniques has been developed.[46] Two important quantifiable aspects of fundus reflectance are its spectral and directional properties. Model analysis of spectral reflectance provides densities of photolabile pigments such as cone visual pigment and of photostable ocular absorbers such as macular pigment, lens, and melanin.[3] Liem *et al.* provided a review of the clinical importance of visual pigment density.[55] Recently, there has been substantial interest in the photostable macular pigment. It is suggested to reduce the risk for age-related macular degeneration.[9–11] Intervention may be possible because macular pigment density has been demonstrated to increase after dietary supplementation of lutein[12,13] and with consumption of spinach, corn, or a combination of both.[14] The directional characteristics of fundus reflectance provide information on the integrity of foveal cones, giving similar insights as obtained with measurement of visual pigment density.[6] Assessment of cone integrity can serve as a differential diagnostic in visual acuity loss of unknown origin.[56] Reduced directionality is associated with macular edema of various origin.[7]In this paper we describe a new apparatus, the foveal reflection analyzer, that is capable of measuring both spectral and directional properties of fundus reflectance simultaneously. The key element is an imaging spectrograph, with its entrance slit placed conjugate to the pupil plane of an eye. Applications concentrate on the fovea, the fundus region corresponding to the area of the visual field with the highest acuity.

Van Norren and Tiemeijer constructed a simple spectral reflectance model using two reflective and four absorbing layers.[1] The model was applied to spectral reflectance at 14 wavelengths, obtained with a densitometer.[57] Delori and Pflibsen equipped a fundus camera with a spectrograph for measuring spectral reflectance of a bleached retina.[2] They elaborated on the spectral reflectance model, an important addition being scattering in the choroid. Following this line of research, Delori build a spectrophotometer, which measures spectral reflectance, and also intrinsic fluorescence of the fundus.[49] Kilbride *et al.* obtained fundus images with a television-based reflectometer at several wavelengths. Analysis of the images revealed the distribution of visual and macular pigment.[31,58] The imaging ability is a large advantage over the other techniques; however, spectral resolution is limited. With imaging spectroscopy, Hammer *et al.* achieved higher spectral resolution and maintained spatial resolution along a bar-shaped field on the retina.[50]

The second important property of light reflected from the fundus is its directionality. Stiles and Crawford demonstrated in a psychophysical experiment that the

luminous efficiency of a narrow ray versus location in the pupil plane shows a bell-shaped curve, with its maximum near the center of the pupil plane.[38] This is now known as the Stiles–Crawford effect of the first kind (SCE I). Reflectance exhibits a similar bell-shaped dependence on location in the pupil plane, also with a maximum near the center.[15–20,59] The psychophysical SCE I and optical SCE originate from directional properties of the receptor cells and their alignment towards the center of the pupil plane. Gorrand and Delori designed a photoreceptor alignment reflectometer for measuring the distribution of reflectance in the pupil.[18] The design was modified and improved by Burns *et al.*[19] Both apparatus are capable of mapping the light distribution in the pupil plane. Using a home-built scanning laser ophthalmoscope (SLO),[53] DeLint *et al.* obtained retinal images while scanning the small entrance and exit pupil configuration along a horizontal line in the pupil plane.[20] The images showed the optical SCE versus location on the retina. Van de Kraats *et al.* simultaneously studied spectral and directional properties of fundus reflectance.[3] With a densitometer[47] they were able to measure spectral reflectance versus location in the pupil plane by jointly scanning a small entrance and exit pupil configuration. Van de Kraats *et al.*[3] added directional properties, and the properties of the visual pigment, to the van Norren and Tiemeijer[1] reflectance model.

In summary, the devices mentioned above measured either spectral reflectance or distribution in the pupil plane. Simultaneous measurement of both was not possible yet. Van de Kraats *et al.*'s analysis required a series of measurements, and spatial resolution in the pupil plane was poor.[3] Both photoreceptor alignment reflectometers[18,19] and the SLO used by DeLint *et al.*[20,47] contained a laser as the light source and therefore yielded limited spectral information. In this present paper we describe an apparatus for measurement of foveal spectral reflectance versus position on a horizontal section of the pupil plane.

3.2 Apparatus

3.2.1 Overview

A schematic representation of the experimental setup is depicted in Fig. 3.1A. Retinal and pupil planes are indicated with R and P and conjugate planes with R' and P'. In some cases, adjacent elements or planes are drawn as a single line. At the top right, the entrance beam emerges from a lamp and passes lenses L1 through L4 and the ophthalmic front lens L_f. The entrance beam defines a small entrance pupil in pupil plane P and illuminates a small spot in the retinal plane R. Light reflected from the eye is captured by lens L_f. Separation of the reflected light from the entrance beam
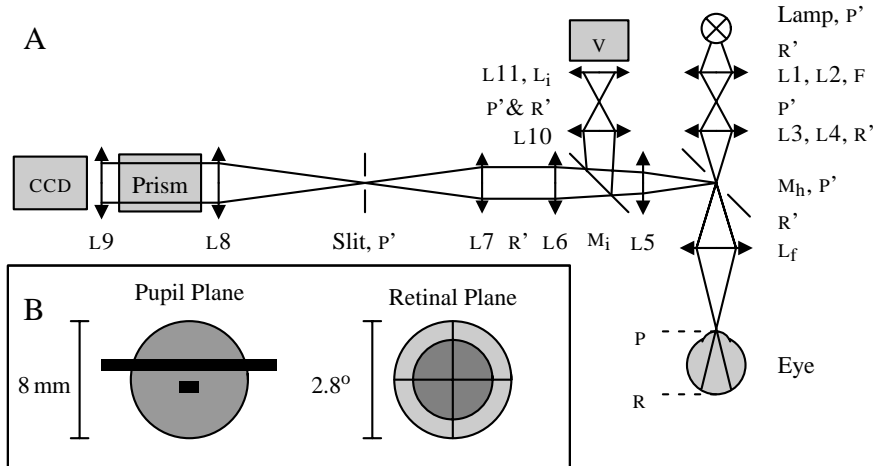
Figure 3.1: (A) Schematic of the apparatus; drawing not to scale. P, pupil plane; R, retinal plane; P' and R', planes conjugate to P and R; Lamp, 30 W halogen lamp; L1-L11, lenses; F, spectral filters; M_h, mirror with central hole; L_f, ophthalmic front lens; M_i, insertable mirror; L_i, insertable lens; V, video camera; Slit, slit conjugate to P; Prism, direct vision prism; CCD, cooled CCD camera. (B) pupil and retinal plane configuration. Left: The disk represents the dilated pupil. The entrance pupil and bar-shaped exit pupil are drawn to scale. Right: The illuminated field, with cross hairs for fixation, and the concentric sampled field.

is achieved with an ophthalmic mirror M_h. The reflected light is either available for observation with a video camera V, or for analysis with an imaging spectrograph. The mode used depends on the position of an insertable mirror M_i. The spectrograph image is captured with a cooled integrating CCD camera.

The retinal and pupil plane configuration is depicted in Fig. 3.1B. In the retinal plane, the illuminated field measures 2.8 deg. The sampled field is concentric, and measures 1.9 deg. This overlap ensures a complete illumination of the sampled field, despite small errors in focus and aberrations in the optics of the eye. The cross wire is centered on the illuminated field. In the pupil plane, the entrance pupil is placed centered with and below the bar shaped exit pupil. Their separation is 0.7 mm. The bar is defined by the slit of the spectrograph. To avoid confusion, the terms entrance and exit are defined with respect to the eye, not the spectrograph.

3.2.2 Entrance Beam

The entrance beam forms a Maxwellian view system, used for controlled illumination of a small spot on the retina. An image of the coil of the 30 W halogen lamp is relayed to the pupil plane with achromatic pairs L1, L2 and L3, L4, and the ophthalmic front lens L_f (20 D, Nikon). The front lens can be moved in the direction of the beam (z direction) to focus on the retina. Eye reflectance is far lower in the blue wavelength region than in the red. In the parallel beam between L1 and L2, glass filters F are placed (FG3 and BG38, 3 mm both, Schott) to increase the ratio of blue over red light and to block most of the infrared light. The intensity of the light entering the eye is 1.10×10^6 Troland (Td). An aperture in plane P' after L2 controls the size of the entrance beam in the pupil plane to 0.8×1.2 mm (with the front lens focussed at infinity). A cross wire for fixation is placed in plane R' close to the lamp. Between L3 and L4 the beam is again parallel. Another retinal conjugate plane R' is available here, where an aperture controls the visual angle of the illuminated field on the retina. A 2.8 deg field is used for measurements. For alignment, the field angle is increased to 16 deg. An additional green filter (VG9, Spindler & Hoyer) is then inserted to increase contrast of the view. The intensity of the alignment beam is 3.35×10^5 Td.

3.2.3 Capturing Light Reflected from the Eye

Light reflected from the eye is captured by lens L_f. The retinal plane is imaged in the focal plane of L_f, the pupil plane in the plane of M_h. Light reflected from the eye is dim compared with the bright entrance beam. To avoid reflections from the cornea, the entrance and exit light are separated with an ophthalmic mirror M_h conjugate to the pupil plane. When the entrance beam, which passes through the central hole of M_h, is correctly focussed in the pupil plane, reflections from the cornea largely disappear in the same hole. Light reflected from the eye is captured by the remaining part of the mirror. This configuration allows observation of the entire pupil, except for the part covered by the hole. Lens L_f is placed slightly out of center and is slightly tilted to redirect reflections at the front and back glass–air interfaces out of the center of the beam. In this way, the reflections are blocked by the retinal aperture at R' in the spectrograph and by a small mask on a glass plate in front of L10 in the observation beam.

3.2.4 Video Observation of the Retina or Pupil

For alignment of the subject, a video observation channel is available. When the mirror M_i is inserted, lenses L5 and L10 act together as a relay pair. Both the retinal

and the pupil plane are relayed to between lens L10 and L11. Lens L_i, moved in or out of the beam with a magnetic solenoid, controls which plane is focused on the video camera chip V (VCB-3512P, Sanyo). Imaging the retina allows us to focus the cross wire and observe whether the subject fixates correctly. Imaging of the pupil allows us to observe the location of the entrance beam within the pupil and is also used to achieve an optimal focus of the entrance beam in the pupil plane.

3.2.5   Imaging Spectrograph

When the mirror M_i is removed from the beam, light is available for the imaging spectrograph. When lenses L5 and L6 are combined, we can image the pupil plane at infinity. In between L6 and L7, a retinal plane R' is available, where an aperture controls the size of the sampled region on the retina to 1.9 deg. A slit, 0.90 mm wide, is placed in the focal plane of lens L7, conjugate to the pupil plane. The slit defines a horizontal bar-shaped exit pupil, which measures 0.8×12 mm in the pupil plane of the eye (with the front lens focussed at infinity). The slit is in the focal plane of lens L8, which images it at infinity. The light traverses a direct vision dispersion prism (Prism, Spindler & Hoyer, Part No. 331120). The spectral image is focused on the chip of a cooled CCD camera (CCD, ST-237, Santa Barbara Instrument Group). The camera is read out in 3×3 binning mode. The spectral image contains 213 points in the spectral direction and 85 points in the spatial direction.

3.3   Methods

3.3.1   Calibration Frames

Reflectance was routinely calibrated with a surface painted with Eastman 6080 white mounted at the end of a black, anodized tube.[3] This painted surface was calibrated against a freshly pressed $BaSO_4$ surface, which we considered the gold standard. The white reference was placed at 445 mm behind the pupil plane and illuminated with the measuring light. The front lens focus was adjusted to place the reference in a retinal conjugate plane. White reference frames calibrate the spectral output of the lamp, transmission of the optics, sensitivity of the CCD camera, as well as sensitivity variations among CCD camera pixels. To account for stray light in the apparatus and dark current in the CCD camera, reference frames of a dark cloth held at approximately 1 m behind the pupil plane were taken. The integration time of the dark frames matched the integration time of the measured spectrum and the white reference frame. White and dark reference frames were obtained prior to each session. In case a refractive

correction was required during the session, additional dark frames for the new position of the front lens were obtained at the end of the session.

3.3.2 Calculation of Reflectance

Each 3×3 binned pixel on the CCD is a detective element, measuring counts at a certain wavelength λ within the range $\Delta\lambda$, and at a certain pixel position x in the spatial direction. In this subsection, we derive an expression for calculating reflectance $R(\lambda,x)$ from the number of counts in the measurement $C_M(\lambda,x)$, the white reference $C_W(\lambda,x)$, and matching dark references $C_{MD}(\lambda,x)$ and $C_{WD}(\lambda,x)$. $R(\lambda,x)$ is an equivalent reflectance: all sources contributing to the reflected light are considered as if they were diffuse reflectors.[1–3] Let $P_h(\lambda)$ be the number of photons per second in the entrance beam, at wavelength λ within the range $\Delta\lambda$, either entering the eye or falling on the white reference surface. Part of the photons will be reflected and backscattered, forming a source of photons in the retinal plane. The number of counts in a pixel is proportional to the photon flux through its detection area and the integration time. The flux through the area A_P spanned by the detective element in the pupil plane at distance d from the retinal plane, is proportional to A_P/d^2. In the measurement situation, the number of detected counts is given by

$$C_M(\lambda,x) = \frac{R(\lambda,x)\gamma P_h(\lambda)t_M A_M S(\lambda,x)}{2\pi d_{\text{eye}}^2} + C_{MD}(\lambda,x), \tag{3.1}$$

with t_M the integration time of the measurement, A_M the detection area in the pupil plane, and d_{eye} the axial length of the eye. The constant γ is the ratio of the sampled and illuminated area in the retinal plane. $S(\lambda,x)$ is a sensitivity factor containing the transmission of the optics, the quantum efficiency, and the gain of the CCD pixels. The factor 2π accounts for light being reflected into half of a sphere.

In the case of the $BaSO_4$ white reference surface, 99% of light in the range 400–800 nm is reflected perfectly diffuse or isotropic into a half-sphere.[25] A relation similar to Eq. (3.1) holds for the white reference images:

$$C_W(\lambda,x) = \frac{0.99\,\gamma P_h(\lambda)t_W A_W S(\lambda,x)}{2\pi d_{\text{ref}}^2} + C_{WD}(\lambda,x), \tag{3.2}$$

with t_W the integration time, A_W the detection area in the pupil plane, and d_{ref} the distance between the white reference and the pupil plane.

Combining Eqs. (3.1) and (3.2), the percentage equivalent reflectance is given by

$$R(\lambda,x) = 0.99\,\frac{t_W}{t_M}\,\frac{A_W}{A_M}\left(\frac{d_{\text{eye}}}{d_{\text{ref}}}\right)^2 \frac{C_M(\lambda,x) - C_{MD}(\lambda,x)}{C_W(\lambda,x) - C_{WD}(\lambda,x)}. \tag{3.3}$$

The factor $A_{\mathrm{W}}/A_{\mathrm{M}}$, which accounts for changes in scale of the pupil plane with the front lens position, is calculated from pixel scale S_{PIX} as $(S_{\mathrm{PIX,W}}/S_{\mathrm{PIX,M}})^2$ (for calibration of S_{PIX}, see Subsection 3.3.3). The axial length of the eye d_{eye} is calculated from the front lens focal adjustment. It is assumed that the cornea and eye lens can be treated as a single flat lens with focal distance 22.29 mm[25] and that all ametropia can be attributed to a variation in axial length of the eye.

An estimation of the error in the reflectance value starts with calculation of the error in the raw pixel data:

$$\sigma = \left(\mathrm{RN}^2 + \frac{N-B}{3}\right)^{\frac{1}{2}}, \tag{3.4}$$

where RN is the read noise of the camera in counts, N is the number of counts read from the pixel, and B is the bias level of the camera in counts. Typical values are RN = 12, N in the range 150–5000, and $B = 100$. The factor 3 accounts for 3×3 on-chip binning. When the appropriate error propagation mathematics and Eq. (3.3) are used, an error is attributed to the reflectance.

3.3.3   Spectral and Spatial Calibration

For spectral calibration of the spectrograph, images of a mercury lamp illuminating the wall opposing the setup were obtained. Pixel positions of seven lines were determined [wavelengths in air: 435.8, 491.6, 546.1, $(577.0 + 579.1)/2$, 623.4, 690.8, and 772.9 nm].[60] The wavelength range covered by the spectrograph was 420–790 nm. Dispersion strongly depended on wavelength. At 420 nm the spectral range covered by one 3×3 binned pixel was approximately 0.4 nm; at 760 nm it was approximately 6 nm. For calibration of pixel scale S_{PIX}, a transparent film containing periodic vertical dark bars was placed in the pupil plane. Images of the wall opposing the setup revealed the periodic pattern, which enabled us to scale the pupil plane to CCD pixels. Scale was calibrated for the complete range of front lens settings. With the front lens focussed at infinity, one 3×3 binned pixel corresponded to 0.14 mm in the pupil plane. Prior to the calculation of reflectance, the images were binned and interpolated to 5 nm spectral and 0.1 mm spatial resolution to correct for the nonlinear dispersion of the prism and variable scaling of the pupil plane.

3.3.4   Protocol

The research followed the tenets of the Declaration of Helsinki and was approved by the local Medical Ethics Committee. The purpose was explained at the beginning

of the experiment, and written informed consent was obtained. The pupil of one eye was dilated with one or two drops tropicamide 0.5%. A chin rest and temple pads, connected to a headrest, were used to maintain head position. The headrest can be adjusted in three dimensions. This allowed us to focus on the pupil plane and to position the entrance beam within the pupil. Subjects were instructed to fixate the cross wire at all times. For adjustment of the headrest, the large field with an additional green filter was used. With the large field the pupil lit up more brightly, focus in the pupil plane was more critical, and a larger part of the retina could be seen. The entrance beam was focused in the pupil plane. Care was taken to avoid reflections from the corneal surface of the eye. Fixation was checked in the retinal image. If required, the front lens focus was adjusted. During focal adjustment the headrest was moved as well to maintain a good focus in the pupil plane.

We then searched the maximum in the directional reflectance (*e.g.*, the maximum of the SCE) using the measuring field. During the search, we continuously read the spatial profiles near 540 nm from the CCD while discarding the remaining part of the data, thereby achieving a short readout time. Integration time was reduced to 0.25 s. At 540 nm the directional reflectance shows up prominently. In the horizontal direction in the pupil plane (along the spectrograph slit) the maximum position is readily observed in a profile plot on a computer display. The maximum in the vertical direction was found by a manual search. While we scanned vertically, the latest profile was compared by eye with the highest profile till then. The search typically took approximately 2 min. In this period, visual pigments are bleached away at approximately 97%.[25] At the optimal entrance position five spectra were obtained. Prior to each measurement, subjects were instructed to blink once, keep their eyes wide open, and fixate on the cross wire. Integration time was 1.0 s. The entire procedure described above, apart from the cross wire focused on the retina, was repeated five times to test repeatability. Settings of the headrest were changed on purpose in between two runs to increase independence.

3.3.5 Subjects

All subjects ($n = 21$) were Caucasian, unfamiliar with any eye disease, and had no complaints on visual acuity. The majority [$n = 15$ (12 females)] fell in the age group 18–27; the mean age was 22. Six of the subjects (male) were aged 40–74. The six older subjects can be considered experienced observers, whereas the younger subjects were all naïve subjects. Fourteen subjects had no refractive correction. For the other cases, refraction was in the range -1.5 to -4 D, except two older subjects having -6 and -7 D.
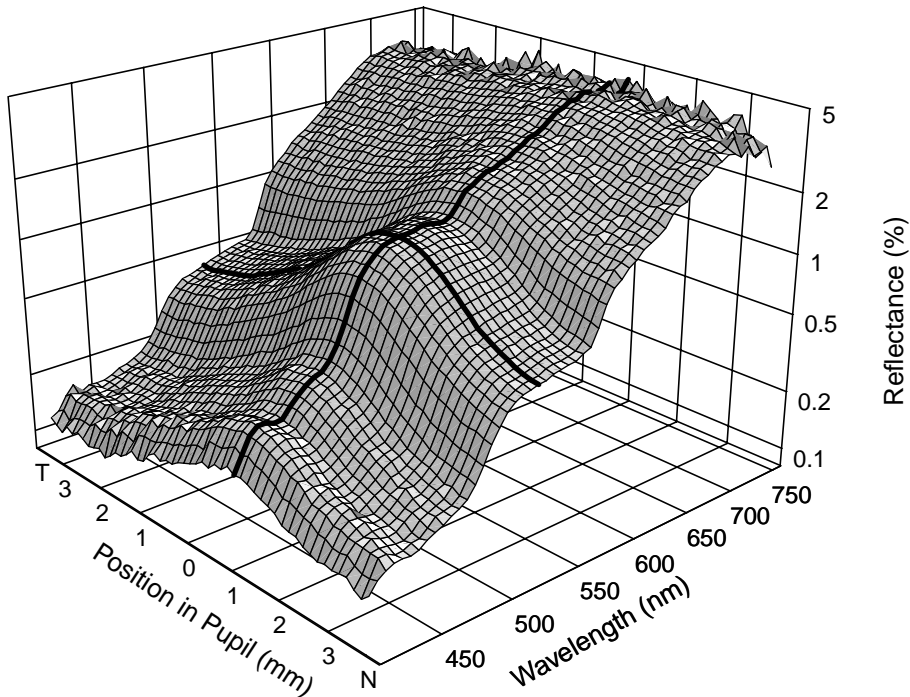
Figure 3.2: Image of foveal spectral reflectance (female subject, age 20). Surface height represents the equivalent reflectance of the fovea, expressed as a percentage on a logarithmic scale, versus wavelength and position in the pupil plane. Temporal (T) and nasal (N) side are indicated.

3.4   Results

3.4.1   Reflectance Spectrum Image

An example of an image of two-dimensional reflectance is presented in Fig. 3.2 (female subject, age 20). Figure 3.2 shows the equivalent reflectance of the fovea, expressed as a percentage on a logarithmic scale, versus wavelength and location in the pupil plane. Temporal (T) and nasal (N) sides are indicated. The image can be looked at in two ways: first, as spectral reflectance versus location in the pupil plane, and second, as an optical Stiles–Crawford profile versus wavelength.

Adopting the first view, the characteristics of spectral fundus reflectance are recognized: a decrease toward short wavelengths, with steeper decrements at 590 nm,

510 nm, and at the lowest recorded wavelengths.[1–3,61] At the longest wavelengths, ocular pigments, except melanin, are fairly transparent. Below 590 nm, light is efficiently absorbed by blood. The contribution to reflectance from deeper, blood rich layers diminishes, causing the first decrement. Reflectance below 590 nm mainly originates from the receptor cell layer.[3] The second decrement at 510 nm is due to macular pigment. The latter also causes a shallow dip near 460 nm. Absorption by the crystalline lens causes a decline at the shortest recorded wavelengths.

The optical SCE is best observed in the region 510–590 nm. The profile near 540 nm, indicated by the thick line in Fig. 3.2, presents a typical example. Reflectance shows a bell-shaped dependence on position in the pupil plane, with a maximum slightly on the nasal side of the pupil center.[15,16,18–20] At longer wavelengths, the directional part of the reflectance dissolves in the much larger nondirectional part. At shorter wavelengths, absorption by the macular pigment and the crystalline lens leaves the bell shape intact, but strongly reduces the amplitude of the directional reflectance.

3.4.2 Spectral Intersections

For each measurement, the spectrum at the pupil position with the highest reflectance at 540 nm was selected (*e.g.*, the spectrum indicated with a thick line in Fig. 3.2). We fitted the spectra with the van de Kraats *et al.* fundus reflectance model using a least-squares method.[3,62] Each data point was assigned a weight of 1 over its error squared. The model describes radiation transfer in the eye with a limited number of reflecting, absorbing, and scattering layers. Spectral properties of the absorbers are taken from the literature. Eight parameters were optimized: reflectance from disks in the outer segments of the photoreceptors R_{disk}, at the inner limiting membrane R_{ilm}, at the cornea R_{cornea}, the optical densities of melanin D_{mela}, macular pigment D_{mac}, the aging component of the lens D_{lens-a}, the thickness of the blood layer Th_{blood}, and a parameter accounting for scattering in the choroid D_{scat}. The parameter R_{cornea} was added to the model. Visual pigment density was assumed zero, and the Stiles–Crawford parameter SC was set at unity. Values for other fixed parameters and a detailed description of the model are given in the original paper.[3]

A sample ($n = 5$) of spectral reflectance curves spanning the full age range is shown in Fig. 3.3A. The solid curves represent model fits. The effect of an increase in lens absorption with age is apparent from the downward trend with age of the spectra below 500 nm. Deviations between the data and the model are largest below 425 nm. Here, both reflectance and the power of the entrance beam are low, resulting in a low signal-to-noise ratio. The mean of all spectra ($n = 5 \times 5 \times 21$) is depicted
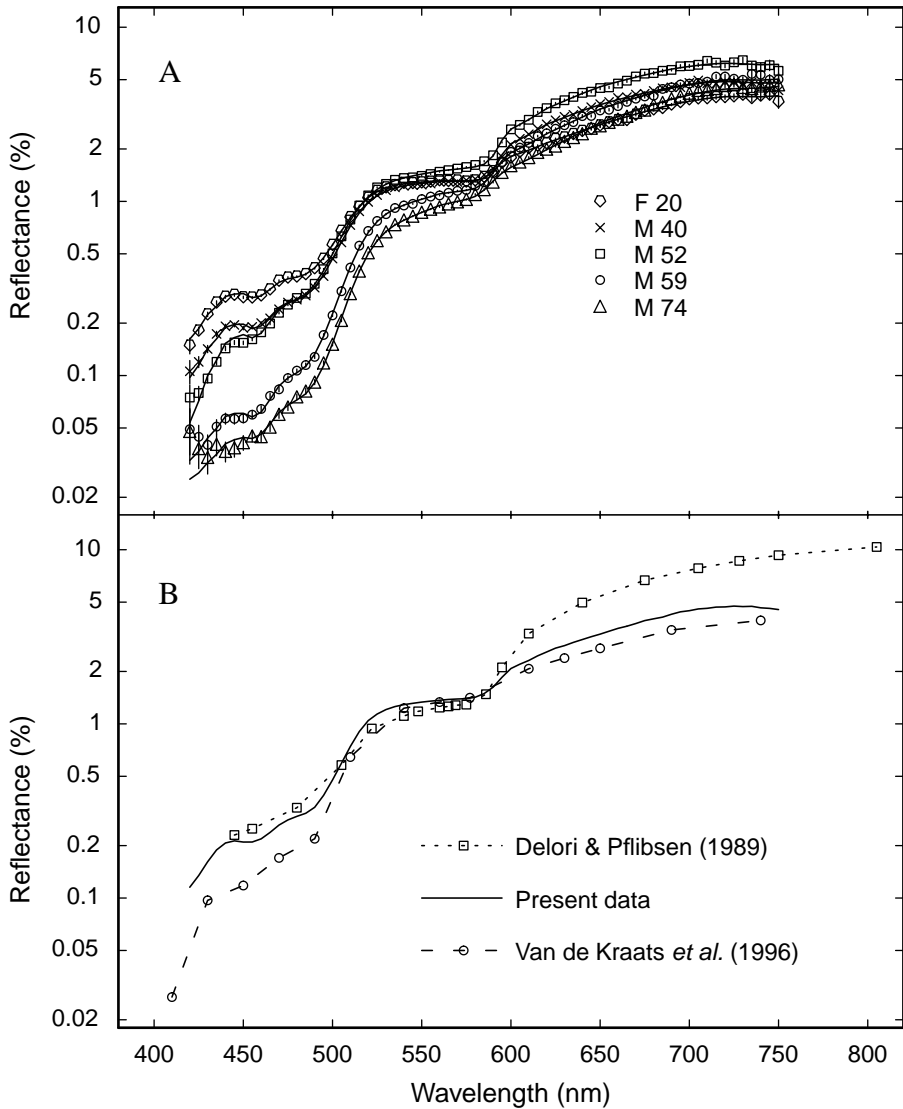
Figure 3.3: (A) Spectral intersections at the pupil position with maximum reflectance at 540 nm. Five subjects spanning the full age range are presented; gender and age are indicated. Vertical bars indicate the error associated with each point (hardly discernable and absent for most points). The solid curves represent model fits. (B) Mean reflectance spectrum (solid curve), together with data from Delori and Pflibsen[2] (1989) and van de Kraats *et al.*[3] (1996). In the mean spectrum, small dips that are due to macular pigment are present at 460 and 490 nm.

Table 3.1: Spectral reflectance data. λ, wavelength; R, mean reflectance; SD, relative between-subjects standard deviation, *i.e.*, the standard deviation of the subject means divided by the mean; RE, relative error

λ (nm)	R (%)	SD	RE (%)	λ (nm)	R (%)	SD	RE (%)
420	0.115	0.39	17	590	1.62	0.16	1.0
430	0.162	0.44	5.7	600	2.08	0.17	1.0
440	0.207	0.45	3.4	610	2.31	0.17	1.1
450	0.210	0.45	2.8	620	2.59	0.18	1.1
460	0.219	0.44	2.2	630	2.81	0.18	1.8
470	0.262	0.43	1.8	640	3.05	0.18	2.0
480	0.294	0.41	1.4	650	3.28	0.18	2.2
490	0.332	0.39	1.3	660	3.53	0.18	2.3
500	0.476	0.34	1.1	670	3.77	0.18	1.6
510	0.742	0.28	0.85	680	4.01	0.18	2.2
520	1.04	0.25	0.75	690	4.26	0.17	1.5
530	1.21	0.24	0.68	700	4.47	0.17	2.2
540	1.29	0.23	0.65	710	4.61	0.17	2.5
550	1.33	0.21	0.56	720	4.69	0.16	3.1
560	1.37	0.20	0.68	730	4.71	0.17	4.0
570	1.39	0.19	0.77	740	4.64	0.16	5.8
580	1.42	0.18	0.94	750	4.53	0.16	9.0

with a solid curve in Fig. 3.3B, together with data from the literature (squares, Delori and Pflibsen;[2] circles, van de Kraats *et al.*[3]). The mean data are also presented in Table 3.1, together with relative standard deviations, *i.e.*, the standard deviation of the subject means divided by the mean of subject means. Also given is the relative error, which was first calculated for each subject from the mean of the estimated measurement errors and mean of 25 spectra and then averaged over subjects.

Table 3.2 gives a summary of the results of the spectral model fit. The parameter mean is the mean of 21 within-subject mean values. The standard deviation σ_N is the standard deviation of the subject means with respect to the parameter means. P_{MIN} and P_{MAX} are the lowest and highest within-subject means. In some cases P_{MIN} reached zero. This was the lower limit set in the fit algorithm. Apart from estimations for the best fit, the Levenberg–Marquardt method returned 68% confidence intervals for the fitted parameters.[62] The mean of 21 for the within-subject mean confidence interval estimations is also shown in Table 3.2. The study design of five measurement

Table 3.2: Spectral model (Top) and Stiles–Crawford parameters (Bottom). PM: parameter mean; σ_N: between-subject standard deviation; P_{MIN}, P_{MAX}: lowest and highest within-subject mean; CI: mean of confidence interval estimations; CR_T, CR_S, CR_M: coefficients of repeatability for the total, within the series, or between the series standard deviation. (N) and (T) stand for nasal and temporal.

	PM	σ_N	P_{MIN}	P_{MAX}	CI	CR_T	CR_S	CR_M
D_{scat}	0.20	0.041	0.11	0.27	0.0066	0.014	0.010	0.010
Th_{blood} (μm)	68	18	29	104	6.5	15	12	10
D_{mela}	1.1	0.11	0.95	1.4	0.022	0.045	0.033	0.032
R_{disk} (%)	2.8	0.50	1.6	3.5	0.050	0.54	0.30	0.47
D_{mac}	0.45	0.11	0.28	0.64	0.010	0.084	0.071	0.047
R_{ilm} (%)	0.034	0.052	0	0.20	8.6	0.049	0.039	0.029
D_{lens-a}	0.11	0.12	0	0.48	0.032	0.058	0.043	0.039
R_{cornea} (%)	0.043	0.028	0	0.10	4.5	0.029	0.024	0.017
x_c (mm)	0.43 N	0.63	1.3 N	1.3 T	0.0063	0.20	0.13	0.16
ρ (mm^{-2})	0.17	0.037	0.12	0.23	0.0037	0.036	0.024	0.028
A (%)	0.77	0.25	0.30	1.14	0.0060	0.22	0.10	0.20
B (%)	0.52	0.080	0.35	0.65	0.0058	0.084	0.062	0.059
A/B	1.5	0.46	0.70	2.4	0.026	0.52	0.29	0.45

series with five replacements allowed an estimation of (1) the total standard deviation σ_T, (2) the standard deviation with respect to the mean of series σ_S, and (3) the standard deviation of the mean of series σ_M. The coefficient of repeatability is defined as the 95% range for the difference in two repeat measurements.[63] The coefficients followed from the mean values of σ_T, σ_S, and σ_M after multiplication by $2\sqrt{2}$.

Figure 3.4 gives an impression of the model predictions for single measurements. Figure 3.4A shows 25 macular pigment density (D_{mac}) estimates for all 21 subjects. D_{mac} is known to vary substantially between subjects. The within-subject variability is occasionally large. Six subjects had experience in this type of experiment (1, 3, 12, 13, 17, and 21). They generally showed low variability. In some of the other subjects, variability was equally low (*e.g.*, 2, 10, and 11). Others, however, show a large variability (*e.g.*, 9 and 19). Fig. 3.4B is a similar scatterplot for melanin density (D_{mela}). For melanin, within-subject variation is much smaller compared with D_{mac}. The stability of the melanin data indicates that the high D_{mac} variability is not related to instrumental errors or head instability of the subject. A probable explanation is given in Section 3.5.
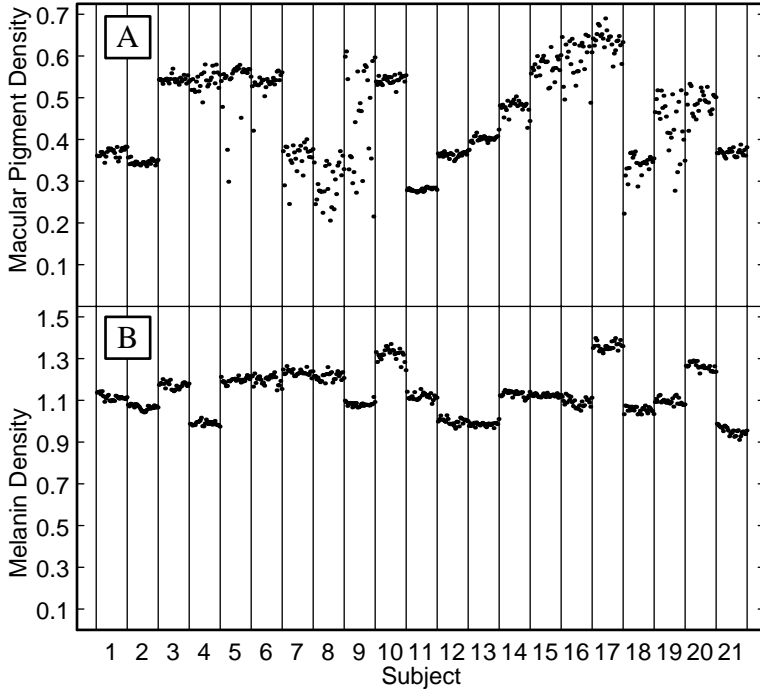
Figure 3.4: (A) Macular pigment (D_{mac}) and (B) melanin density (D_{mela}) estimates for all 25 measurements per subject. For macular pigment, both between- and within-subject variations are large. For melanin they are much smaller. Macular pigment for the within-subject variation is markedly different between subjects; *e.g.*, subject 11 has little variation, whereas for subject 9 the data are highly scattered. The latter subject had difficulties maintaining rigid fixation during alignment.

3.4.3 Spatial Intersections: Stiles–Crawford Effect Profiles

For each measurement, the profile at 540 nm was selected and fitted with

$$R(x) = B + A10^{-\rho(x-x_c)^2}, \tag{3.5}$$

with R the percentage reflectance, x the location in the pupil plane in millimeters, B the nondirectional background reflectance, A the amplitude of the directional reflectance, ρ a measure for the peakedness, and x_c the center position.[18–20] The fit used a least-squares method with each data point assigned a weight of 1 over its error squared.[62] Data included in the fit met two conditions: distance to either of the pupil edges more of than 1 mm and distance to the entrance beam of less than 3 mm.
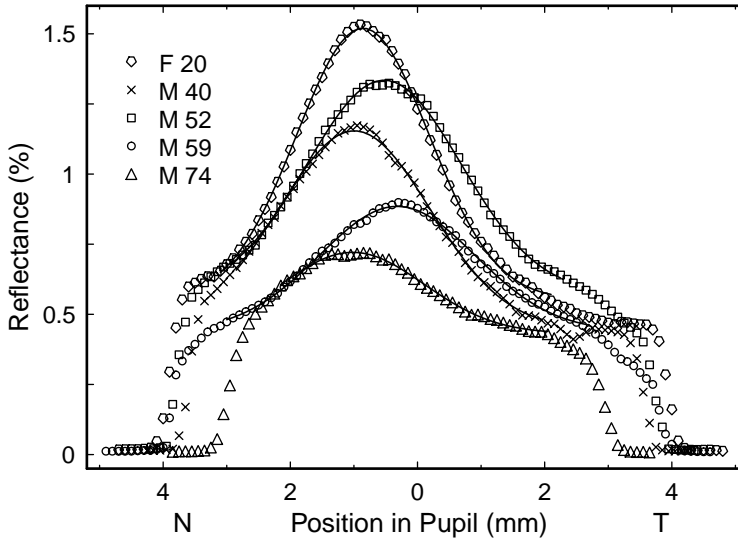
Figure 3.5: Profiles at 540 nm demonstrating individual differences in the optical SCE. Data are for the same subjects as in Fig. 3.3A; gender and age are given. Solid curves represent fits to the data. Nasal (N) and temporal (T) side are indicated. Pupil edges are recognizable as the sharp drops in the region 3–4 mm. Maximum reflectance shows up near the center of the pupil, with a tendency toward the nasal side.

Optical SCE profiles at 540 nm ($n = 5$) are shown in Fig. 3.5 for the same subjects as in Fig. 3.3A. The solid curves represent fits with Eq. (3.5). At the pupil edges, the profiles drop to zero. The edge of the pupil may span numerous pixels when the bar is far below or above the pupil center because the vertical width of the bar is much larger than the horizontal width of the pixels. As usual, the maxima show up near the pupil center, with a tendency to the nasal side.[18–20] Table 3.2 gives a summary of the SCE parameter fit results (see explanation in Subsection 3.4.2).

3.5 Discussion

3.5.1 General Discussion

We have demonstrated the feasibility of simultaneous measurement of spectral and directional fundus reflectance. Both aspects hitherto have been studied separately.[1–3, 15–20, 31, 50, 59, 61] The course of the spectra and directional aspects agree with earlier results. In the model by van de Kraats *et al.* differences between spectra ob-

tained at the maximum of the optical Stiles–Crawford effect and 2 mm nasally were fitted with a single parameter.[3] The model lacks a quantitative relation between the single parameter and the position in the pupil plane. Furthermore, the model assumes simultaneous scanning of the entrance and exit pupil. In contrast, we aligned the entrance pupil with the maximum of the SCE and obtained spectra for a range of exit pupil positions. Thus the van de Kraats *et al.* model as it is cannot be applied to entire spectrograph images. To our knowledge, other models including both spectral and directional fundus reflectance are not available. For a more detailed comparison with the literature, intersections of the data set were analyzed: spectra at the pupil position with the highest reflectance at 540 nm and profiles at 540 nm.

3.5.2 Mean Spectrum

In Fig. 3.3B, the mean spectrum (solid curve) is compared with literature data. Differences between the spectra depend on (at least) three factors: composition of the population, size of the illuminated and sampled retinal field, and configuration of the entrance and exit pupil. The large differences between subjects are apparent from Fig. 3.3A, with the largest variation below 500 nm. There is a strong influence of age on the spectra, as absorption in the crystalline lens increases with age.[64] Delori and Pflibsen measured subjects aged 22–38 years.[2] The lack of older subjects may explain the somewhat higher reflectance below 500 nm.

Above 600 nm, a strong dependence on illuminated field size is expected. At the longest wavelengths, where blood does not absorb, light scatters laterally in the deeper fundus layers.[3] Hence, the larger the illuminated field size, the larger the reflectance. Delori and Pflibsen illuminated 5 deg and sampled 1.2–1.6 deg.[2] Van de Kraats *et al.*[3] illuminated 1.9 deg and sampled 1.6 deg. In the present study, field sizes were 2.8 and 1.9 deg. As can be seen in Fig. 3.3B above 600 nm, the reflectance slightly raises with the increment from 1.9 to 2.8 deg, whereas the leap to 5 deg substantially increases the reflectance in the red. Below 500 nm, field sizes also influence the spectra. Macular pigment is highly concentrated toward the center of the fovea.[29–32] The slightly larger sampled retinal field in the present study reduces macular pigment content and gives rise to higher reflectance in the blue part of the spectrum. The agreement in the range 520–590 nm is rather remarkable. The present mean spectrum was selected at the Stiles–Crawford maximum. The corresponding pupil plane configuration is similar to the one used by van de Kraats *et al.*:[3] small, closely separated entrance and exit pupils. Both are sensitive for directional reflection, and spectra are equally high. Delori and Pflibsen[2] used a modified Zeiss fundus camera, which uses a rather large annular entrance pupil and a concentric circular

exit pupil, and should be less sensitive to the directional light. Modification of this arrangement was not reported. It is therefore unclear why the latter spectrum is as high as the other two. Perhaps there is a difference in the absolute calibration of the spectra.

Below 630 nm, mean relative errors in Table 3.1 are smaller than obtained by van de Kraats *et al.*[3] The errors are larger at longer wavelengths. Van de Kraats *et al.*[3] included both instrumental errors and errors due to instability of the subject. In this study, integration time was short, largely eliminating errors that were due to movement of the subject. The errors are largest below 430 nm, where the output of the lamp drops and reflectance is low, and above 730 nm, where the spectral filters block almost all deep-red and infrared light.

3.5.3   Spectral Model Results

The results of the spectral model fit are given in Table 3.2. Parameters are discussed as in the Table 3.2, upward from the sclera. Deep scatter loss D_{scat} was 0.20, slightly less than 0.23 found by van de Kraats *et al.*[3] The mean thickness of the blood layer Th_{blood} was 68 μm. Van de Kraats *et al.* found 22.7 μm,[3] and Delori and Pflibsen found 168 μm.[2] Delori and Pflibsen used a model with a Kubelka–Munk scattering description of the deeper layers.[2] This increased the estimated blood layer thickness. Melanin density D_{mela} (1.1 at 500 nm, range 0.95–1.4) is comparable to the densities found by van de Kraats *et al.* (1.32 at 500 nm, 0.98–1.68).[3] Delori and Pflibsen found a higher mean and a much larger range (2.13 at 500 nm, 0.19–7.9).[2] The former two studies contained only Caucasians, the latter included two Blacks with three to four times higher melanin content. This probably explains the differences at the high end of the range.

Receptor disk reflectance R_{disk} cannot be discerned from a reflecting layer at the level of the retinal pigment ephithelium in a single bleached spectrum at the Stiles–Crawford maximum. The arguments for attributing reflectance at this level in the retina to the disks in the receptor outer segments are given by van de Kraats *et al.*[3] Mean disk reflectance was 2.8%, similar to van de Kraats *et al.*, who found 2.75%.[3] The results can also be compared with the retinal pigment ephithelium reflectance of 2.3% in the model by Delori and Pflibsen.[2] The high mean disk reflectance demonstrates the effectiveness of alignment with the Stiles–Crawford maximum. Mean macular pigment density D_{mac} was 0.45 at 460 nm, with a range of 0.28–0.64. Van de Kraats *et al.* found higher values (0.54 at 460 nm, 0.42–0.83).[3] As stated above, this was caused when a smaller retinal field was sampled. Delori and Pflibsen found lower values (0.21 at 460 nm, 0.12–0.31).[2] In a more recent paper, Delori *et al.* re-

ported 0.23 for a reflectometric method (sampled field of 2 deg).[65] With a method based on the autofluorescence of lipofuscin, a fluorophore posterior to the macular pigment, they found 0.48 (sampled field 2 deg).[65] The cause for the low reflectometric values may reside in their model because it lacks reflectors anterior to the macular pigment, *e.g.*, inner limiting membrane and cornea. Accounting for light that is reflected posterior to the macular pigment gives a higher macular pigment level. Berendschot *et al.* studied the effect of lutein supplementation on D_{mac} in eight male subjects with a reflectometer and a SLO.[13] At baseline, mean D_{mac} was 0.47 for the reflectometric and 0.26 for the SLO technique.

Reflectance from the inner limiting membrane R_{ilm} is small and problematic to fit. In many cases the parameter reached the lowest allowed value of zero. Mean R_{ilm} was 0.034%; even the maximum 0.20% is lower than the mean R_{ilm} of 0.26% found by van de Kraats *et al.*[3] They also included data from dark-adapted spectra in the model fit. Undoubtedly, this allowed a better estimate of R_{ilm}. The mean age-dependent lens density D_{lens-a}, added with an age-independent density 0.31, gives a mean lens density of 0.42 at 420 nm, with a range of 0.31–0.79. For some of the young subjects, D_{lens-a} reached the lowest allowed value of zero. As expected, D_{lens-a} showed a trend with age (data not shown). Van de Kraats *et al.* found a lens density of 0.54 at 420 nm, with a range of 0.42–0.83 for subjects aged 20–51 years, 32 years on average.[3] Delori and Pflibsen found a lens density of 0.66 for a group of 10 subjects aged 22–38 years, with an unknown mean.[2] The latter result is fairly high given the age of the subjects. The aging algorithm by Pokorny *et al.* predicts a total lens density at 420 nm of 0.66 at age 22, 0.73 at age 32, and 0.89 at age 50.[64] Compared with these values, reflectometric methods produce systematically low values. Reflectance from the cornea R_{cornea} was on average 0.043%. This is low in the absolute sense, but is of equal magnitude as light that is reflected from the fundus at wavelengths below 500 nm, especially in older subjects, *e.g.*, see Fig. 3.3A.

The mean confidence interval states how accurately parameters are determined in the model fit. A large confidence interval indicates large measurement errors or bad convergence of the fit. For most parameters, except R_{ilm} and R_{cornea}, the confidence interval was smaller than σ_N and the range P_{MIN} to P_{MAX}. Apparently, in some cases, R_{ilm} and R_{cornea} did not strongly contribute to reflectance and were attributed to a large error. The weakness of the current model is that sometimes parameters are optimized in the fit while being insignificant or that parameters reach the lower (physical) limit set to zero.

The coefficient of repeatability derived from the total standard deviation CR_T contains the total experimental error. CR_T was smaller or hardly larger than σ_N and smaller than the range P_{MIN} to P_{MAX}. This means that the measurements discriminate

well between subjects. CR_T is much larger than the confidence interval for D_{mac} and R_{disk}. This indicates that the uncertainty in D_{mac} and R_{disk} results mainly from experimental errors. A high within series CR_S points to errors in fixation and movements of the subject. Between series, CR_M is mainly connected to errors in the alignment procedure. For R_{disk}, CR_M is largest; most variation is due to variation in alignment on the optical Stiles–Crawford maximum. For D_{mac}, CR_S is largest. Macular pigment is highly concentrated toward the center of the fovea.[29–32] This makes D_{mac} sensitive to errors in fixation. The influence of fixation was illustrated in the scatterplot in Fig. 3.4A. Experienced subjects showed low variability; and for some inexperienced subjects (*e.g.*, 9 and 19), variability was large. Figure 3.4B demonstrates that variability in melanin is similar for all subjects. The distribution of melanin pigmentation near the fovea is much smoother than for macular pigment.[31] Therefore melanin will not be influenced as strongly by fixation errors as will macular pigment. With further automation of the setup and optimization of the protocol, an improvement in the assessment of macular pigment might be expected. It is crucial to observe fixation just before each measurement. Coefficients of repeatability for macular pigment, achieved by Berendschot *et al.*, were 0.27 for a reflectometric technique and 0.17 with a SLO based technique.[13] Despite the problem with fixation, the present coefficient of repeatability 0.084 was better.

3.5.4   Stiles–Crawford Profiles

Profiles at 540 nm clearly showed the optical SCE. The profiles were fitted with the commonly used Gaussian model [Eq. (3.5)]; results are given in Table 3.2. The results are discussed in relation to three earlier studies. Gorrand and Delori scanned the pupil plane with a small exit and entrance pupil configuration.[18] A 3-deg retinal field was illuminated with 543 nm He–Ne light, and the central 2 deg were sampled. Burns *et al.* used a small entrance pupil and imaged the entire pupil plane on a CCD camera.[19] A series of images was obtained for several entrance pupil positions. The image with the highest directional reflectance was selected afterwards. A 2-deg retinal field was illuminated with 543 nm He–Ne light, the central 1 deg was sampled. DeLint *et al.* used an SLO with a small entrance and exit pupil configuration.[20] The horizontal meridian of the pupil plane was scanned with both pupils, and retinal images were obtained in 514 nm argon light. The series of images show the optical SCE versus location on the retina. The difference in wavelength with the other studies is considered of minor influence.

In the present study mean x_c was 0.43 ± 0.63 mm nasal (given are the mean parameter plus or minus σ_N). Gorrand and Delori reported 0.86 ± 0.84 mm nasal,[18] and

DeLint *et al.* reported 0.23 ± 0.41 mm nasal.[20] In the scatter plot of x_c given by Burns *et al.*, the trend to the nasal side is also present.[19] The slight tendency toward the nasal side is common to all studies. Our mean peakedness ρ was 0.17 ± 0.037 mm^{-2}. When compared with the results by Burns *et al.*,[19] 0.0813 ± 0.013 mm^{-2}, this is on the high side. The higher ρ may result from the larger field size (1.9 versus 1.0 deg) because, for small angles, ρ increases with eccentricity.[20] Gorrand and Delori[18] and DeLint *et al.*[20] use a double scanning method that results in a higher ρ: 0.204 ± 0.035 mm^{-2} and 0.226 ± 0.049 mm^{-2} for the central 2×2 deg of the SLO images. For a more detailed discussion on the differences in ρ between the different techniques, see Marcos and Burns[23] and Berendschot *et al.*[66] Mean ratio A/B of directional light A over the nondirectional background B was 1.5 ± 0.46. This is lower than for Gorrand and Delori, who reported 2.59 ± 0.82,[18] and by DeLint *et al.* who found 4.9 ± 1.8.[20] The latter authors used a small aperture confocal to the SLO spot on the retina, which strongly suppresses the diffuse background component that is present with larger fields. With a 1.3 deg confocal aperture their, mean A/B decreased to 3.0. Interpretation of the confidence interval, $\mathrm{CR_T}$, $\mathrm{CR_S}$, and $\mathrm{CR_M}$ was discussed above in Subsection 3.5.3. The confidence intervals are small compared with the natural variation. The experimental errors $\mathrm{CR_T}$ are much larger. Discrimination between subjects was reasonable. For directional reflectance A, $\mathrm{CR_M}$ is much larger than $\mathrm{CR_S}$. Variation in A mainly originates from alignment on the optical SCE maximum, similar to R_{disk} (see Subsection 3.5.3).

3.6 Conclusion

Simultaneous measurement of spectral and directional reflectance with a simple chinrest and headrest proved possible. A video observation channel and a fast method for optimization of the optical SCE at 540 nm allowed alignment with respect to the apparatus and on the Stiles–Crawford maximum within a few minutes. Application of a short integration time reduced errors that were due to movement of the subject. Spectral analysis provided densities of photostable ocular absorbers such as macular pigment, lens, and melanin and reflectivity of the disks in the outer segment of the cone receptor cells. Analysis of spatial profiles delivered Stiles–Crawford parameters. Use of all data, not just one spectrum, awaits extension of the fundus reflectance model. Errors in fixation were found to be the main source of within-subject variation in macular pigment density. This might be avoided if fixation is checked just prior to the measurement. The new apparatus provides a novel diagnostic tool. It might also greatly facilitate epidemiological studies of ocular pigments.

Chapter 4

Wavelength Dependence of Reflectometric Cone Photoreceptor Directionality

N.P.A. Zagers, T.T.J.M. Berendschot, and D. van Norren

Abstract:
We present evidence for the wavelength dependence of the directionality of light reflected from cone receptor cells (optical Stiles–Crawford effect): Blue light is more directional than red. According to the waveguide-scattering model of Marcos *et al.* [J. Opt. Soc. Am. A **15**, 2012 (1998)], directionality is the sum of a waveguide component and a scattering component. The latter is proportional to 1 over wavelength squared, and it is related to the row-to-row spacing of the cone lattice. Our results allow a firm confirmation of Marcos *et al.*'s theory. For a 1.9 deg foveal area, group mean ($n = 18$) cone spacing was 3.42 μm, in good agreement with anatomical data. Group mean waveguide directionality was 0.077 mm^{-2}.

4.1   Introduction

Stiles and Crawford discovered that light entering near the center of the pupil is perceived brighter, compared with light entering at the edge.[38] Relative luminous efficiency showed a bell-shaped dependence on the entrance beam location in the pupil plane, with a maximum near the center of the pupil. This phenomenon is generally referred to as the psychophysical Stiles–Crawford effect of the first kind (SCE I). Light reflected from cone receptor cells exhibits an optical counterpart of the SCE I.[15–23] In a typical experiment a narrow beam enters near the pupil center and illuminates a small spot on the retina, centered with the fovea. The visual pigments are bleached away. The distribution of light reflected and scattered from the retina is then recorded in the pupil plane. Reflectance shows a bell-shaped directional component, again with a maximum near the center of the pupil. The directional component originates from the cone receptor cells.[3] In addition, light scattered in other layers, *e.g.*, the choroid, gives rise to a constant background, filling the entire pupil. The directionality of light reflected from cone receptor cells is referred to as the optical Stiles–Crawford effect (optical SCE).

In the fovea, cone receptor cells are tightly packed, with their long axes pointing toward a location near the center of the pupil.[24] From the SCE I it follows that light entering near this location, traveling parallel to the receptor's long axis, is more effective in eliciting a visual response compared with light from the pupil edges, impinging on the receptors under a slight angle. Directional sensitivity has been attributed to the antenna and/or waveguide properties of the receptors,[67–69] and leakage of light out of the receptors at oblique incidence.[3,70] Optical reciprocity states that the emitting and receiving characteristics of an antenna or waveguide are equal. This argument has been used extensively to explain the similarities between the SCE I and the optical SCE. The main discrepancy between the two phenomena is that the psychophysical SCE I distribution is broader compared with the optical SCE one. Gorrand and Delori proposed that some of the modes excited in a photoreceptor waveguide are poorly excited backward.[71] Their model calculations predicted a higher directionality for the optical SCE. Berendschot *et al.* predicted that optical SCE directionality does not depend on wavelength, although evidence for their model curve was limited to data from five subjects, at two wavelengths.[66]

It may seem that the comprehension of the SCE I and the optical SCE in terms of waveguides is fairly complete. However, Marcos *et al.*[22] and Marcos and Burns[23] introduced a new factor. They treated reflectance from the layer of receptor cells as scattering from a rough surface. Each receptor outer segment can be considered a separate source contributing to reflectance in the pupil plane, with a random phase

difference that is due to random differences in outer segment length. The resulting far-field distribution of light in the pupil is again bell-shaped, in particular, a Gaussian. Light scatters preferentially in the direction of the photoreceptor long axes, which explains the alignment with the psychophysical SCE I. To account for the emitting pattern of the cones, one must multiply the scattering distribution with a second Gaussian. The shape factor or directionality of the resultant Gaussian distribution is given by

$$\rho(\lambda) = \rho_{\mathrm{wg}}(\lambda) + \rho_{\mathrm{scatt}}(\lambda), \tag{4.1}$$

where λ is the wavelength, ρ_{wg} is the waveguide component, and ρ_{scatt} is the scattering component.[22, 23] The scattering component was predicted to be proportional to 1 over wavelength squared and should be related to row-to-row spacing s of the cone lattice. With two types of experiment, differently sensitive for the two components, Marcos and Burns managed to separate the waveguide component and the scattering component. This allowed them to test the predicted dependence on wavelength and to estimate cone spacing.[23] Because the technique was quite laborious, experiments were limited to three subjects and two wavelengths.

We recently described an apparatus for simultaneous measurement of spectral and directional reflectance (Chapter 3).[72] In the present paper we used the same database to determine whether the shape factor ρ depends on wavelength. The results allow a firm confirmation of the theory presented by Marcos *et al.*[22] and Marcos and Burns.[23] In addition, we compared resulting data on cone spacing with anatomical values.

4.2 Methods

4.2.1 Instrument, Subjects, and Protocol

The instrument, subjects, and protocol have been described in detail elsewhere (Chapter 3).[72] The essentials are summarized below. The key element of the instrument is an imaging spectrograph with its entrance slit conjugate to the pupil plane. The spectral range of the spectrograph is from 420 to 790 nm. The slit of the spectrograph defines a 0.8×12 mm exit pupil, placed over the dilated pupil of the subject. The coil of a 30 W halogen lamp is relayed to the pupil plane of the eye, defining a 0.8×1.2 mm entrance pupil. The intensity of the light entering the eye is 1.10×10^6 Td. The entrance pupil is placed centered with, and below, the bar-shaped exit pupil. Their separation is 0.7 mm. A 2.8 deg spot centered on the fovea is illuminated. The subject fixates on a central cross wire. The central 1.9 deg of the illuminated spot is sampled. The spectral image is focused on the chip of a cooled CCD camera. The front-lens focus setting provides an estimation of the axial length

of the eye, under the assumption that all ametropia is caused by an error in the axial length of the eye. A chin rest and temple pads connected to a headrest were used to maintain head position.

For calibration purposes, white and dark reference frames were obtained in each session. For each pixel, the counts in the measurement and reference frames were converted into an equivalent percentage reflectance R and an estimate of the error in reflectance. Prior to the calculation of reflectance, the images were binned and interpolated to 5 nm spectral resolution and 0.1 mm spatial resolution. The array of reflectance values can be looked upon as pupil profiles exhibiting cone photoreceptor directionality versus wavelength.

All subjects ($n = 21$) were Caucasian, unfamiliar with any eye disease, and they had no complaints on visual acuity. The majority ($n = 15$, 12 females) fell in the age group of 18–27, mean 22. Six subjects (all male) were aged from 40 to 74. The six older subjects can be considered experienced observers, whereas the younger subjects were all naïve subjects. Fourteen subjects had no refractive correction. For the other cases, refraction was in the range from -1.5 to -4 D, except for two older subjects having -6 and -7 D. The research followed the tenets of the Declaration of Helsinki and was approved by the local Medical Ethics Committee. The purpose was explained at the beginning of the experiment, and written informed consent was obtained.

The pupil of one eye was dilated with one or two drops of tropicamide 0.5%. Subjects were instructed to fixate on a cross wire centered on the illuminated field at all times. The entrance beam was focused in the pupil plane by moving the headrest in the z direction. Fixation and front-lens focus were checked in the retinal image. Thereafter the pupil location in which directional reflectance is maximal (*e.g.*, the maximum of the optical SCE) was searched for. The search typically took approximately 2 min. In this period, 97% of the visual pigments were bleached away.[25] At the optimal entrance position, five spectra were obtained. Integration time was 1.0 s. The procedure described above, apart from dilatation and adjustment of retinal focus, was repeated five times. Settings of the headrest were changed on purpose in between two runs to increase independence.

4.2.2 Analysis of Directionality versus Wavelength

For each 5 nm band in the range from 420 to 780 nm, a pupil profile was independently fitted with

$$R(x) = B + A\ 10^{-\rho(x-x_c)^2}, \tag{4.2}$$

where R is the percentage reflectance, x is the location in the pupil plane in millimeters, B is the nondirectional background, A is the amplitude of the directional reflectance, ρ is a measure for the directionality, and x_c is the center position.[18–20] Parameters B, A, ρ, and x_c were fitted with a least-squares method.[62] Each data point was assigned a weight 1 over its error squared. Data included in the fit met two conditions: distance to either of the pupil edges of more than 1 mm and distance from the entrance beam of less than 3 mm.

The subsequent steps of the analysis concentrated on directionality ρ versus wavelength. The mean ρ of five measurements (within a series) was calculated, which improved the signal-to-noise ratio. Rather than to sift out measurements with irregularities at either extremity of the spectrum, we limited the wavelength to 480–720 nm. The wavelength was further restricted by two criteria: the within-series standard deviation in ρ was less than 0.05 mm^{-2} and the inflexion points of the Gaussian were within the fitted pupil range. The largest united wavelength range, with all data fulfilling both criteria, was selected.

Starting from Ref. 30 in the paper by Marcos *et al.*,[22] an equation for the scattering directionality $\rho_{scatt}(\lambda)$ is derived here. The diffused rough-surface scattering distribution is given by $\exp\{-[\pi T \sin(\theta_M)/\lambda_M]^2\}$, where T is the correlation length of the surface, θ_M is the angle of scattering, and λ_M is the wavelength. The subscript M stresses that these parameters are to be considered inside the eye, within a medium with index of refraction n. The wavelength $\lambda_M = \lambda/n$, where λ is the wavelength in air. The factor n was neglected by Marcos *et al.*[22] and Marcos and Burns.[23] For small angles, $\sin(\theta_M) = (x - x_c)/d_{eye}$, where x is position in the pupil plane, x_c is the center position, and d_{eye} is the axial length of the eye. Parameter T is replaced with $0.4s$, where s is the row-to-row cone spacing. In concordance with earlier research on the SCE, a power of 10 notation instead of an exponential is used. Taking the above terms together, a comparison with Eq. (4.2) reveals that $\rho_{scatt}(\lambda) = (ns/kd_{eye}\lambda)^2$, where $k = [\ln(10)]^{1/2}/(0.4\pi) = 1.20753$, a constant.[23] As a first-order approach, we assumed $\rho_{wg}(\lambda)$ to be independent of λ. This assumption will be justified in Section 4.4.

A least-squares fit of the form

$$\rho(\lambda) = \rho_{wg} + \frac{\alpha}{\lambda^2} \tag{4.3}$$

was made to the data, with free parameters ρ_{wg} and α.[62] Each value of $\rho(\lambda)$ was assigned a weight 1 over the within-series standard deviation squared. Parameter α was converted into cone spacing s with $n = 1.336$.[25] The axial length d_{eye} was calculated from the front-lens focus setting (22.29 mm for an emmetropic eye).[25] A fit was also made to mean ρ versus wavelength for all subjects. In that case the

spectral range was 440–690 nm, and data were weighted with 1 over the between-subjects standard deviation squared.

4.3   Results

Figure 4.1 presents the optical Stiles–Crawford effect directionality ρ versus wavelength for all 21 subjects. Symbols represent the mean ρ of five measurements. Four additional series of five measurements each are not shown. Error bars (not discernible in some cases) indicate the standard deviation. The solid curves depict model fits of Eq. (4.3) to the data. Data of most subjects exhibit a decrease with wavelength, as predicted by the scattering theory. In some subjects, *e.g.*, 7 and 19, systematic deviations between the data and the fit are present, but the weighing of data according to the standard deviation ensured a reduced influence of the outlying points on the model fit. Although not all variation in the data is explained, the model fit is still deemed acceptable. The wavelength range differs between subjects, owing to the application of the two selection criteria described in Section 4.2.

In subjects 9 and 17, directionality does not vary with wavelength or increase with increasing wavelength. In the latter case the parameter α is negative, which impedes taking its square root and hampers the calculation of cone spacing. Subject 9 had great difficulties with fixation on the crosshair, resulting in extreme differences between measurements. Subject 17, aged 74, had a high density of the crystalline lens. Signal-to-noise ratio was low at the shortest wavelengths and floaters were present. Subject 21, aged 57, also suffered from floaters and had large variation between series (data of the other series are not shown), and the selected wavelength range was very small in some series. The data of these subjects were not used for calculating the group mean directionality versus wavelength (Fig. 4.2). Whereas in the analysis of individual series the lower limit was 480 nm, for the group mean data it was possible to reduce the lower limit to 440 nm. Again, as was already seen for most subjects individually in Fig. 4.1, a marked decrease with wavelength as predicted by scattering theory is readily observed. The solid curve represents a model fit of Eq. (4.3). Waveguide directionality ρ_{wg} was 0.085 ± 0.002 mm^{-2} ($\pm$ statistical error). With the axial length of the eye set to the group mean, row-to-row cone spacing s was 3.38 ± 0.57 μm. It should be noted that both ρ_{wg} and s represent a spatial average over our 1.9 deg central foveal field.

The results for waveguide directionality ρ_{wg} and row-to-row cone spacing s for individual subjects are depicted in Figs. 4.3A and 4.3B. Squares represent the mean of five series. Triangles are used in the case that one of the five series was discarded. Crosses, *e.g.*, as for subject 21, indicate all data was discarded. The error
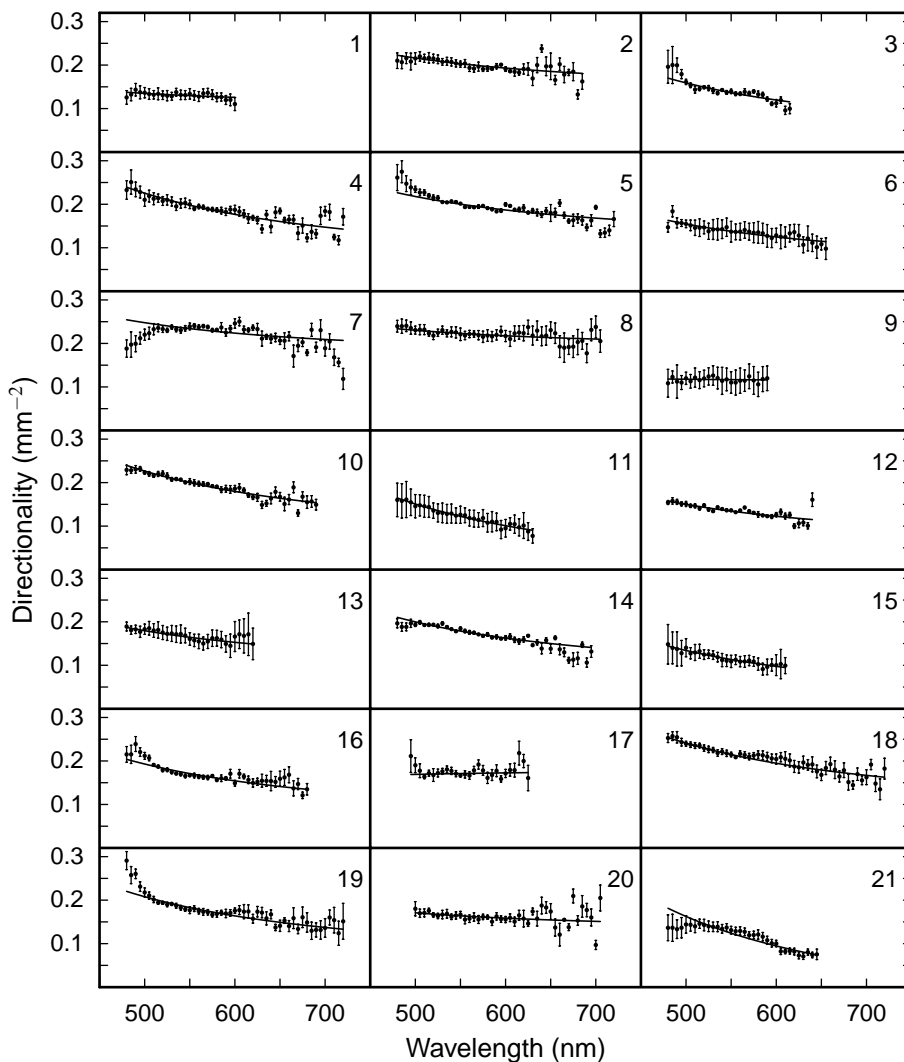
Figure 4.1: Optical Stiles–Crawford effect directionality ρ versus wavelength for all 21 subjects. Data shown are the mean of five measurements within a series. Error bars (not discernable in some cases) indicate the standard deviation. The solid curves represent model fits to the data. Most subjects show the expected decrease with 1 over wavelength squared. The wavelength range varies between subjects owing to selection criteria defined in Section 4.2.
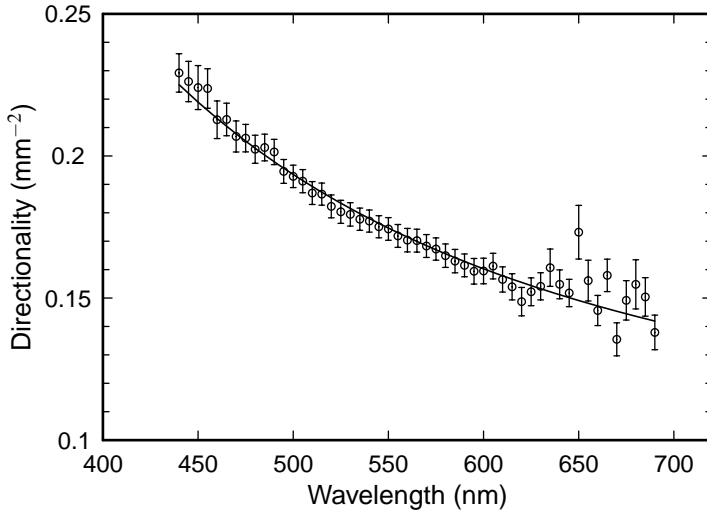
Figure 4.2: Mean optical SCE directionality ρ versus wavelength for all subjects except 9, 17, and 21. The solid curve is a model fit to the data. The decrease with 1 over wavelength squared as predicted by theory is clearly present. Error bars represent the between-subjects standard error.

bars represent between-series standard deviation. The group mean waveguide directionality ρ_{wg} was 0.077 mm^{-2}, and the between-subjects standard deviation was 0.044 mm^{-2}. The group mean row-to-row cone spacing s was 3.42 μm, and the between-subjects standard deviation was 0.67 μm. Again, it should be noted that these data represent a spatial average over our 1.9 deg central foveal field. Each mean value is depicted with solid horizontal lines in Figs. 4.3A and 4.3B. Subjects with five or four valid series were weighted equally.

4.4 Discussion

The dependence of directionality ρ on wavelength, as predicted by the scattering theory by Marcos *et al.*[22] and Marcos and Burns,[23] is clearly present in our data. The results demonstrate that ρ versus wavelength can be described by the sum of waveguide directionality ρ_{wg}, independent of wavelength, and a contribution proportional to 1 over wavelength squared, attributed to scattering. From the latter, row-to-row cone spacing s was calculated. In the original papers by Marcos *et al.*[22] and Marcos and Burns,[23] the model was derived and tested for coherent, monochromatic light.
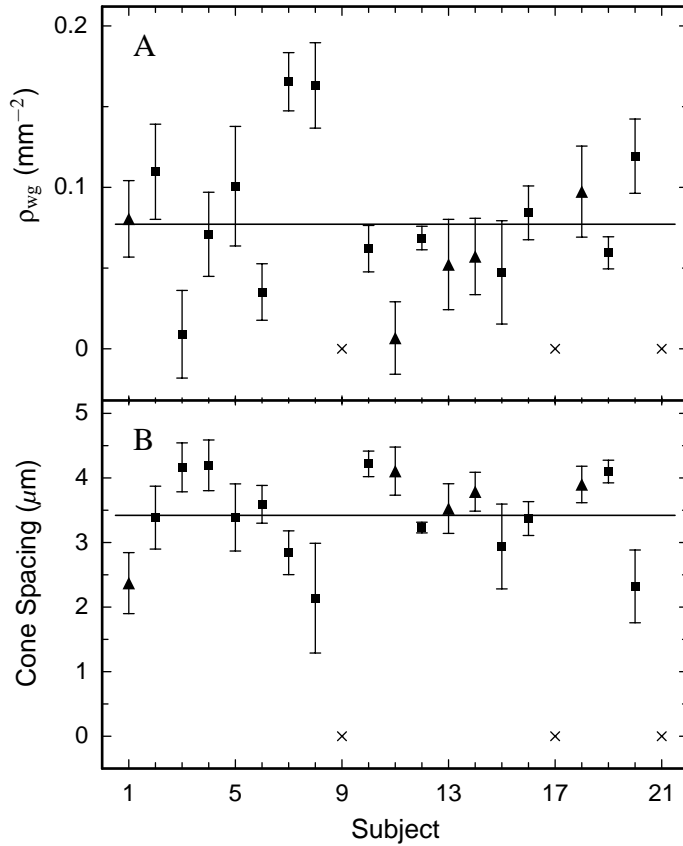
Figure 4.3: Mean waveguide directionality ρ_{wg} and row-to-row cone spacing *s*. Squares depict the mean of five series; triangles, the mean of four series. Error bars represent between-series standard deviation; solid horizontal lines show the group mean. Crosses indicate all data was discarded.

In contrast, the present technique uses incoherent broadband light. The scattering theory predicts that each cone will act as a secondary light source. Given the small size of the cones, they act as coherent sources, independent of the coherency of the illuminating light. In the theoretical calculations, simulated retinal patches with homogeneous cone density were used. The influence of rods was not taken into account. Cone density within our 1.9 deg sampled field is far from homogeneous.[34] Furthermore, the field is larger than the rod-free zone.[34] Although the experimental circumstances are different from the theoretical assumptions, the concordance between the

predicted behavior with wavelength and experimental results indicates the model still holds. Berendschot *et al.*[66] predicted a nearly constant value for $\rho(\lambda)$ with a model by van de Kraats *et al.*[3] The van de Kraats model describes radiation transfer in the eye with a limited number of reflecting, absorbing, and scattering layers. Reflectance from the photoreceptor layer is an essential ingredient, as in Marcos *et al.*'s model.[22] Clearly, photoreceptor reflectance is presently incorrectly modeled. Modification of the van de Kraats model will allow simultaneous description of spectral and directional properties of fundus reflectance.

In our analysis we made some simplifications. First, we neglected the differential absorption of central and marginal rays in the crystalline lens.[73,74] The effect is strongest at wavelengths below 450 nm, where absorption in the lens is high.[75] Nearly all our data for the present analysis are above this wavelength. Second, waveguide directionality ρ_{wg} was assumed to be independent of wavelength. Marcos and Burns[23] measured ρ_{wg} at 543 and 632 nm and found little variation. To our knowledge, no other measurements exist. Berendschot *et al.* made a survey of SCE I directionality versus wavelength and provided a mean curve.[66] It is expected from theory that ρ_{wg} is similar to SCE I directionality. SCE I directionality had a maximum of 0.066 mm^{-2} near 420 nm, dropped to 0.043 mm^{-2} near 550 nm, increased again to 0.054 mm^{-2} around 670 nm, and decreased slightly to 750 nm onward. The variations with wavelength with respect to the mean are in the order of 10–30%. This probably represents an overestimate because the dip observed near 550 nm results from self-screening by the visual pigments.[70] In the present experiment the visual pigments were nearly fully bleached. In view of the variation in the SCE I directionality, the assumption of a constant ρ_{wg} seems right for the present first-order analysis.

We found a group mean waveguide directionality ρ_{wg} of 0.077 mm^{-2} for our 1.9 deg central foveal field. The between-subjects standard deviation was 0.044 mm^{-2}. Analysis of the group mean ρ versus wavelength yielded 0.085 ± 0.002 mm^{-2} ($\pm$ statistical error). For three subjects, with 543 nm light, Marcos and Burns found 0.094 mm^{-2} at the fixation point and 0.100 mm^{-2} at 2 deg eccentricity.[23] They compared their values with the psychophysical ρ obtained in the same three subjects and concluded ρ_{wg} to be systematically higher. Applegate and Lakshminarayanan produced a normative SCE I database.[76] For mean directionality in the horizontal direction, they give 0.047 ± 0.013 mm^{-2}. Although ρ_{wg} is supposed to be more closely linked to the psychophysical estimates of ρ than the total optical SCE ρ, there is no direct quantitative agreement. He *et al.*[21] and Marcos and Burns[23] give an overview of possible causes of disagreement.

We found a group mean row-to-row cone spacing of 3.42 μm for our central foveal field of 1.9 deg. The between-subjects standard deviation was 0.67 μm. Analy-

sis of the mean directionality for all except three subjects gave $3.38 \pm 0.57\,\mu m$ ($\pm$ statistical error). These values come close to most findings in the literature. Anatomical data obtained from excised retinal sections are provided by Curcio *et al.*[34] Assuming a triangular cone lattice, we converted their cone density D to cone spacing s with the relation $s = 3^{1/4}(2D)^{-1/2}$. For conversion of a measure on the retina in micrometers into an angle in degrees, we used $1\,\deg = 291.2\,\mu m$.[25] We further assumed axial symmetry, and data were averaged by area. The mean spacing within a 1.9 deg diameter field was calculated to be $3.33\,\mu m$. Individual data for seven eyes were processed similarly. The between-subject standard deviation for a 1.9 deg field was $0.32\,\mu m$, thus lower than in our data. Perhaps variations in the axial length of the eye not yet accounted for in our simplified model contribute to the variation in cone spacing. In particular, in the emmetropic subjects, differences in axial length were neglected. With an indirect method similar to that applied in the present paper, Marcos and Burns calculated cone spacing in three subjects.[23] They also found their results in agreement with the anatomical data by Curcio *et al.*[34] Williams assessed cone spacing with a psychophysical method based on projecting interference fringes exceeding the cone lattice resolution, which produce visible moiré patterns.[77] From his data we calculated mean cone spacing within a 1.9 deg field as $3.75\,\mu m$. Direct, physical *in vivo* measurements of cone spacing are hampered by the poor optical quality of the eye for large pupil sizes.[78–81] To overcome this problem, Artal and Navarro applied speckle interferometry.[78] The speckle technique was refined by Marcos *et al.*[79] On the basis of their data, we arrived at $s = 4.3\,\mu m$, for a 1.9 deg field. Miller *et al.* obtained conventional high-resolution images after best correction for defocus and astigmatism[80] and obtained values for cone spacing in agreement with Curcio *et al.*[34] and Williams.[77] Liang *et al.* combined a Hartmann–Shack wave-front sensor and a deformable mirror into an adaptive optics system.[81] After correction of the eye's optical aberrations, direct imaging of the cone mosaic was possible. They found for two subjects' cone spacing to be $2.6\,\mu m$ at the foveal center and approximately $3.6\,\mu m$ at 1 deg eccentricity, again values in the same range as discussed in this paragraph.

4.5 Conclusion

The dependence on wavelength of optical SCE directionality as predicted by Marcos *et al.*[22] and Marcos and Burns[23] is clearly present in our data. Both individual as well as the group mean estimates for waveguide directionality ρ_{wg} and row-to-row cone spacing s are in agreement with the literature. The results allow a strong confirmation of Marcos *et al.*'s theory.

Chapter 5

Absorption of the Eye Lens and Macular Pigment Derived from the Reflectance of Cone Photoreceptors

N.P.A. Zagers and D. van Norren

Abstract:
We measured the amplitude of the directional component of the bleached fundus reflectance, the so called optical Stiles–Crawford effect, as a function of wavelength. The directional reflectance originates from within the outer segments of the photoreceptors. Thus, only two anterior absorbers are of importance: macular pigment and the crystalline lens. Analysis of spectra obtained in pseudophakes established that the cone photoreceptors act as spectrally neutral reflectors. The reflectance spectra, expressed in density units, resembled the macular pigment density spectrum. Studying age effects in the lens of normal subjects resulted in a description of the optical density of the lens in terms of a "young" and an "aged" template. The young template represents the pigment 3-HKG, which dominates the light absorption in young eyes and decreases with age. The aged template represents the pigments accumulating in the lens with age. The total optical density increased with age, but it was

lower in the wavelength region 500–650 nm than was previously assumed on base of psychophysical studies. Analysis of the spectra also provided precise individual estimates of the optical density of macular pigment. Finally, we observed a decrease of the photoreceptor reflectivity with age, possibly reflecting a degradation of the photoreceptors.

5.1   Introduction

Light reflected from the fundus exhibits directional and spectral properties (Chapters 3 and 4).[1–5, 15–23, 72, 82] The directional property has become known as the optical Stiles–Crawford effect. In a typical experiment dedicated to reveal this phenomenon, a small spot centered at the fovea is illuminated through a small entrance pupil. The distribution of the reflected light, as measured in the dilated pupil, shows a bell shaped directional component superimposed on a flat background.[19] The maximum reflectance is generally located slightly nasal to the center of the pupil. Van de Kraats *et al.* argued that the flat background represents diffusely reflected and backscattered light.[3] This diffuse component originates from various layers in the fundus, with a major contribution from the choroid.[3] The directional reflectance stems from the highly organized outer segments of the photoreceptors, containing a large number of parallel membranes or disks.[3] Recently, we developed a new instrument based on an imaging spectrograph, capable of measuring both the spectral and directional aspects of fundus reflectance in the wavelength range 420–790 nm (Chapter 3).[72] This enables a separation of the spectra for the diffuse and directional component of fundus reflectance.

In the past decades, several models for the spectral reflectance of the fundus have been published.[1–5] The development of these models was recently reviewed by Berendschot *et al.*[45] One of the major challenges has been to provide a proper description of the diffusely scattered non-directional light. The directional reflectance received much less attention, except in the earlier mentioned model by van de Kraats *et al.*[3] The present paper concentrates on the amplitude of the directional reflectance

from the bleached fovea, as a function of wavelength. With regard to possible reflectors, we assume that the only source of reflectance resides in the outer segments of the photoreceptors.[3] Thus, all the other reflecting layers, *e.g.*, the inner limiting membrane, the retinal pigment epithelium, the choroid, and the sclera, play no significant role. With regard to possible absorbers, in a condition with the photopigments bleached, light is only absorbed in the eye media, mainly the crystalline lens, and in the macular pigment, located predominantly along the axons of the nerve cells in front of the receptors.[29, 30]

To eliminate uncertainty about age effects in the spectral absorption of the crystalline lens, we first studied the spectral behavior of the directional component in pseudophakic subjects. Their implant lenses required only a minor spectral correction. The optical density spectrum of the macular pigment is available from the literature and contains little uncertainty. The pseudophakes' spectra corroborated an assumption in the model of van de Kraats *et al.*,[3] *viz.* that the reflection from the photoreceptors is spectrally flat. With that answer available, we could achieve the second aim of this study, *viz.* an analysis of age effects in the crystalline lens. For that purpose we obtained data on a group of healthy subjects, aged 18 to 64 years. In addition, analysis of the directional reflectance yielded precise values for the macular pigment density. Finally, we studied receptor reflection as a function of age.

5.2 Methods

5.2.1 Instrument

The instrument has been described in detail elsewhere (Chapter 3).[72] A number of essentials are summarized below. The key element of the instrument was an imaging spectrograph with its entrance slit conjugate to the pupil plane. Spectral range of the spectrograph was 420–790 nm. The slit of the spectrograph defined a horizontal 0.8×12 mm exit pupil, placed over the dilated pupil of the subject. The coil of a 30 W halogen lamp was relayed to the pupil plane of the eye, defining a 0.8×1.2 mm entrance pupil. This small entrance pupil was placed centered with, and below the bar shaped exit pupil. Their separation was 0.7 mm. The intensity of the measuring light entering the eye was 1.10×10^6 Troland. A 2.8 deg diameter spot centered at the fovea was illuminated. Ametropia was corrected for with the front lens focus. The subject fixated on a central cross hair. The central 1.9 deg of the illuminated spot was sampled. A chin rest and temple pads connected to a headrest were used to maintain head position. A video channel was available for observation of both retina and pupil.

With the imaging spectrograph, a spectral image of the bar shaped field in the pupil plane was projected on the chip of a cooled CCD camera. For calibration purposes, reference spectral images were obtained from a diffuse reflecting surface painted with Eastman 6080 white paint and a dark black cloth in each session. For each pixel of the CCD, the counts in the measurement and reference spectral images were converted to an equivalent percentage reflectance R, and an estimate of the error in reflectance. Prior to the calculation of reflectance, the images were binned and interpolated to 5 nm spectral and 0.1 mm spatial resolution. The array of reflectance values can be looked upon as the distribution of light within a narrow bar placed over the pupil, versus wavelength.

5.2.2 Protocol

The research followed the tenets of the Declaration of Helsinki and was approved by the local Medical Ethics Committee. The purpose was explained at the beginning of the experiment, and written informed consent was obtained. The first part of the study included five eyes of five subjects with an intra-ocular lens made of poly-methylmethacrylate with bonded UV-absorbers. These pseudophakic subjects were aged 39, 57, 58, 61, and 84 years. The second part of the study included 39 eyes of 39 normal subjects aged 18–64 years; 23 of them were typically young adults, in the age bracket 18–27 years, the other 16 were roughly evenly spread over the 32–64 years age bracket. The pupil of one eye was dilated with one or two drops tropicamide 0.5%. Subjects were instructed to fixate a cross hair centered on the illuminated field at all times. The entrance beam was focused in the pupil plane by moving the headrest back and forth. Fixation and front lens focus were checked in the retinal image. We then searched for the maximum in the directional reflectance (*i.e.*, the maximum of the optical Stiles–Crawford effect) using the measuring field. During the search, continuously directional profiles near 540 nm were read from the CCD. At that wavelength the directionality showed up prominently. In the horizontal direction in the pupil plane (along the spectrograph slit) the maximum position was readily observed in a profile plot on a computer display. The maximum in the vertical direction was found by manual search. While moving the headrest vertically, the actual profile was compared by eye to the highest profile till then. The search procedure took approximately 2 minutes. In this period, visual pigments were bleached away by the measuring light at approximately 97%.[25] At the optimal entrance position 5 spectra were obtained. In the pseudophakic subjects between 3 to 10 spectra were obtained. The integration time was set at 1.0 s.

5.2.3 Separation of the Directional Reflectance

For each 5 nm band in the range 420–650 nm, the 5 measured profiles were independently fitted with

$$R(x) = B + A_{\text{dir}} \; 10^{-\rho(x-x_{\text{c}})^2}, \tag{5.1}$$

with R the fractional reflectance, x the location in the pupil plane in mm, B the non-directional background, A_{dir} the amplitude of the directional reflectance, ρ a measure for the directionality, and x_{c} the center position.[18–20] Parameters B, A_{dir}, ρ, and x_{c} were fitted with a least-squares method.[62] Each data point was assigned a weight 1 over its error squared. Data included in the fit met two conditions: distance to either of the pupil edges more than 1 mm, and distance from the entrance beam less than 3 mm. Because the background rose steeply above 600 nm, it became increasingly difficult to achieve a reliable fit. For this reason, the wavelength range was limited to 650 nm. The subsequent steps of the analysis concentrated on the amplitude A_{dir} versus wavelength. This amplitude, given as a percentage reflectance, was converted to optical density $D_{\text{dir}} = -^{10}\log A_{\text{dir}}$.

Two sources contributed to the error in D_{dir}. The first (σD) resulted from the error in A_{dir}, which was estimated in the fit with Eq. (5.1). The second (σE) was the experimental variation between the five measurements within a series, which was estimated from the standard deviation of D_{dir} at 540 nm. The total error $\sigma_{\text{D−tot}} = (\sigma D^2 + \sigma E^2)^{\frac{1}{2}}$. Data points were rejected when the calculated amplitude was larger than 5% or smaller than zero, or when the error σD was larger than 0.5. These choices were somewhat arbitrary, but guaranteed that a minority of cases, where the fit with Eq. (5.1) failed, was discarded in the next steps of the analysis. After application of these criteria, the mean density within a series was calculated for each subject, which improved the signal to noise ratio. We also produced mean density data representing a typical young and typical aged eye. Among the youngest and oldest subjects, ten subjects having the best signal to noise ratio at the shorter wavelengths were selected. Five measurements were included for each subject. In the young and aged group the mean ages were 20 and 56 years, the standard deviations were 1.3 and 5 years.

5.3 Experiment I: Pseudophakes

5.3.1 Model for the Directional Reflectance

Following van de Kraats *et al.*,[3] we assumed that the directional reflectance originates from a location within the outer segments of the cone photoreceptors. Before reaching the receptor layer, and after being reflected, light is absorbed in the macular

pigment and the ocular media. These considerations led to a model for the amplitude of the directional component:

$$A_{\mathrm{dir}}(\lambda) = R_{\mathrm{recep}}(\lambda)\, 10^{-2[D_{\mathrm{mac}}\alpha_{\mathrm{mac}}(\lambda) + D_{\mathrm{media}}\alpha_{\mathrm{media}}(\lambda)]} \qquad (5.2)$$

with $A_{\mathrm{dir}}(\lambda)$ the amplitude of the directional component versus the wavelength λ in nm, $R_{\mathrm{recep}}(\lambda)$ the reflectance of the photoreceptors, D_{mac} the optical density of macular pigment at 460 nm, $\alpha_{\mathrm{mac}}(\lambda)$ the optical density spectrum of macular pigment normalized to unity at 460 nm, D_{media} the optical density of the eye media at 420 nm, and $\alpha_{\mathrm{media}}(\lambda)$ the optical density spectrum of the eye media normalized to unity at 420 nm. Since the retina was nearly fully bleached by the measuring light, absorption in the visual pigments could be neglected. The macular pigment optical density spectrum has a maximum near 460 nm, so this wavelength was preferred for normalization. The optical density spectrum of the media increases continuously with decreasing wavelength, the normalization wavelength is somewhat arbitrary here.

In van de Kraats *et al.*'s model, reflectance from the stack of disks was postulated to be a spectrally neutral source of reflectance.[3] We based our model fit on this assumption, that is, we too assumed $R_{\mathrm{recep}}(\lambda)$ independent of wavelength. The optical density spectrum of macular pigment was obtained from the equation:

$$
\begin{aligned}
\alpha_{\mathrm{mac}}(\lambda) = f_{\mathrm{norm}}\Big(\;\; & 0.32\exp[-0.0012(436-\lambda)^2] + \\
& 0.32\exp[-0.0012(480-\lambda)^2] - \\
& 0.123\exp[-0.0012(458-\lambda)^2] + \\
& 0.12042\exp[-0.006(457-\lambda)^2] \; \Big),
\end{aligned}
\qquad (5.3)
$$

with λ the wavelength in nm.[85] The above equation was derived by Walraven[85] to represent the macular pigment data in the review by Vos.[83] We incorporated the scalar f_{norm}, set to $1/0.35$, which normalized the equation to unity at 460 nm. In Fig. 5.1A, this macular pigment template is compared with several data sets taken from the literature, all normalized to unit density at 460 nm.[25, 65, 83, 84]

Absorption and scattering losses in the natural eye media, *e.g.*, the cornea,[87–89] the lens capsule,[90] the aqueous humor,[87, 88] and the vitreous humor,[87, 88] were considered negligible in the wavelength region 420–650 nm. The media absorption term in Eq. (5.2) was replaced by a minor correction for absorption in the intra ocular lens. A typical optical density spectrum for an intra ocular lens was taken from an Alcon product information booklet.[86] A small neutral optical density was dropped; the optical density at 650 nm was set to zero. Fig. 5.1B depicts discrete data points for the
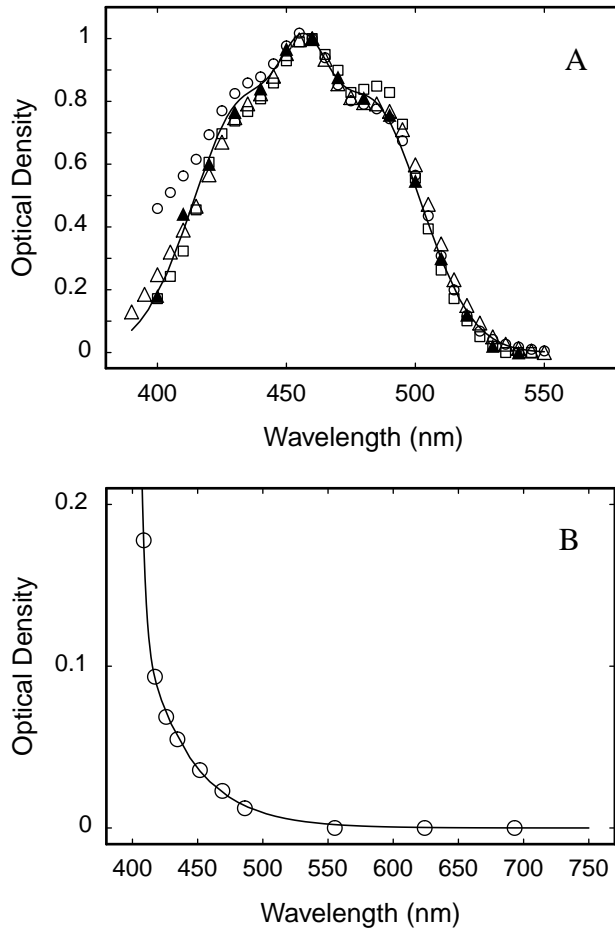
Figure 5.1: (A) Optical density spectra of macular pigment, taken from the literature and normalized to unity at 460 nm. Solid triangles, literature review by Vos[83] (1972); squares, literature review by Wyszecki and Stiles[25] (1982); open triangles, data by Stockman *et al.*[84] (1999); circles, data by Brown, cited by Delori *et al.*[65] (2001). The solid curve was calculated with the template Eq. (5.3) by Walraven.[85] Note that the spectra are not independent, the reviews by Vos and by Wyszecki and Stiles largely rely on the same data. (B) The optical density spectrum of an intra ocular lens adapted from an Alcon product information booklet.[86] The solid curve produced with Eq. (5.4) closely follows the discrete data points.

intra ocular lens density, which could be empirically described (solid curve) by:

$$D_{\mathrm{IOL}}\alpha_{\mathrm{IOL}}(\lambda) = 0.0838\exp\left[-\frac{\lambda - 420}{36.6}\right] + 8.55\exp\left[-\left(\frac{\lambda - 380}{12.9}\right)^2\right]. \qquad (5.4)$$

After insertion of the intra ocular lens absorption term, and by taking minus the logarithm to base 10 on the left and right side of Eq. (5.2), the model becomes a linear combination of three terms:

$$D_{\mathrm{dir}}(\lambda) = C_r + 2D_{\mathrm{mac}}\alpha_{\mathrm{mac}}(\lambda) + 2D_{\mathrm{IOL}}\alpha_{\mathrm{IOL}}(\lambda), \qquad (5.5)$$

with $D_{\mathrm{dir}}(\lambda)$ the optical density equivalent of the amplitude $A_{\mathrm{dir}}(\lambda)$, C_r a measure for the spectrally neutral reflection of light by the photoreceptors, and D_{mac}, $\alpha_{\mathrm{mac}}(\lambda)$, and $D_{\mathrm{IOL}}\alpha_{\mathrm{IOL}}(\lambda)$ as defined above. This model, with only two free parameters C_r and D_{mac}, was fitted to the density data with a least-squares method.[62] Each value $D_{\mathrm{dir}}(\lambda)$ was assigned a weight 1 over its total error.

5.3.2 Results

The upper part of the panels A-E in Fig. 5.2 depicts the amplitude of the directional reflectance converted to a density, versus wavelength for the five pseudophakic subjects. The solid curves depict model fits of Eq. (5.5) to the data. In the upper part of Fig. 5.2F the mean of the five subjects' data is given. The solid curve is a model fit with Eq. (5.5) to this mean data. All density spectra reflect the shape of the macular pigment density spectrum. Above 540 nm the data suggest no variation with wavelength. The mean single pass optical density of the macular pigment was 0.52. The spectrally neutral reflectance of the cone layer can be read from the average long wavelength value 2.5, which converts to $R_{\mathrm{recep}} = 10^{-2.5}$, corresponding to 0.32%. At the bottom of each panel in Fig. 5.2 the differences between the data and the model fit are shown. In general, the model provides a good fit to the data and validates the assumption that the reflectance of the receptors is spectrally neutral.

5.4 Experiment II: Normal Subjects

5.4.1 Model with Pokorny *et al.*'s Lens Templates Applied to Young and Aged Group

When making the transition from the pseudophakes' model to a model for normal eyes, absorption in the natural crystalline lens is introduced as a new element. We adopted, in a first try, Pokorny *et al.*'s model for the optical density of the lens as a
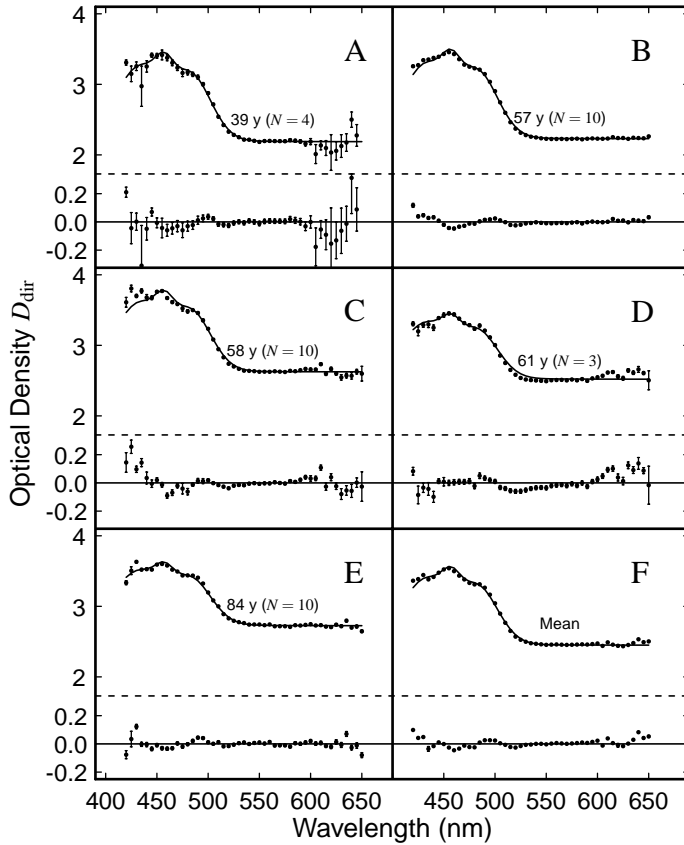
Figure 5.2: (A-E) Top: The amplitude of the directional reflectance converted to a density $D_{\text{dir}}(\lambda)$, for the pseudophakic subjects. The symbols represent the mean density. Error bars indicate the total errors in the mean. The subjects' ages and the number of averaged spectra are indicated. The solid curves depict model fits of Eq. (5.5) to the data. Bottom: The differences with the fit at an enhanced scale. (F) The same results for the mean of the five subjects' data. All the six spectra reflect the optical density spectrum of macular pigment, *c.f.*, Fig. 5.1A.

function of age.[64] This model describes lens absorption in terms of a template with a
fixed density of 0.30 at 420 nm ($\alpha_{\text{lens}-\text{na}}$), and a template with a density affected by
aging ($\alpha_{\text{lens}-\text{a}}$). The model becomes a linear combination of four terms:

$$D_{\text{dir}}(\lambda) = C_r + 2D_{\text{mac}}\alpha_{\text{mac}}(\lambda) + 2D_{\text{lens}-\text{a}}\alpha_{\text{lens}-\text{a}}(\lambda) + 2\,0.30\,\alpha_{\text{lens}-\text{na}}(\lambda), \quad (5.6)$$

with $D_{\text{dir}}(\lambda)$, C_r, D_{mac}, and $\alpha_{\text{mac}}(\lambda)$ as defined above, $D_{\text{lens}-\text{a}}$ and 0.30 the optical
densities of the two lens components at 420 nm, and $\alpha_{\text{lens}-\text{a}}$ and $\alpha_{\text{lens}-\text{na}}$ the lens
optical density spectra normalized to unity at 420 nm. The optical density spectra
$\alpha_{\text{lens}-\text{a}}$ and $\alpha_{\text{lens}-\text{na}}$ were derived from the templates $T_{\text{L}_1}(\lambda)$ and $T_{\text{L}_2}(\lambda)$ as given in
Pokorny *et al.*'s Table I, page 1439.[64] In the model fit implementation, $D_{\text{lens}-\text{a}}$ was
rewritten as $10^{\delta_{\text{lens}-\text{a}}}$, which ensured that $D_{\text{lens}-\text{a}}$ remained positive. We applied the
model on the mean data for the young and aged eyes (*c.f.*, Methods). These mean data
sets had a high signal to noise ratio, which facilitated a thorough test of the model.

5.4.2   Comparison of the Model with the Young and Aged Group Data

Figure 5.3A shows the mean density D_{dir} versus wavelength for the young (bottom
spectrum, mean age 20 years) and aged group (top spectrum, mean age 56 years).
The symbols represent the mean of in total 50 measurements, 5 for each of the 10
subjects in both groups. The data were not shifted vertically; the optical density in
aged eyes is larger at longer wavelengths as well. In contrast to the pseudophakes'
spectra in Fig. 5.2, the normal subjects' spectra in Fig. 5.3 steeply rise below 450 nm.
The imprint of macular pigment absorption on the density spectra is apparent: both

Table 5.1: Model fit parameters and their statistical errors estimated from the fit.

	Pokorny *et al.*'s model		New templates	
Mean, young	D_{mac}	0.443 ± 0.015	D_{mac}	0.465 ± 0.004
	R_{recep} (%)	1.04 ± 0.02	R_{recep} (%)	0.970 ± 0.005
	$D_{\text{lens}-\text{na}}$	0.30 (fixed)	D_{young}	0.31 ± 0.02
	$D_{\text{lens}-\text{a}}$	0.11 ± 0.02	D_{aged}	0.11 ± 0.02
Mean, aged	D_{mac}	0.54 ± 0.03	D_{mac}	0.560 ± 0.009
	R_{recep} (%)	0.58 ± 0.02	R_{recep} (%)	0.485 ± 0.003
	$D_{\text{lens}-\text{na}}$	0.30 (fixed)	D_{young}	negligible
	$D_{\text{lens}-\text{a}}$	0.24 ± 0.04	D_{aged}	0.501 ± 0.011
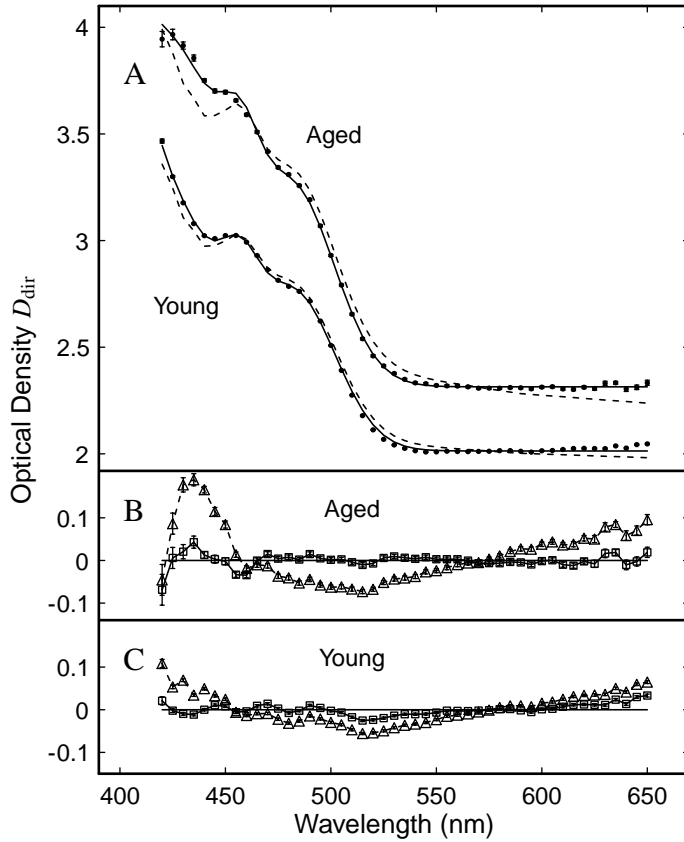
Figure 5.3: (A) The mean optical density $D_{\text{dir}}(\lambda)$ for 10 young and 10 aged subjects. The error bars, not discernable in most cases, indicate the total errors in the mean. The data were not shifted vertically; the optical density in aged eyes is larger at longer wavelengths as well. The rise in optical density from 450 to 420 nm is due to absorption in the crystalline lens. The dashed curves depict the best fit with the Pokorny *et al.*[64] lens aging model. The solid curves represent the simultaneous fit of Eq. (5.8) to both data sets in order to derive two new templates for the absorption in the lens. (B, C) The differences between the mean aged and young data and the model fit based on the Pokorny et al.[64] lens aging model (triangles) and the model based on Eq. (5.8) (squares). The new templates improved the fit to the data.

spectra show the absorption edge below 520 nm and a slight local maximum near 460 nm.

The dashed curves in Fig. 5.3A represent the best fits with the model Eq. (5.6). Table 5.1 gives values for the model parameters. The dashed model curve shown in comparison with the top data set in Fig. 5.3A clearly has a slope in the wavelength region 540–650 nm, while the data suggests no variation with wavelength within this range. The triangles in Figs. 5.3B and C illustrate the differences between the mean aged and mean young data and the model fits. Small, but systematic differences between the data and the model based on Pokorny *et al.*'s lens templates are present, in particular for the mean aged data. The discrepancies warranted a search for an improvement of the model.

5.4.3   Derivation of New Templates

The age-related increase in light absorption by the eye lens has been extensively discussed in the literature.[64, 96, 97] The biochemical processes causing this change are probably complex. However, two main physiological aspects have been identified. In young lenses, absorption is dominated by the pigment O-β-glucoside of 3-hydroxykynurenine, or 3-HKG (some authors use 3-OHKG).[40, 92, 98–101] The optical density spectrum of 3-HKG presents an absorption band near 365 nm, with a tail up to 450 nm.[40, 91–93] With age, the amount of 3-HKG in the lens decreases.[92, 99–101] Nevertheless, there is a net increase in lens absorption, because other light absorbing pigments accumulate in the lens.[40, 92, 102] These pigments, probably proteins, have a maximum absorption at 320 nm and show a shallow tail extending considerably further in the visible wavelength range than 3-HKG.[40, 92] As a result of the concomitant decrease in 3-HKG and the accumulation of the other pigments, the absorption maximum shifts from 365 to 320 nm, and a shallow tail shows up in the visible wavelength region.[40]

In view of the physiological considerations described above, and in line with Pokorny *et al.*'s model,[64] we aimed at optimizing the shape of two spectral templates. The contribution of both templates was allowed to vary with age. For the first template we propose to use the optical density spectrum of 3-HKG. We coin this the "young" template. Figure 5.4A depicts several spectra taken from the literature, normalized to unity at 370 nm.[40, 91–95] The solid curve in Fig. 5.4A represents a model fit with a single Gaussian in the wavelength range 350–450 nm to the recent 3-HKG spectrum by Heckathorn *et al.*[93] The model fit represents their data well, but also comes close to Pokorny *et al.*'s choice for the non-aging component.[64] The latter was multiplied by a scalar to fit the 3-HKG data at 400 nm. The Gaussian curve, after
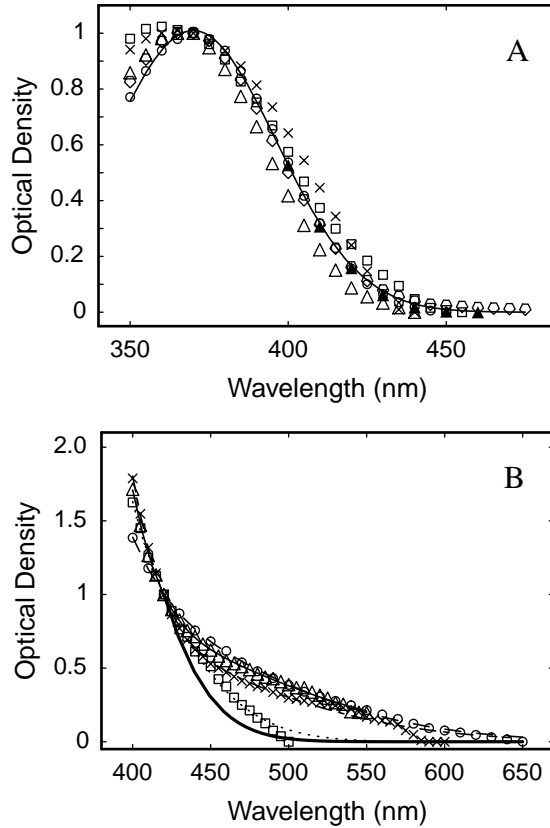
Figure 5.4: (A) The optical density of 3-HKG, normalized to unity at 370 nm; crosses, Dillon *et al.*[91] (1984); squares, Dillon *et al.*[92] (1990); circles, Heckathorn *et al.*[93] (2001). The diamonds represent the spectrum of 3-hydroxy-kynurenine (3-HK) by Stutchbury *et al.*[94] (1993), which is similar to the 3-HKG spectra. Dillon *et al.*'s (1990) spectrum[92] was first reported representing 3-HK, but in 1991 Dillon presented the same data as a 3-HKG spectrum.[95] The spectrum of the eye of a young monkey (triangles) by Gaillard *et al.*[40] (2000) is similar to the 3-HK and 3-HKG spectra. The solid curve depicts a single Gaussian fitted to Heckathorn *et al.*'s 3-HKG data.[93] The solid triangles represent Pokorny *et al.*'s non aging template.[64] It has the same shape as the 3-HKG spectra. (B) Various suggested optical density spectra for the pigments accumulating with age, normalized to unity at 420 nm; squares, Dillon *et al.*[92] (1990); crosses, Dillon *et al.*[39] (1999), triangles, Gaillard *et al.*[40] (2000). The circles depict the Pokorny *et al.*[64] template affected by aging. The curves drawn through the above data sets represent a fit with the tail of a single, or the sum of two Gaussians centered at 320 nm. The thick solid curve depicts the newly proposed aged template Eq. (5.9).

normalization to unity at 420 nm, was taken as the young template:

$$\alpha_{\text{young}}(\lambda) = 6.09 \exp\left[-\left(\frac{\lambda - 370}{37.2}\right)^2\right]. \tag{5.7}$$

As to the second lens absorption template the literature is divided. Three spectra of the pigments accumulating with age, as well as Pokorny *et al.*'s template for the component affected by aging are depicted in Fig. 5.4B.[39,40,64,92] Making a choice for a particular curve was difficult. First, there were large differences between the three sources. Second, all three were obtained from excised material. Third, the spectra were obtained with a light source containing UV and blue light, but were not corrected for fluorescence in the lens. Finally, the spectra were corrected for scattered light by fitting the data in the wavelength range 600–700 nm with a power law. This correction was then extrapolated to shorter wavelengths and subtracted from the data. An error in this correction is expected when it is extrapolated down to 400 nm.

Because a spectrum for the pigments accumulating with age was not readily available, we derived a new template, which we will refer to as the "aged" template. First, we sought a mathematical function suitable for representation of the aged template in the model fit. There is consensus in the literature that the lens spectrum gradually rises with decreasing wavelength, asymptotically approaches a constant value at longer wavelengths, and has little or no fine structure. A priori, the tail of a Gaussian seemed appropriate for describing the lens spectra. To assure that this choice does not pose too large a limitation on the outcome of the aged template, we first tested our assumptions on the literature data in Fig. 5.4B. It proved possible to fit the three spectra as well as Pokorny *et al.*'s template for the component affected by aging with a single, or with the sum of two Gaussians. The resulting model curves are drawn through the data in Fig. 5.4B. Since the pigments accumulating with age have an absorption maximum at 320 nm (not shown here), we fixed the center position of the Gaussians to this value.[40] Dillon *et al.*'s data[92] (1990) do not show the tail at longer wavelengths; they could be fitted well with a single Gaussian.

In the second step, we used the same mathematical model to derive the aged template from the mean aged and young group data. With the young template known, and with a single Gaussian at 320 nm, Eq. (5.6) transforms to:

$$\begin{aligned} D_{\text{dir}}(\lambda) \;=\; & C_r + 2D_{\text{mac}}\alpha_{\text{mac}}(\lambda) + 2D_{\text{young}}\alpha_{\text{young}}(\lambda) + \\ & 2D_{\text{aged}} \exp\left[\left(\frac{320 - 420}{\Delta}\right)^2\right] \exp\left[-\left(\frac{\lambda - 320}{\Delta}\right)^2\right], \end{aligned} \tag{5.8}$$

with $D_{\text{dir}}(\lambda)$, C_r, D_{mac}, and $\alpha_{\text{mac}}(\lambda)$ as defined earlier, D_{young} and D_{aged} the optical density of the young and aged component at 420 nm, $\alpha_{\text{young}}(\lambda)$ the young template

given by Eq. (5.7), and the expression following D_{aged} a single Gaussian with a free width Δ, representing the aged template. The first exponential serves to normalize the aged template to unity at 420 nm. In the model fit implementation, D_{young} and D_{aged} were rewritten as $10^{\delta_{\text{young}}}$ and $10^{\delta_{\text{aged}}}$, which ensured that D_{young} and D_{aged} remained positive. The model, with free parameters C_r, D_{mac}, δ_{young}, δ_{aged}, and Δ was simultaneously fitted to the mean young and aged data with a least-squares method.[62] Parameters C_r, D_{mac}, δ_{young}, and δ_{aged} were optimized for each group separately. The width of the aged template Δ was optimized as well, but kept equal for the young and aged group.

The solid curves in Fig. 5.3A represent the model fit with Eq. (5.8). The model fit parameters are given in Table 5.1. We also evaluated a model fit with the sum of two Gaussians at 320 nm, but found no improvement. The aged template is characterized by the parameter Δ, which was 76.0 ± 2.4 nm. Normalized to unity at 420 nm, it is given by:

$$\alpha_{\text{aged}}(\lambda) = 5.65 \exp\left[-\left(\frac{\lambda - 320}{76.0}\right)^2\right]. \tag{5.9}$$

It is shown in Fig. 5.4B as a thick solid curve. It runs an even steeper course than Dillon *et al.*'s (1990) data.[92] The differences between the mean $D_{\text{dir}}(\lambda)$ data and the model, plotted as squares in Figs. 5.3B and C, have diminished to the order of 0.02 density units in almost the full wavelength range.

5.4.4 Model with New Templates Applied to Individual Data

The final model is arrived at after insertion of the two new templates in Eq. (5.6):

$$D_{\text{dir}}(\lambda) = C_r + 2D_{\text{mac}}\alpha_{\text{mac}}(\lambda) + 2D_{\text{young}}\alpha_{\text{young}}(\lambda) + 2D_{\text{aged}}\alpha_{\text{aged}}(\lambda), \tag{5.10}$$

with $D_{\text{dir}}(\lambda)$, C_r, D_{mac}, and $\alpha_{\text{mac}}(\lambda)$ as defined before, the templates $\alpha_{\text{young}}(\lambda)$ and $\alpha_{\text{aged}}(\lambda)$ given by Eqs. (5.7) and (5.9), and D_{young} and D_{aged} the optical densities of the two lens components at 420 nm. The model Eq. (5.10) was fitted to the data for individuals with a least-squares method.[62] The lens densities D_{young} and D_{aged} were rewritten as $10^{\delta_{\text{young}}}$ and $10^{\delta_{\text{aged}}}$. Free parameters were C_r, D_{mac}, δ_{young}, and δ_{aged}.

The upper parts of the panels in Fig. 5.5 depict the amplitude of the directional reflectance, converted to a density, versus wavelength for a sample of six normal subjects spanning the full age range. The solid curves depict model fits of Eq. (5.10) to the data. At the bottom of each panel in Fig. 5.5 the differences between the data and the model fit are shown at an enhanced scale. Generally a good fit of the model to the data was obtained. Figure 5.6 shows the density of the young component, the aged component, and the total lens density versus age at 420 nm. The solid curves
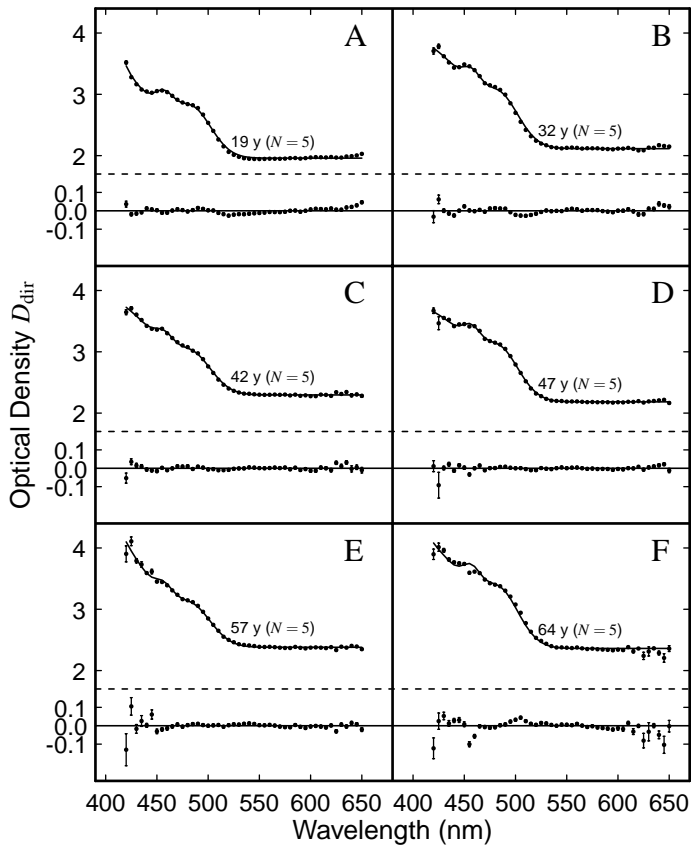
Figure 5.5: (A-F) Top: The amplitude of the directional fundus reflectance, converted to a density, versus wavelength for a sample of six normal subjects spanning the full age range. The symbols represent the mean density within a series of five measurements. Error bars indicate the total errors in the mean. Ages are indicated above each spectrum. The solid curves depict model fits of Eq. (5.10) to the data. Compared with Fig. 5.2, the spectra steeply rise below 450 nm. The additional optical density is caused by absorption in the crystalline lens. Bottom: The differences between the data and the model fit.
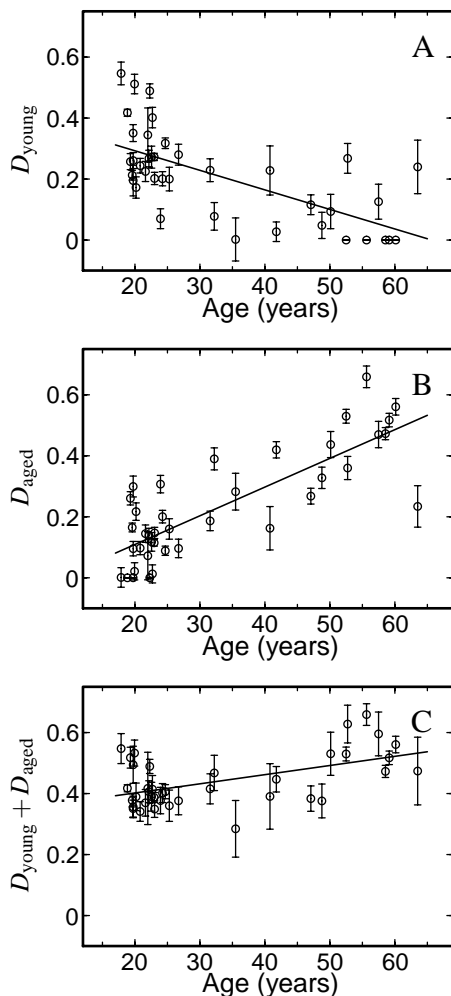
Figure 5.6: (A) The density of the young and (B) the aged components, and (C) the total lens density versus age at 420 nm. The error bars indicate the statistical error estimated in the model fits. The solid curves depict linear regression lines, their parameters are given in Table 5.2. The density of the young component decreased with age. The density of the aged component strongly increased with age. The total optical density of the lens slightly increased with age.
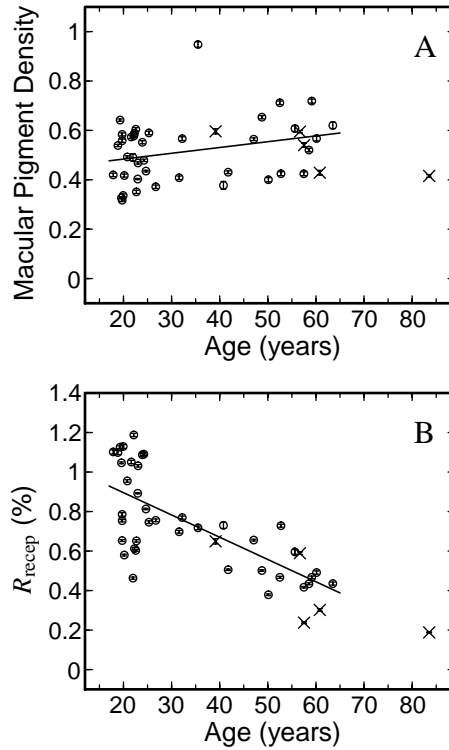
Figure 5.7: (A) Macular pigment density and (B) the reflectivity of the receptors versus age. The circles represent individual estimates for the 39 normal subjects; the crosses depict data obtained in the pseudophakes. The error bars are smaller than the symbols in most cases. The solid curves depicts a linear regression to the normal subjects' data, parameters are given in Table 5.2. The receptor reflectance strongly decreased with age.

represent linear regression lines. Parameters for the regression analysis are given in Table 5.2.

The density of the young component D_{young} (Fig. 5.6A), representing 3-HKG, decreased with age. In some of the oldest subjects D_{young} reached zero. The density of the aged component D_{aged} (Fig. 5.6B), representing the pigments accumulating with age, strongly increased with age. In some of the young subjects, it was absent. As a result of the two concomitant changes, the total lens density at 420 nm (Fig. 5.6C)

Table 5.2: Parameters derived from linear regression with age.

	Intercept	Slope $(10^{-3}\ \text{year}^{-1})$	R	P
D_{young}	0.42 ± 0.04	-6.4 ± 1.2	-0.66	< 0.001
D_{aged}	-0.08 ± 0.04	9.4 ± 1.1	0.81	< 0.001
$D_{\text{young}} + D_{\text{aged}}$	0.34 ± 0.03	3.0 ± 0.8	0.53	< 0.001
D_{mac}	0.44 ± 0.05	2.3 ± 1.3	0.28	0.09
R_{recep} (%)	1.12 ± 0.07	-11 ± 2	-0.70	< 0.001

slightly increased with age. The total optical density of the eye media as a function of age can be described with a combination of the regression models given in Table 5.2, and the two known templates:

$$D_{\text{media}}(\lambda, A) = (0.42 - 0.0064\,A)\alpha_{\text{young}}(\lambda) + (-0.08 + 0.0094\,A)\alpha_{\text{aged}}(\lambda), \quad (5.11)$$

with $D_{\text{media}}(\lambda, A)$ the total optical density, A the age in years, and $\alpha_{\text{young}}(\lambda)$ and $\alpha_{\text{aged}}(\lambda)$ given by Eqs. (5.7) and (5.9).

The model fit also provided individual estimates of the optical density of the macular pigment and the reflectivity of the photoreceptors. Figures 5.7A and B depict both parameters versus age. The circles represent the data for the thirty-nine normal subjects. The crosses represent the data obtained in the five pseudophakic subjects in Section 5.3. The solid curves represent linear regressions to the normal subjects' data. Parameters for the regression analysis are also given in Table 5.2. Macular pigment (Fig. 5.7A) showed no significant change with age ($P = 0.09$). The mean macular pigment optical density was 0.51. The between subjects standard deviation was 0.13. In the normal subjects, the reflectance of the photoreceptors (Fig. 5.7B) strongly decreased with age. The reflectance ranged from 1.19% to 0.38%. The reflectance of the photoreceptors in the pseudophakes did not show any sign to deviate from the downward trend.

5.5 Discussion

We measured spectra for the amplitude of the directional component of fundus reflectance. This type of spectral reflection could be described with a simple model. The single reflecting layer resides in the outer segments of the photoreceptors, and light is only absorbed in the crystalline lens and in the macular pigment. Model analysis of the pseudophakes' spectra validated the assumption that the source of directional reflectance is spectrally neutral. The second part of the study concentrated on

the age changes in the absorption of the lens. We first tested Pokorny *et al.*'s model for absorption in the crystalline lens.[64] We found small but significant differences between their model and our mean data for young and aged observers. Therefore, we derived a new lens aging model. Similar to Pokorny *et al.*'s model,[64] it comprises a combination of two templates: a "young" template representing 3-HKG, and an "aged" template representing the pigments accumulating in the lens with age. A new element is that the young component decreased with age; the old component increased with age. Both changes are reported in the literature.[40, 92, 99–101] In addition, we observed a hitherto unreported decrease of the photoreceptor reflectivity with age.

5.5.1   Directional Reflection From the Layer of Cone Photoreceptors

An important assumption throughout this paper was that the source of the directional reflectance resides in or near the photoreceptor layer, as was proposed before by van de Kraats *et al.*[3] Gorrand and Delori suggested that the retinal pigment epithelium also plays a role.[71] The tips of the outer segments of the photoreceptors are intertwined with the microvilli of the retinal pigment epithelium cells. This alternative assumption would lead to practically the same model for the directional reflectance. Burns *et al.* measured the distribution of the fluorescence in lipofuscin in the pupil plane and found no directionality. This indicates that recapture of light from behind the receptors does not play a major role.[103] The pseudophakes' spectra (Fig. 5.2) closely resembled the shape of the macular pigment optical density spectrum. This indicates that the source of directional reflectance lies behind the nerve fiber layer. Because no other retinal absorbers, *e.g.*, no melanin or blood, were required to explain the data, reflectance from the choroid can be excluded. This pinpoints the source of directional reflectance to the anterior layers of the retinal pigment epithelium, the receptor layer, or a combination of both.

None of the spectra (Figs. 5.2, 5.3, and 5.5) varied strongly with wavelength above 540 nm. There are no pigments in front of the receptors absorbing in this wavelength range. Below 540 nm absorption by the macular pigment and the eye media come into play. But, because the model satisfactorily described the data, the assumption that the directional reflectance is spectrally neutral below 540 nm as well seems tenable. This is in line with a model calculation of the electrodynamics of a receptor cell by Piket-May *et al.*[104] They demonstrated that the waveguide properties of the bleached photoreceptors are independent of wavelength. Experimentally this is corroborated by the fact that the spectral sensitivity of the photoreceptors does not deviate from the spectral absorption of their visual pigments.[25] In a previous paper we analyzed the directionality, a measure for the peakedness of the distribution in the

pupil plane, versus wavelength (Chapter 4).[82] It was found that the waveguide directionality of the cone photoreceptors, to first order, is independent of wavelength, in line with Piket-May *et al.*'s results.[104] Recently, assessment of the waveguide properties of single photoreceptor cells became possible *in vivo*.[105] It would be worthwhile to examine the amplitude of the reflectance and its directionality of individual cells as a function of wavelength.

5.5.2   Lens Aging, Objective, *in vivo*

Objective, *in vivo* assessment of light absorption in the lens requires a source of reflectance in the eye with known properties. Johnson *et al.*[106] and Savage *et al.*,[107] following a method originally devised by Said and Weale,[108] measured the amount of light reflected at the back of the lens (the fourth Purkinje image). Van Norren and Tiemeijer,[1] Delori and Burns,[109] van de Kraats *et al.*,[3] and Zagers *et al.*[72] (Chapter 3) relied on a model analysis of light reflected from the retina. Xu *et al.* followed a similar approach using the spectral reflectance of the optic disk.[110] Thus far the spectral reflectance models could only be made more or less compatible with experimental data by assuming, without really understanding, diffusely scattered light. Our analysis, with its split up in a directional and non-directional component, removes this difficulty. Assessment of the directional component as a function of wavelength provides a unique method for studying light absorption in the living eye lens. Unfortunately, the lens is an inhomogeneous structure and the central and marginal path lengths are different.[41] In the present experiments the entrance beam was confined to a small region near the center of the pupil, but the exit beam typically spanned 5–6 mm of the pupil. As a result, the lens optical density represents an average over the pupil with most weight placed on the region centered with the maximum of the optical Stiles–Crawford effect. Several authors have proposed corrections for the differences in path length of central and marginal rays.[41, 73, 111] It is not straightforward to implement these corrections, because the maximum of the optical Stiles–Crawford effect and the center of the lens in general do not coincide. The former has a unique location in different individuals. Furthermore, the shape of the lens is not uniquely determined and a purely geometrical correction would not do justice to the inhomogeneous distribution of the absorbing pigments in the lens. Therefore, we have neglected this second order correction.

Analysis of the spectra of the normal subjects provided individual estimates for the optical density of the pigment 3-HKG and the pigments accumulating with age. Many authors have suggested that these or two similar components are the main factors determining lens absorption,[40, 64, 92, 96, 112–114] yet a quantitative analysis with use
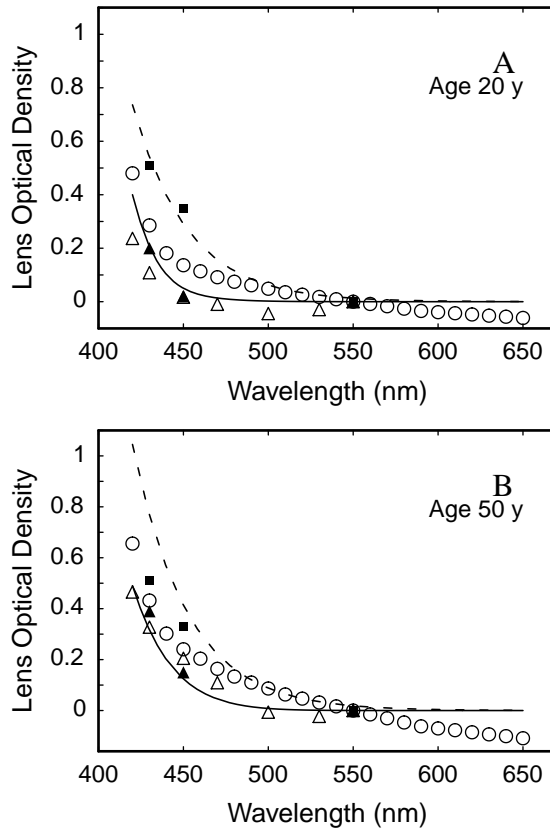
Figure 5.8: Comparison of lens optical density spectra for (A) observers aged approximately 20 years and (B) observers aged approximately 50 years. The solid curves represent the present model calculated with Eq. (5.11). Data obtained with the Purkinje image method: open triangles, Johnson *et al.*[106] (1993), age groups 21–30 and 41–50 years; solid triangles, Savage *et al.*[107] (2001), for observers with an average age of 24 and 50 years. Psychophysical data: circles, Pokorny[64] *et al.*'s (1987) model; dashed curves, Savage[97] *et al.*'s (1993) model; solid squares, Savage *et al.*[107] (2001), in the same observers with an average age of 24 and 50 years that provided the objective data represented by the solid triangles.

of the known 3-HKG absorption spectrum was, to our knowledge, never published. The decrease of the young component (Fig. 5.6A), the aged component (Fig. 5.6B), and the increase of the total lens density at 420 nm with age (Fig. 5.6C) have been reported.[40, 64, 92, 96, 97, 99–101] The absence of 3-HKG in some of the oldest lenses is also in agreement with earlier findings.[101] The aged component also reached zero, but not

surprisingly only in some of the youngest subjects. In a previously published study on the spectral reflectance of the fovea (Chapter 3),[72] we applied Porkorny *et al.*'s model[64] for assessment of lens density, and found zero density for the component affected by aging in some of the youngest subjects. In addition, van den Berg and Felius fitted the optical density of excised lenses with the Porkorny *et al.* model[64] and found zero density for the component affected by aging in some of the youngest specimens.[114] In contrast, the Porkorny *et al.* model[64] predicts a considerable contribution of the component affected by aging, even in the age range 20–30 years.

The total lens density at 420 nm (Fig. 5.6C) only slightly increased with age. The two underlying processes compete and the increase of the aged component just overcompensates the decrease of the young component. The increase of the total optical density at 420 nm with age was obscured by the large variation between subjects of comparable age. This large spread within age groups was encountered in previous studies on large groups of subjects as well.[75,97,107,109,115,116] As in our data, it was regularly observed that the highest densities at age 20 are as high as the lowest at age 60.[97,107,115,116] Gaillard *et al.* suggested that the spectral changes in the lens are the result of chemical or photochemical modifications, not biological aging.[40] The environment, in particular the light history, poses different levels of chemical or photochemical stress to an individual. Thus, age might be a poor determinant for the changes in the lens.

In Figs. 5.8A and B the solid curves, predicted with Eq. (5.11) for subjects aged 20 and 50 years, are compared with data from the literature. Johnson *et al.*'s data is depicted by the open triangles.[106] They represent the mean optical density in the age groups 21–30 and 41–50 years. Savage *et al.* (2001) provided data for a group of subjects with mean age 24 and 50 years (solid triangles).[107] We conclude that there is good agreement between our data and the results derived with the objective Purkinje image method. Both data sets show no changes with age above 540 nm.

5.5.3 Lens Aging, Psychophysics

The curves in Fig. 5.8 for the total lens density can also be compared with psychophysical data. The circles in Figs. 5.8A and B were calculated with Pokorny *et al.*'s lens aging model for a 20 and 50 year old observer.[64] The data were shifted vertically to normalize the optical density to zero at 550 nm. The dashed curves were calculated with Savage *et al.*'s (1993) psychophysical model for observers aged 20 and 50 years.[97] The solid squares represent psychophysical data obtained by Savage *et al.* (2001) in the same observers of average age 24 and 50 years that provided the objective data (solid triangles).[107] The psychophysical data exhibit systematically

higher optical densities for wavelengths below 550 nm than the objective data. Savage *et al.* (2001) discussed this difference and suggested that an additional absorbing pigment is located in front of the peripheral receptors.[107] More extensive research with both types of measurement in the same set of subjects would be helpful to clarify this interesting phenomenon.

Pokorny *et al.*'s model predicts age-related changes at wavelengths as high as 640 nm.[64] As stated before, our data suggests no variation with age above 540 nm. For the discussion of the differences between the present results and the Pokorny *et al.* model, it is of interest to review the fundaments of the latter.[64] One of the starting points was the compromise curve in the first edition of the book "*Color Science*" by Wyszecki and Stiles (1967).[117] For wavelengths above 420 nm, this curve was mainly based on donor eyes obtained by Ludvigh and McCarthy[118] ($n = 4$) and Weale[119] ($n = 2$; ages 48 and 53 years). Ludvigh and McCarthy measured four complete eyes with an average age of 62 years.[118] They also measured the lenses of these eyes separately, as well as 5 lenses with an average age of 21.5 years. From this data, they calculated the transmission of a whole eye, as if it had contained a young lens. One of the lenses used by Weale had been invaded by a melanoma, and in both lenses a control experiment clearly demonstrated postmortem effects.[119] Two decades later, van Norren and Vos reviewed the literature available at that time and compared it with the Wyszecki and Stiles compromise curve.[75] They concluded that this curve was adequate for the visual region, but too low for the ultraviolet. Also, they derived a new ocular density curve from the CIE scotopic sensitivity function and the absorption curve of human rhodopsin. Below 430 nm, the new curve followed the literature data more closely. Above 430 nm, the Wyszecki and Stiles compromise curve was maintained. On their turn, in the second edition of "*Color Science*", Wyszecki and Stiles (1982) referred to van Norren and Vos and concluded that an update of the compromise curve from the first edition was not required.[25] Pokorny *et al.* took Wyszecki and Stiles' (1982) curve as the starting point for their lens aging model.[64] Analysis of the color matching data for subjects aged 16–55 years published by Stiles and Burch[120] yielded the spectral shape of the partition of lens optical density affected by aging L_1 and a fixed residual component L_2.[64] The fixed component reached zero at 460 nm. From our analysis of the cited literature sources, it can be concluded that Pokorny *et al.*'s total optical density T_L in the visible wavelength range relates to only six donor eyes. As a consequence, for wavelengths above 460 nm, the shape of the aging component also relates to the same six donor eyes. In our view, this provides a rather weak experimental basis for the model in the visible wavelength region in particular at the longest wavelengths. This might at least partly explain why we have found a considerably higher transmission in the wavelength region 500–650 nm.

5.5.4 Macular Pigment

The model analysis of the normal subjects' spectra also yielded values for the optical density of the macular pigment. The mean macular pigment optical density in the normal subjects was 0.51, well within the range of values reported in earlier studies (Chapter 3).[2,3,72] Previously, macular pigment was found to be constant with age,[121–124] or to show a minor decline with age.[125,126] In agreement with these findings, no significant trend with age was found. It must be noted that the macular pigment optical densities represented an average by area over the sampled field, in our case 1.9 deg. The macular pigment distribution is highly concentrated toward the center of the fovea. This is a complicating factor when comparing different methods for assessment of macular pigment. Delori *et al.* discussed other difficulties involved when comparing different techniques.[65] As was stated before, isolation of the directional component removed many of the difficulties normally encountered in assessment of macular pigment by means of fundus reflectometry.

5.5.5 Reflectance of the Photoreceptors

The reflectivity of the receptors (Fig. 5.7B) strongly decreased with age. From the model Eq. (5.2) it can be inferred that this cannot be distinguished from an increase in spectrally neutral light losses in the eye media. The observed loss in reflectivity between age 20 and 60 years corresponds to the accumulation of a single path optical density of 0.14 density units. Psychophysical studies found forward-scattered light to be independent from wavelength.[127,128] When scattered outside the measurement field this scattered light is lost for detection. However, for our 1.9 deg field, the scatter losses seem too small to explain the entire neutral component. Van den Berg and IJspeert measured on average only 0.09 density units absorption at 700 nm in donor lenses, with the major part of them having cataract.[129] In a similar study on normal lenses aged 59 ± 20 years, van den Berg and Felius found 0.04 ± 0.04 density units at 700 nm.[114] In view of this low value, an increase of a spectrally neutral absorbing pigment is considered an unlikely explanation of the density increase.

The number of cones in the fovea is stable with age,[130] but the disks in the outer segments undergo a gradual but major disruption.[131] This phenomenon is the most probable cause of the loss of reflectivity with age. To our knowledge, the present data represent the first observation of this kind *in vivo*.

Chapter 6

Spectral and Directional Reflectance of the Fovea in Diabetes Mellitus

N.P.A. Zagers, M.C.A. Pot, and D. van Norren

Submitted

Abstract:
Aim: To assess the integrity of the photoreceptors in the fovea, and to measure the optical density of the macular pigment and the eye lens in patients with diabetes mellitus, and to compare the results with those of a group of healthy subjects. **Methods:** The directional and spectral properties of the light reflected from a 1.9 deg field centered on the fovea were measured simultaneously, in a single one second flash, with the Foveal Reflection Analyzer. The directional characteristics, i.e., the optical Stiles-Crawford effect, provided information on the integrity of the foveal photoreceptors. Model analysis of the spectral reflectance yielded optical densities of the macular pigment and the lens. **Results:** The amplitude of the directional reflectance in diabetic eyes was significantly lower compared to controls ($P < 0.001$). Surprisingly, the directionality (a measure for the peakedness) was similar in diabetics and controls ($P = 0.3$). The density of macular pigment was not different from that in controls

($P = 0.3$). The optical density of the lens increased with age in both groups, but the rate of increase was larger in the diabetics. ($P < 0.05$). **Conclusion:** The integrity of the photoreceptors in the fovea was altered in diabetics. Possibly, the lens optical density increasing at a higher rate with age reflects changes preceding cataract formation.

6.1   Introduction

Diabetes mellitus is one of the largest threats to health in the western world,[132] and its incidence is expected to rise.[132, 133] The main characteristic of the disease is an elevated blood glucose level.[134, 135] Many if not all patients develop visual complaints. Major complications are the development of diabetic retinopathy and cataract.[136] Diabetes causes vascular changes in the retina. These changes play an important role in the development of the retinopathy, and can be divided in two opposing effects: Capillary dilatation, which causes edema, and capillary occlusion, leading to ischemia.[137] The amount of retinal edema is to be monitored closely after first detection. Common methods for assessment of retinal edema are fluorescein angiography, stereo fundus photography, and optical coherence tomography.[137, 138] These methods are suitable for mapping the posterior pole and they facilitate general diagnoses.

Detecting retinal edema specifically in the macula, where it is most threatening to visual acuity, asks for dedicated techniques. Additional tests on the structural integrity of the foveal region could be useful for diagnosis and prognosis. DeLint *et al.* compared results on visual pigment density and the optical Stiles–Crawford effect and concluded that both provide information on the integrity of the cone photoreceptors in the fovea.[6] Lardenoye *et al.* observed reduced visual pigment density and a decrease in the directionality of the optical Stiles–Crawford effect in eyes with macular edema.[7] It must be noted that the etiology of the edema was not always diabetes, but also uveitis. Furthermore, the authors compared patient eyes with and without edema. Direct comparison of the optical Stiles–Crawford effect in diabetic versus healthy eyes is still lacking.

Retinopathy and the associated occurrence of retinal edema as discussed above are well known phenomena. Davies and Morland recently reported a hitherto unknown retinal abnormality in diabetes, *viz.* reduced levels of macular pigment.[139] The pigment is a collection of the carotenoids lutein and zeaxanthin,[8] and absorbs blue light with a peak absorption at 460 nm.[25] It is located along the axons in the

center of the fovea, in front of the receptors, and as such acts as a preretinal filter for blue light.[29,30] Several authors have suggested that macular pigment reduces the risk for age-related macular degeneration.[9–11] For the macular pigment being reduced in diabetes, Davies and Moreland discussed three possible causes.[139] First, the difference could result from a genetic influence, but this was considered unlikely. Second, diabetics might have a lower dietary intake of lutein and zeaxanthin, or a lower absorption in the gut. And third, as preferred by the authors, the reduction could point to a change in either the rate of deposition or removal of lutein and zeaxanthin in or from the retina. In that case, understanding of the deficit might be valuable in a broader context, *i.e.*, in relation to age-related macular degeneration.

Diabetes also affects the anterior segment of the eye; it is a well known risk factor for cataract.[140] During the phase preceding the appearance of cataract, which may take years, diabetic lenses are already abnormal in various aspects.[141] One property, the transmission of light, can be inferred from the ratio of the autofluorescence in the posterior and anterior part of the lens.[142–145] Zeimer *et al.* and Mosier *et al.* found no significant difference between diabetic eyes and healthy controls.[142,145] Van Best *et al.* observed a strong decrease in lens transmission of healthy subjects above the age of about 50 years.[143] In a second paper, for a subgroup with duration of diabetics longer than 10 years, the steep decrease in transmission occurred about 15 years earlier.[144] While two of the three of the autofluorescence studies did not report significant differences, two psychophysical studies have demonstrated a lower transmission at 420 nm in diabetes compared with age matched subjects.[139,146] The autofluorescence method yields a transmission at approximately 500 nm. Possibly the transmission changes are limited to lower wavelengths and were not noticed.

In the present paper we tested three hypotheses in a group of diabetic patients: first, that photoreceptor integrity is affected, second, that macular pigment is reduced, and third, that the optical density of the lens is increased compared with age matched subjects. The patients were of both type I and II, diabetes duration was on average 19 years, and almost all patients showed signs of retinal pathology. In most studies, the retina and anterior segment are studied separately. Our study of such differing hypotheses was facilitated by a recently developed instrument: the Foveal Reflection Analyzer (Chapter 3).[72] This apparatus is capable of simultaneous assessment of the spectral and directional properties of the light reflected from the retina. Model analysis of spectral reflectance provides optical densities of photo stable ocular absorbers such as the lens and macular pigment (Chapter 3).[2,3,72] The directional characteristics exhibit the optical Stiles–Crawford effect (Chapter 3),[16–20,72] which contains information on the integrity of foveal cones.[6,7] The investigated properties of diabetic eyes were obtained in single snap shot measurements.

Table 6.1: Clinical data for the 14 diabetic eyes. [*]Age, gender, type of diabetes, duration of the disease and visual acuity were obtained from the medical record. [†]The presence of edema, small hard exudates, and ischemia in the measurement region (− absent, + present) was assessed from a fluorescein angiography and red-free and color photographs, obtained immediately after our investigations. [‡]Availability or absence of the early phase (EP) recording (+/−). Without an early phase recording, the state of ischemia is uncertain. Three patients' profiles and spectra are depicted with triangles[§], squares[¶], and crosses[#] in Figs. 6.1 and 6.2.

Age[*] (years)	Gender[*]	Type[*]	Duration[*] (years)	Acuity[*]	Edema[†]	Exudates[†]	Ischemia[†]	EP[‡]
23	M	I	19	1.0	−	−	−	−
31	F	I	25	1.0	−	−	−	−
34	F	I	23	1.0	+	−	−	+
42[§]	M	I	21	1.0	+	−	−	+
42	M	I	13	1.0	−	−	−	+
43	F	II	6	1.0	−	−	−	+
44[¶]	M	II	21	0.63	+	−	+	+
52	M	?	?	0.32	+	−	+	+
53	M	II	?	0.6	+	−	−	+
53	M	II	14	0.63	+	+	−	−
55	M	I	20	0.5	+	+	−	+
56	M	II	15	0.8	+	−	−	−
58[#]	F	I	27	0.4	−	−	−	+
61	M	I	28	0.8	+	−	−	−

6.2 Methods

6.2.1 Subjects

The research followed the tenets of the Declaration of Helsinki and was approved by the local Medical Ethics Committee. Before testing, all subjects gave written informed consent after the nature and possible consequences of the study were explained. Diabetic patients were recruited randomly from all the patients who had an appointment for a fluorescein angiography consult in our clinic. Exclusion criteria based on the medical record were age above 65 years, correction outside the range −5 D to +3.5 D, cataract, visual acuity less than 0.2, large hard exudates within the

fovea, intra ocular lens implant, having other ocular or systemic diseases, or a history of allergic reactions on fluorescein. In total 14 eyes of 14 subjects were included; an overview of the clinical data is given in Table 6.1. In general, the right eye was selected. In a single case the left eye was measured. The patients' ages, rounded to the nearest integer, ranged from 23 to 61 years, mean 46 years, with a standard deviation of 11 years. Both type I and II diabetics were included. Duration of the disease ranged from 6 to 28 years, mean 19 years, with a standard deviation of 6 years. Visual acuity as obtained with a letter projection system was taken from the medical record and can only serve as a rough indication. The presence of edema, hard exudates and ischemia in the measurement region was assessed by an ophthalmologist of our clinic from fluorescein angiography recordings, and red-free and color photographs. Table 6.1 also indicates whether an early phase (EP) recording was obtained for the included eye. The assessment of ischemia is hampered without an early phase recording. The control group consisted of 14 eyes of 14 age matched healthy subjects, without a history of eye disease and no complaints on visual acuity. They were aged 23 to 60 years, mean 47 years, with a standard deviation of 11 years.

6.2.2 Instrument

The instrument has been described in detail elsewhere (Chapter 3).[72] A number of essentials are summarized below. The key element of the instrument was an imaging spectrograph with its entrance slit conjugate to the pupil plane. Spectral range of the spectrograph was 420–790 nm. The slit of the spectrograph defined a horizontal 0.8×12 mm exit pupil, placed over the dilated pupil of the subject. The coil of a 30 W halogen lamp was relayed to the pupil plane of the eye, defining a 0.8×1.2 mm entrance pupil. This small entrance pupil was placed centered with, and below the horizontal bar shaped exit pupil. Their separation was 0.7 mm. The intensity of the measuring light entering the eye was 1.10×10^6 Troland. A 2.8 deg diameter spot centered on the fovea was illuminated. Ametropia was corrected for with the front lens focus. The subject fixated on a central cross hair. The central 1.9 deg of the illuminated spot was sampled. A chin rest and temple pads connected to a headrest were used to maintain head position. A video channel was available for observation of both retina and pupil.

With the imaging spectrograph, a spectral image of the bar shaped field in the pupil plane was projected on the chip of a cooled CCD camera. For calibration purposes, reference spectral images were obtained from a diffuse reflecting surface painted with Eastman 6080 white paint and a dark black cloth in each session. For each pixel of the CCD, the counts in the measurement and reference spectral images

were converted to an equivalent percentage reflectance R, and an estimate of the error in reflectance. Prior to the calculation of reflectance, the images were binned and interpolated to 5 nm spectral and 0.1 mm spatial resolution. The array of reflectance values can be looked upon as the distribution of light within a narrow bar placed over the pupil, versus wavelength.

6.2.3   Protocol

The pupil of one eye in the controls was dilated with one or two drops tropicamide 0.5%. In the patients, for the purpose of the fluorescein angiography assessment following immediately after our investigations, the pupils of both eyes were dilated with tropicamide 0.5% and phenylephrine 5%. Both drops were administered a second time after ten minutes. Subjects were aligned with the instrument and instructed to fixate the cross wire at all times. The entrance beam was focused in the pupil plane by moving the headrest back and forth. Fixation and front lens focus were checked in the retinal image. We then searched for the maximum in the directional reflectance (*i.e.*, the maximum of the Stiles–Crawford effect) using the measuring field. During the search, continuously directional profiles near 540 nm were read from the CCD. At that wavelength the directionality showed up prominently. In the horizontal direction in the pupil plane (along the spectrograph slit) the maximum position was readily observed in a profile plot on a computer display. The maximum in the vertical direction was found by manual search. While moving the headrest vertically, the actual profile was compared by eye to the highest profile till then. The search procedure took approximately 2 minutes. In this period, visual pigments were bleached away by the measuring light at approximately 97%.[25] At the optimal entrance position 5 spectra were obtained. In some of the patients it was impossible to observe a directional component in the reflectance. In that case, the measurements were obtained near the center of the pupil. Integration time was set at 1.0 s. All patients underwent fluorescein angiography as part of their regular treatment immediately after our measurements. Before injection of the fluorescein, red-free and color photographs were obtained.

6.2.4   Data Analysis

The array of reflectance values obtained from the spectrograph can be looked upon as pupil profiles exhibiting the directional reflectance (*i.e.*, the optical Stiles–Crawford effect) versus wavelength (Chapter 3).[72] Only the profile at 540 nm was used. The array can also be interpreted as spectra versus location along the bar shaped exit pupil. We selected a single spectrum, at the location where the 540 nm profile

had a maximum. In cases where no such maximum was present, the spectrum was obtained at the center of the pupil.

The spectra were fitted with the van de Kraats *et al.* fundus reflectance model using a least-squares method.[3,62] Each data point was assigned a weight 1 over its error squared. Spectral data at wavelengths above 750 nm was discarded because the signal to noise ratio in this region was too low (Chapter 3).[72] The fundus reflectance model describes radiation transfer in the eye with a limited number of reflecting, absorbing, and scattering layers. Spectral properties of the absorbers are taken from the literature. Eight parameters were optimized: reflectance from disks in the outer segments of the photoreceptors, at the inner limiting membrane, and at the cornea, the optical densities of melanin, macular pigment, and the aging component of the lens, the thickness of the blood layer, and a parameter accounting for scattering in the choroid. The parameter accounting for reflectance of the cornea was added to the model. Visual pigment density was assumed zero, Stiles–Crawford parameter SC was set at unity. The non-aging component of the optical density of the lens at 420 nm was fixed at 0.31. Values for other fixed parameters and a detailed description of the model are given in the original paper.[3] The optical density of the lens is given at 420 nm and the optical density of macular pigment at 460 nm.[3]

In healthy subjects, the reflectance versus location in the pupil plane can be described as a bell-shaped peak on top of a constant background (Chapter 3).[72] Usually, two sharp drops at about 4 mm nasal and temporal are present, corresponding to the edge of the dilated iris. With pathology, the bell-shaped peak may disappear, leaving a block shaped profile. For both patients and controls, the distribution of reflectance versus location in the pupil plane was fitted with:

$$R(x) = B\Big(\exp[-\exp[-r_1(x-x_{\mathrm{L}})]] + \exp[-\exp[r_2(x-x_{\mathrm{R}})]]\Big) + A10^{-\rho(x-x_{\mathrm{c}})^2}, \quad (6.1)$$

where R is the percentage reflectance, x is the location in the pupil plane in mm, B is the non-directional background reflectance, A is the amplitude of the directional reflectance, ρ is a measure for the peakedness, x_{c} is the center position, x_{L} and x_{R} are the location of the left and right edge, and r_1 and r_2 are a measure for the steepness of the drop at the edges of the profile. The fitted data included a few points at level zero left and right to the pupil edges. As can be inferred from the equation, the left and right edge are modeled in terms of a growth curve from zero to $B/2$. All profiles were fitted with Eq. (6.1) using a least-squares method, with all data points assigned equal weights.[62]

The observed amplitudes A and B are reduced due to absorption in the lens. The non-aging component of lens absorption is zero at 540 nm, and can be neglected.[64] The same is true for macular pigment.[25] A correction for light losses due to the aging
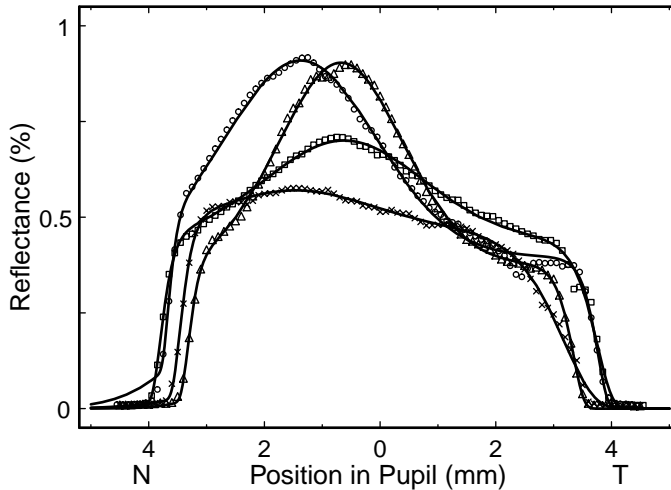
Figure 6.1: Percentage reflectance at 540 nm versus location in the pupil plane for three diabetic patients (triangles, squares, and crosses) and one healthy subject (circles). Nasal (N) and temporal (T) side are indicated. The solid lines represent model fits to the data with Eq. (6.1). The drop in amplitude of the directional reflectance in two of the patients (squares and crosses) indicates that the integrity of the photoreceptors was altered.

component of the lens absorption was obtained from a model fit to the accompanying spectra. The corrected amplitude is given by:

$$A' = A10^{fD_{lens-a}}, \tag{6.2}$$

where A is the amplitude of the directional reflectance as found in the original fit, D_{lens-a} is the aging component of the lens density, and $f = 0.247$, the ratio of lens aging density at 540 nm to 420 nm.[64] The same relation holds for B' and B. Directionality and the maximum position are far less altered by absorption in the ocular media, although in theory the shape of the profile might be altered, even at 540 nm.[41,73] We neglected these minor differences.

6.3   Results

Four examples of a pupil profile exhibiting the directional reflectance from the fovea, *i.e.*, the optical Stiles–Crawford effect, are shown in Fig. 6.1. The symbols depict the amount of reflected light versus location along a horizontal bar in the pupil. The edges of the dilated pupil can be recognized as the sharp drops at about 4 mm nasal
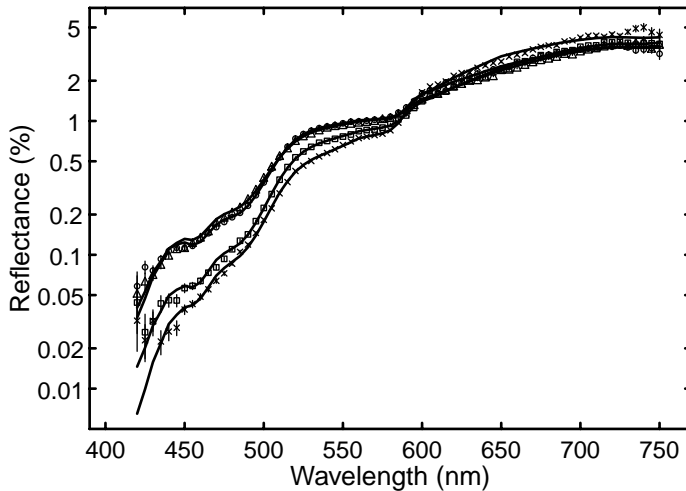
Figure 6.2: Spectral reflectance for the same subjects as in Fig. 6.1, three diabetic patients (triangles, squares, and crosses) and one healthy subject (circles). The solid curves are fits to the data with van de Kraats *et al.*'s model.[3] Vertical lines (not discernable in most cases) indicate measurement errors. A low reflectance at the shortest wavelengths is indicative of a high optical density of the lens. For two patients (squares and crosses) reflectance was reduced between 540 and 580 nm, in accordance with their lowered directional reflectance at 540 nm (*c.f.*, Fig. 6.1). The absorption edge of macular pigment near 520 nm was clearly present in all the spectra.

and temporal. The solid curves are model fits with Eq. (6.1). The circles represent data obtained from a healthy male control, aged 42 years. Reflectance showed a prominent maximum 1.4 mm nasal of the pupil center. The triangles represent a male type I diabetic subject, aged 42 years. Duration of his diabetic condition was 21 years and visual acuity was 1.0. Fluorescein angiography and fundus photography revealed macular edema, no ischemia in the fovea, and no hard exudates in or near the fovea. The pupil profile had a normal shape. The squares represent a male type II diabetic subject, aged 44 years. Duration of his diabetic condition was 21 years, visual acuity was 0.63. He had macular edema and ischemia in the fovea, but no hard exudates. The directional component of the reflectance was clearly reduced in amplitude. A female type I diabetic subject aged 58 presents a more extreme example (crosses). Duration of her diabetic condition was 27 years and visual acuity was 0.4. No edema or exudates were present in or near the fovea, there was no ischemia in the fovea.

Four reflectance spectra, for the same subjects as in Fig. 6.1, are shown in Fig. 6.2. Reflectance at the lowest wavelengths was substantially lower for two diabetic subjects (squares and crosses), indicative of absorption in the lens being higher.[3] Note
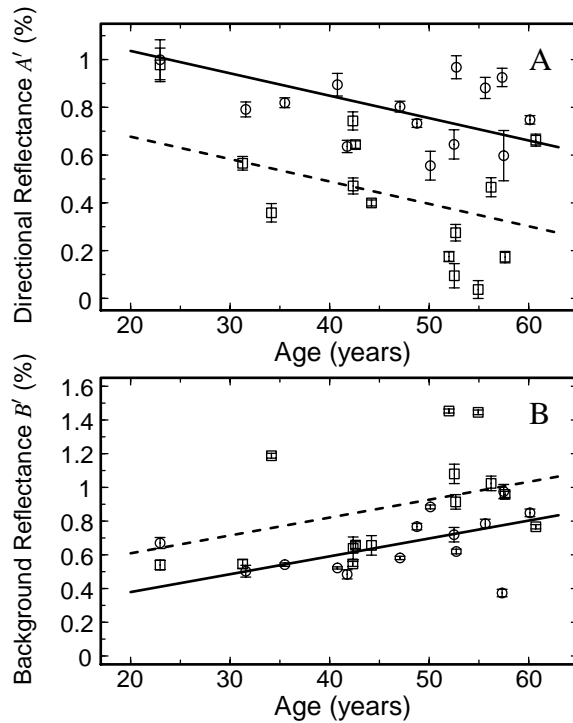
Figure 6.3: (A) The amplitudes of the directional component A' and (B) the diffuse background B' corrected for absorption in the lens versus age in normal subjects (circles) and patients (squares). Symbols depict the mean of five measurements. Error bars indicate the standard deviation within a series of five measurements. The directional component decreased with age and was reduced in the diabetics group. The diffuse component increased with age and was higher in the diabetics group.

that the first diabetic subject (squares) and the control subject (circles) were of similar age. Absorption by the macular pigment caused a decline from 520 nm towards lower wavelengths.[3] The absorption edge was clearly present in all four subjects. Between 540 and 580 nm a plateau was present. The level of reflectance in this wavelength region is a measure for reflectance of the photoreceptors.[3] As expected, the plateau was reduced for the subjects with a decreased directional reflectance (squares and crosses).

Photoreceptor integrity was assessed from the profiles as were shown in Fig. 6.1.

The corrected amplitudes A' and B' for the directional reflectance and the non-directional background reflectance are plotted versus age in Figs. 6.3A and B for the diabetics (squares) and controls (circles). Differences between the two groups were assessed with univariate analysis of variance with age as a covariate. The directional reflectance A' (Fig. 6.3A), adjusted for absorption in the lens with Eq. (6.2), decreased with $(9.4 \pm 3.4) \times 10^{-3}$ percentage reflection year^{-1} ($P = 0.01$, regression parameters are presented as mean $\pm$ standard error). There was no significant difference in the slope for diabetics and controls ($P = 0.1$). The directional reflectance was lowered by 0.36 percentage reflection in the diabetics ($P < 0.001$). The non-directional background reflectance B' (Fig. 6.3B), also adjusted for absorption in the lens, increased with $(11 \pm 4) \times 10^{-3}$ percentage reflection year^{-1} ($P < 0.05$). There was no significant difference in the slope for diabetics and controls ($P = 0.3$). The background reflectance was 0.23 percentage reflection higher in the diabetics ($P < 0.05$).

Figures 6.4A and B depict the directionality ρ and the position of the maximum of the directional reflectance x_c versus age for the diabetics (squares) and controls (circles). The results of two diabetic eyes for ρ were discarded, because they had virtually no directional component and ρ could not be assessed with reasonable accuracy. Again, univariate analysis of variance with age was applied. Directionality (Fig. 6.4A) did not change with age ($P = 0.4$). For the diabetics mean ρ was 0.15 ± 0.07 mm^{-2}, in the controls it was 0.17 ± 0.04 mm^{-2}, which was not significantly different ($P = 0.3$, population means are given $\pm$ the standard deviation). The position of the maximum (Fig. 6.4B) did not change with age ($P = 0.6$). The mean position was 0.56 ± 0.89 mm nasal in the diabetics and 0.95 ± 0.56 mm nasal in the controls. The mean position of the maximum and its standard deviation were not significantly different in the two groups ($P = 0.2$, Levine's test for equality of variances: $P = 0.2$).

Analysis of the spectra as in Fig. 6.2 with van de Kraats *et al.*'s fundus reflectance model[3] provided, among other parameters, the optical density of the macular pigment at 460 nm and the aging component of the optical density of the lens at 420 nm. Both parameters are plotted versus age in Figs. 6.5A and B for the diabetics (squares) and controls (circles). Again, univariate analysis of variance with age was applied. Macular pigment (Fig. 6.5A) did not change with age ($P = 0.6$). For the diabetics mean macular pigment was 0.38 ± 0.17, in the controls it was 0.44 ± 0.14. This 14% reduction was not significantly different ($P = 0.3$). The optical density of the lens (Fig. 6.5B) in the controls increased with $(7.5 \pm 2.5) \times 10^{-3}$ year^{-1} ($P < 0.01$). In the diabetics there was an additional increase of $(7.8 \pm 3.5) \times 10^{-3}$ year^{-1} ($P < 0.05$). When corrected for age, the lens density in both groups was not significantly different ($P = 0.5$).
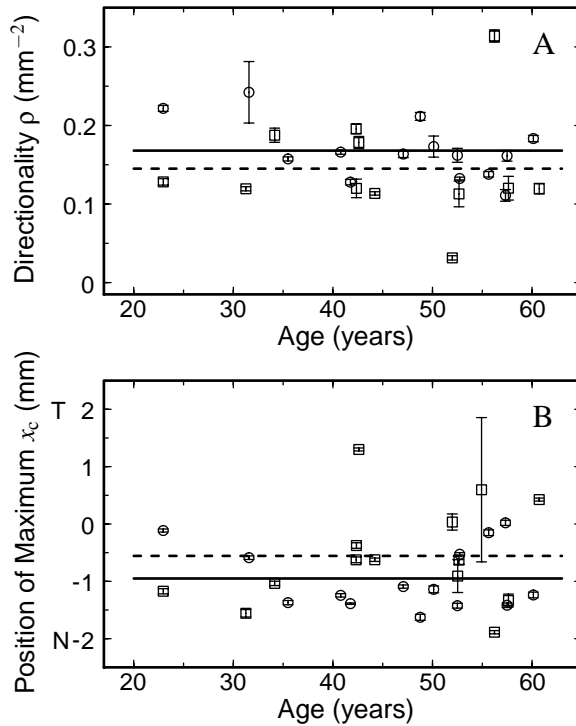
Figure 6.4: (A) The directionality of the directional component ρ and (B) the position of the maximum reflectance x_c for normal subjects (circles) and patients (squares). Nasal (N) and temporal (T) side are indicated. Symbols depict the mean of five measurements. Error bars indicate the standard deviation within a series of five measurements. Both the directionality and the maximum position were similar in normal and diabetic eyes.

6.4 Discussion

The strong reduction of the amplitude of the directional reflection in the diabetics group indicates changes in the integrity of the foveal cone-photoreceptors. Surprisingly, the directionality of the cones was not reduced. Macular pigment was not significantly lower in diabetics. Lens density increased at a substantially higher rate in diabetics, compared with the normal age-related increase in the controls.

The amplitude of the directional component A' in the controls decreased with
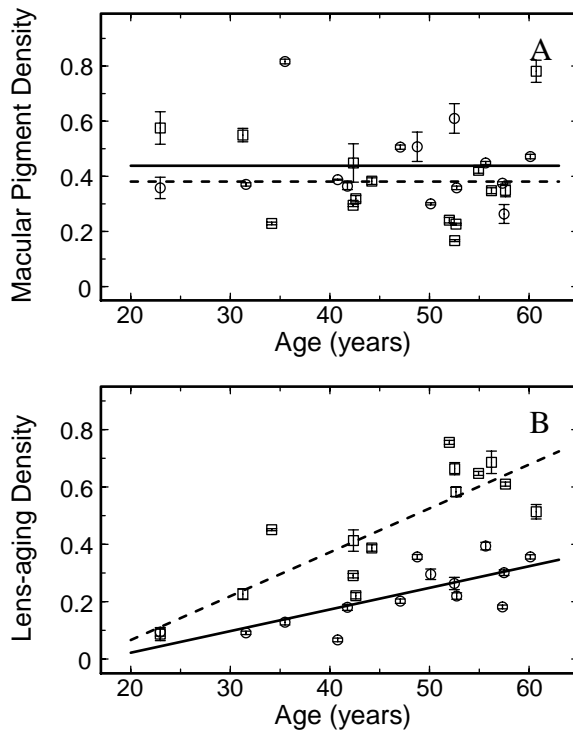
Figure 6.5: (A) Macular pigment density (at 460 nm) and (B) the aging component of the lens density (at 420 nm) versus age in normal subjects (circles) and patients (squares). Symbols depict the mean of five measurements. Error bars indicate the standard deviation within a series of five measurements. Macular pigment density in the diabetic and normal eyes was not significantly different. The optical density of the lens in the controls increased with age in both groups, in the diabetics this effect was stronger.

age, even after correction for absorption losses in the lens. This indicates that the degradation of the receptors is a normal age-related phenomenon. The anatomical alterations in the cone outer segments in normal aged retinas reported by Marshall support this finding.[131] The non-directional background B' slightly increased with age. Possibly, we have applied an over-correction for absorption in the eye lens. In that case, the actual decrease of the directional component with age might be stronger than our present estimate. After correction for age, the amplitude A' was

lower in diabetes. For as far as this reduction is of concern, we agree with Lardenoye *et al.*[7] that the integrity of the cone-photoreceptors is altered in diabetes. This finding is also in agreement with Elsner *et al.*,[147] who found cone photopigment bleaching abnormalities in diabetes, and with Weiner *et al.*,[148] who observed changes in foveal cone electroretinography. In contrast to Lardenoye *et al.*[7] we did not find a decrease in the directionality.

How can the alteration of the optical Stiles–Crawford effect in diabetes be understood? The first requisite for a normal directional reflectance is a precise alignment of the individual receptor cells toward a common location near the center of the pupil.[24] Second, it requires a sharply peaked back reflectance from each single receptor. Whether considered a sign of the antenna or waveguide properties of the receptor cells,[67–69] or a directional reflectance from the stack of the disks in the outer segments of the photoreceptors,[3] this demands healthy photoreceptors. Because only the amplitude dropped, and because there were no major changes in the maximum position, a common tilt or random disruption of the orientation of all the receptors can be excluded. At least part of the receptor population was still commonly aligned near the center of the pupil. Because the cells are closely packed, it seems impossible that the cells still aligned, and those deviating, are mixed. As a first possible explanation for the reduced amplitude, we propose that groups of cells are deviating, while other groups remain aligned. Alternatively, the amplitude might also drop when a fraction of the cells no longer acts as a directional reflector, whatever the cause. Possibly, the age-related alterations in the outer segments as *e.g.* reported by Marshall, occur at an earlier age in the diabetics.[131] However, the difference in age between the two linear regression lines was 38 years, a rather large value. It seems likely that diabetic retinopathy inflicts additional damage to the photoreceptors. Again, we can conclude on the basis of the high directionality that the cells are probably not massively affected. Recently, Roorda and Williams demonstrated *in vivo* assessment of the waveguide properties of single photoreceptors.[105] It would be worthwhile to examine the affection of the photoreceptor reflectance in diabetes with this technique, to narrow down the possible causes of the abnormalities.

Although our results corroborate the findings of Lardenoye *et al.*,[7] a critical note can be made on their analysis of the directional reflectance, which also concerns the work of DeLint *et al.*[6] They both applied a fit with a simpler version of Eq. (6.1), with a single parameter *B* accounting for the diffuse background component (see also Gorrand and Delori,[18] and Burns *et al.*[19]) A fit with such an equation works well in healthy subjects, but becomes unstable when the directional part of the reflectance decreases. When this occurs, the amplitude of the directional component *A* increases and fits the entire signal in the pupil center, while the diffuse background parameter

B decreases or may even be negative. The directionality becomes very low. DeLint *et al.* made a comment on this, but continued using the spuriously low directionality values.[6] Lardenoye *et al.*[7] quoted values for the directionality as low as 0.01 mm^{-2}, indicative of an unstable fit. Analysis of our profiles with the more elaborated model as given by Eq. (6.1) was stable in all cases; this improves interpretation of the pupil profiles. We note that the apparatus used in the aforementioned studies was also built in our laboratory. The new instrument applied in the present study offers a number of benefits. Instead of the formerly used bitebar, a simple chinrest suffices. Previously, a series of images were required, which makes the technique vulnerable to errors in fixation or slight head movements during the series. The new technique merely requires capturing a single reflection image, obtained in a second. Our results illustrate the potential of the new instrument as a fast test on photoreceptor integrity in a clinical setting.

The reduction of macular pigment was approximately 14%. This difference is small compared to the natural variation in macular pigment, and was not significant. Davies and Morland found a mean reduction of 59% in a population of 34 diabetics.[139] Our much smaller reduction is probably not related to a lack of diabetic retinal complications in our population. The clinical data in Table 6.1 provide evidence that many patients suffered from retinopathy in the foveal region. Duration of diabetes ranged from 6 to 28 years, mean 19 years, with a standard deviation of 6 years; in Davies and Morland's patients duration ranged from 2 to 38 years, mean 13.8 years, standard deviation 10.3 years.[139] Searching for other sources of the discrepancy, we wonder whether their subjects were capable of performing a complicated psychophysical test. The experimental errors were large; for half of their diabetics the confidence interval included zero, and 8 patients and 4 controls were not included in the macular pigment test for reasons unknown. We conclude that if a reduction in macular pigment in diabetics exists, it is probably small.

The density of the lens in healthy subjects strongly correlated with age. In the normal controls, the increase in lens density was $(7.5 \pm 2.5) \times 10^{-3}$ year^{-1}, which is of the same order as the increase of 8.66×10^{-3} year^{-1} for subjects aged less than 60 years in Pokorny *et al.*'s aging model.[64] In the diabetics, the increase in lens density was $(15 \pm 4) \times 10^{-3}$ year^{-1}, a factor of two higher. Lutze and Bresnick also found a faster increase in lens density in diabetics compared to normals.[146] The increase in lens density in young diabetics was similar to that of their controls above age 60 years. They concluded that the aging mechanism in diabetics and elderly must be similar. We do not agree with this conclusion. In Pokorny *et al.*'s aging model,[64] subjects over age 60 have an increase in lens density of 28.9×10^{-3} year^{-1}, almost twice the rate we found in our diabetics. Possibly, other factors besides an accelera-

tion of the normal aging process exist. Pigments with other spectral signatures might accumulate in the diabetic lens, or scattering of light might increase. In conclusion, the increased optical density of the lens reflects early changes in the diabetic lens. Possibly, these early changes are predictive for cataract formation. They could serve to monitor the affection of the lens by the disease or as a marker in clinical studies.

Chapter 7

General Discussion

The first aim of this thesis was the development of a new instrument for simultaneous measurement of the spectral and the directional reflectance of the living human eye. The analysis of existing instruments in Chapter 2 demonstrates that this was hitherto not achieved. In Chapter 3, the new instrument is described in detail, and its functionality is demonstrated on a group of healthy subjects. In Section 7.1 of this General Discussion, we will compare the new instrument with the previous designs that are reviewed in Chapter 2. Whereas Chapter 3 focusus on experimental results, this discussion will deal with the technical aspects of the design. The second aim of this investigation was to derive a model for analysis of the reflectance images produced by the apparatus. The results of Chapters 4 and 5 provide important intermediate steps towards a model capable of fitting the entire two-dimensional data sets simultaneously. The development of such a fundus reflectance model will be addressed in Section 7.2. In the final part of this thesis (Chapter 6), the first application of the new instrument in a clinical setting is presented. In general, the results offer good prospects for further clinical studies. The possible future applications of the instrument will be discussed in Section 7.3.

7.1   Development of the Instrument

In Chapter 2, we review existing instruments for fundus reflectometry. Table 2.1 on page 16 gives a qualitative overview of the characteristics of the previous and new designs. The new instrument is described in detail in Chapter 3. In this Section, we will compare the design of the new and previously existing instruments. Many elements of the new instrument were derived from the earlier designs. Imaging spectroscopy on the living human eye was demonstrated before by Hammer *et al.*[50] In their in-

strument, the entrance slit of the spectrograph was conjugate to the retinal plane. In contrast, we have placed the entrance slit of an imaging spectrograph conjugate to the pupil plane. This feature is unique to the new instrument.

For all the single spot instruments, the size of the illuminated and sampled region was in the range 1–5 deg. In order to decrease the influence of imperfect imaging, the illuminated fields were in general slightly larger. The diameters of the illuminated and sampled fields of the new instrument were 2.8 deg and 1.9 deg. This is of the same order as in the other single spot instruments, and it is about the size of the foveal region. A decrease of the field sizes would result in less light available for analysis, and possibly the signal to noise ratio would become too low. A larger field size would make the instrument less sensitive to changes in the cone photoreceptors in the center of the fovea. Furthermore, the average macular pigment optical density would be reduced, and the differences between individuals would be more difficult to detect. In view of these considerations, the present field sizes seem a reasonable compromise.

The two photoreceptor alignment reflectometers described in the literature had the highest resolution in the pupil plane.[18, 19] Moreover, they sampled the pupil plane in two dimensions. In van Norren and van de Kraats' densitometer and scanning laser ophthalmoscope, the configuration of the pupil plane was small and could be scanned through the subject's pupil plane.[3, 20] The other instruments were not capable of sampling the pupil plane. In the new instrument, the entrance pupil was formed by the image of the filament of its halogen lamp light source, and measured 0.8×1.2 mm. This principle was taken over from van Norren and van de Kraats' densitometer.[47] The bar shaped exit pupil comprises a series of 0.14×0.8 mm exit pupils. The first measure of 0.14 mm was set by the pixel size of the CCD camera in the spectrograph. The second measure was set by the width of the slit of the spectrograph. A fairly large width was required to capture enough light. The separation of the entrance pupil and bar shaped exit pupil was 0.7 mm. This was the closest separation that could be achieved with the presently used ophthalmic mirror. A decrease in this separation would lead to reflections and stray light at the edges of the hole in the mirror. For optimal assessment of the directional reflectance, it is important that the entrance and exit pupil configuration is not too large. Otherwise, the directional component would decrease too much relative to the diffuse background component. For the present dimensions of the pupil configuration, it can be estimated that the measured amplitude of the directional reflectance is approximately 75% of what could be achieved maximally. Thus, the present size of the pupil configuration seems sufficiently small. The half width at half maximum of the distribution of the directional reflectance is in the order of a few millimeters. The spatial resolution along the bar shaped exit pupil

was more than adequate to sample this distribution.

Delori's spectrophotometer[48, 49] and Hammer *et al.*'s imaging spectrograph[50] produced continuous spectra. In van Norren and van de Kraats' densitometer, the spectra were limited to discrete points in wavelength, set by the transmission window of the interference filters.[47] Delori and Pflibsen used only 19 wavelengths in their analysis, while their apparatus was capable of returning a larger number.[2] The scanning laser ophthalmoscopes and the photoreceptor alignment reflectometers operated at one, or a small number of particular laser wavelengths. The new instrument produced continuous spectra in the wavelength range 420–790 nm. This was the maximal possible range given the dispersion of the prism and the size of the CCD chip. Unfortunately, the spectral filters blocked too much light above 750 nm, giving a poor signal to noise ratio above this wavelength. While developing the instrument as an experimental setup, we opted for a practical solution, and experimented with spectral filters that were available in our laboratory at that time, to find a reasonable combination. The present filters worked well in the wavelength range 420–750 nm, which was sufficient for our purpose.

Some of the instruments were optimized to operate at light levels low enough to keep the visual pigments unbleached. In other cases, it was possible to align the dark-adapted subject to the apparatus using near infrared wavelengths where visual pigments do not absorb, and measure the dark-adapted reflectance in a single, or few flashes. DeLint *et al.* used a scanning laser ophthalmoscope with a fast shutter synchronized to the scanning electronics, enabling the capture of single frames.[20] With a sufficiently low frame rate, dark-adapted measurements over longer periods were possible. In the new instrument, the high spectral and spatial resolution demanded a high illuminance of the measuring light to maintain a sufficient signal to noise ratio. Consequently, all the measurements were performed in bleached conditions.

The number of photons available for detection in each pixel of the CCD camera is related to the factors discussed above, *e.g.*, the size of the illuminated and the sampled field, the size of the entrance pupil, the width of the spectrograph's slit, the spectral resolution, the spatial resolution in the pupil plane, the illuminance of the measuring light, the choice for the spectral filters, the spectral sensitivity of the CCD, and the integration time. It requires a delicate trade-off to reach sufficient signal, in particular at wavelengths below 450 nm, because the retinal reflectance, output of the light source, and quantum efficiency of the CCD are lowest in this region. The sizes of the entrance pupil and the retinal fields were chosen to be similar to the values used in earlier experiments. The integration time and the spectral filters were optimized, in order to achieve the highest possible signal in the blue, while preventing the signal at longer wavelengths from saturating the CCD. It can be concluded that we have

adopted a reasonable choice for the combination of the parameters.

Recently, the optics of the instrument were completely redesigned, which resulted in a tabletop version. In the design and construction, several improvements have been made. First, the tabletop version has a CCD camera with less dark current and readout noise, and a larger chip. Second, the choice of spectral filters has been optimized for the new CCD. The new combination of filters and the larger chip facilitated extending the spectral range to 400–950 nm.

Both the experimental setup and the new tabletop version of the instrument rely on a continuous light source with a high illuminance. This will inevitably bleach the visual pigments to a transparent state. To measure the reflectance with the visual pigments present (dark-adapted) as well, the illuminance of the measuring beam should be reduced with a neutral density filter. This could be compensated with an increase in integration time, larger retinal field sizes, and a decrease in spectral resolution and spatial resolution in the pupil plane. Another possible solution would require flash light illumination and a fast, synchronized shutter for the camera. Possibly, this would allow capturing a single recording before the measuring light bleaches the visual pigment.

7.2   Fundus Reflectance Model

7.2.1   The Present Model

At present, we rely on van de Kraats *et al.*'s reflectance model for analysis of foveal reflectance spectra.[3] In this thesis, the first purpose was to analyze the results obtained with the new instrument, in order to compare them with those reported in the literature (Chapter 3). The second purpose was to compare the optical density of the lens and the macular pigment in diabetic eyes with that in normal eyes (Chapter 6). In Chapters 4 and 5, we have presented new aspects that are not accounted for in the present model. In addition, as will be discussed below, the description of light originating from the choroid could be improved. Although the present model describes the data satisfactorily, possibly the fitted parameters contain systematic errors. How sensitive are our conclusions to these errors? Reconsideration of the work presented in Chapters 3 and 6 seems appropriate.

Regarding Chapter 3, the correctness of the model is of less concern. We compared our spectral model parameters mainly with the parameters obtained by Delori and Pflibsen[2] with a comparable model, and those obtained by van de Kraats *et al.*[3] with exactly the same model. In Chapter 6, we have applied the model for analysis of the normal and diabetic subjects' spectra. Of main interest were the differences be-

tween the two groups. If the model would produce systematic errors in one or more of its parameters, these would to first order affect the outcome in both groups similarly. Thus, for the comparison between groups, certain uncertainties in the correctness of the model are acceptable. Regarding *in vivo* methods, there is no gold standard for measurement of the optical density of the lens or macular pigment. Notwithstanding that, it would be highly interesting to compare our technique with different independent methods in the same group of subjects. An example of such a study, on three methods for assessment of macular pigment optical density, was published by Delori *et al.*[65] In conclusion, application of van de Kraats *et al.*'s model[3] for analysis of single spectra can be justified. However, as will be discussed below, an update of the model seems necessary.

7.2.2 Towards a Model for Spectral and Directional Reflectance

The new instrument produces images of the spectral and directional reflectance $R(x,\lambda)$, with x the location in the pupil in millimeters and λ the wavelength in nm (*c.f.*, Fig 3.2, page 26). Van de Kraats *et al.*'s reflectance model[3] cannot be applied to the two-dimensional $R(x,\lambda)$ data. We set out to expand the model, with the aim to fit the entire two-dimensional data set simultaneously. In Chapters 4 and 5, we have analyzed the two-dimensional $R(x,\lambda)$ spectra by fitting a Gaussian to individual profiles at each wavelength (*c.f.*, Eq. (4.2), page 42; Eq. (5.1), page 55):

$$R(x,\lambda) = B(\lambda) + A(\lambda)10^{-\rho(\lambda)(x-x_c)^2}, \tag{7.1}$$

with $B(\lambda)$ the non-directional background, $A(\lambda)$ the amplitude of the directional reflectance, $\rho(\lambda)$ a measure for the directionality, and x_c the center position. Here, we have explicitly denoted the dependence of B, A, and ρ on wavelength λ. The parameter x_c is expected to be independent from λ. The spectra for ρ and A were presented in Chapters 4 and 5. We successfully derived a new model for both spectra. These models are important steps towards improvement of van de Kraats *et al.*'s model.[3] Unfortunately, an analysis of the spectra for the non-directional component $B(\lambda)$ is lacking.

Below, we will briefly discuss van de Kraats *et al.*'s model.[3] They divided the different layers in the eye into three groups: First, the pre-receptor layers, *e.g.*, the eye media, the inner limiting membrane, and the layer of nerve fibers containing the macular pigment, second, the receptor layer, and third, the post-receptor or "deeper" layers.[3] We will follow the same division. Starting at the level of the cornea, a ray of light encountering the successive layers in the eye will be traced. Of interest are the processes that contribute to the measured reflectance, such as reflectance or backscatter of the light, and in the mechanisms attenuating the light. An important notion is

that the ray of light passes the layers twice, first on the entrance path and second on
the way back to the pupil. This is accounted for by multiplying the optical densities
of the layers by a factor of two. Because the reflectivity of the layers is small, sec-
ondary reflections are generally neglected. It is assumed that the interference of light
between different layers plays no significant role: Light reflected at different levels
in the retina is simply added.

7.2.3   Pre-Receptor Layers

Reflection

The reflections at the surfaces of the cornea and the lens, referred to as the Purkinje
images, are considered artefacts when measuring the reflectance of the fundus. The
more the paths of the entrance and exit beam are kept separated till they intersect
the back surface of the lens, the weaker the contribution of these reflections. In
the arrangement we have applied to separate the reflected light from the entrance
beam, the specular reflection of the cornea largely disappears in the central hole of
the ophthalmic mirror. To correct for a small remnant reflection, and possibly light
back-scattered in the lens as well, we have added the parameter R_{cornea} to the model
(Chapters 3 and 6). It was assumed to be independent from wavelength.

Another source of reflectance is the boundary between the vitreous body and
the retina, the inner limiting membrane (ILM). On fundus images, the specular re-
flectance of this layer is clearly visible as a ring-shaped reflex surrounding the mac-
ula, on top of and along the larger blood vessels, and sometimes as a tiny speck in
the center of the fovea.[149] In van de Kraats *et al.*'s model, the ILM is assumed to be a
source of diffuse reflectance as well.[3] As the authors noted, it cannot be distinguished
from minor backscatter in the vitreous.[3] We found the ILM reflectance R_{ilm} small and
problematic to fit; in many cases it reached zero (Chapter 3). Although diffuse, van
de Kraats *et al.* assumed the ILM reflectance to be due to a transition in refractive
index, *viz.* Fresnel reflectance, and to be spectrally neutral.[3] To our knowledge, there
is no experimental evidence for this assumption. A second reflecting layer in the su-
perficial retina is the nerve fiber layer.[150] The reflectance of this layer is proportional
to its thickness and is strongly dependent on wavelength.[150] Because the nerve fibers
are nearly absent in the fovea, reflectance from this layer is neglected.

Attenuation

At least three mechanisms play a role in the attenuation of light in the pre-receptor
layers. Reflections at the cornea and the inner limiting membrane present small light

losses. The second source of attenuation is scattering in the media, *e.g.*, the cornea, the lens, and the vitreous. Apart from losses due to back scattering, light scattered forward outside the detection field is lost as well. Finally, light is absorbed in the media, mainly the lens, and in the macular pigment. Part of this light is converted to heat, another part may appear at longer wavelengths as fluorescent light.

We will first discuss the spectrally neutral light losses in the media. Van de Kraats *et al.*'s model parameter (D_{medscat}) accounting for these losses was estimated at 0.15 for a single pass.[3] Earlier, Delori and Pflibsen[2] proposed a density of 0.10. The value of 0.15 might be too high: With a correction this large, the reflectivity of all the retinal reflecting layers is multiplied by a factor of two. How much do the three mechanisms for attenuation add to the spectrally neutral density? First, the outermost layer of the cornea (the tear film) has a refractive index of 1.336 with respect to air.[25, 27] With the Fresnel equations,[27] the reflection at the front surface of the cornea can be estimated at 2%. This corresponds to a minute optical density of 0.009. The other reflection losses, *e.g.*, at the back of the lens or the inner limiting membrane, are even smaller. Second, psychophysical studies[127, 128] found forward-scattered light to be independent from wavelength; in that case a spectrally neutral correction would be appropriate. Because most of the light is scattered within a narrow solid angle, the light loss is expected to be small for our 1.9 deg field. Forward scattering in the cornea was reported to depend on wavelength,[89] but it is also negligible for our 1.9 deg field. Third, the spectrally neutral absorption losses in the lens are also small: Van den Berg and Felius reported a mean optical density of 0.04 ± 0.04 density units at 700 nm for donor lenses aged 59 ± 20 years.[114] This value included losses due to back scattering as well. In view of this low value, D_{medscat} is estimated at approximately 0.05, much smaller than the present value of 0.15. It should be noted that this parameter, because it is spectrally neutral, does not improve the goodness of fit of the model.

Spectrally selective attenuation in the pre-retinal layers is mainly due to absorption. The spectral absorption of the pre-retinal layers was studied in detail in Chapter 5. The main absorbers are the pigments in the eye lens and the macular pigment. At wavelengths above 700 nm, absorption in water comes into play. The other components of the ocular media have a negligible absorption in the visible wavelength range. With regard to the first source of absorption, the eye lens, van de Kraats *et al.*'s model could remain largely the same. We suggest to replace the templates that are referred to as "non-aging" and "aging" with the "young" and "aged" templates, representing the pigment O-β-glucoside of 3-hydroxykynurenine (3-HKG) and the pigments accumulating with age. The non-aging template had a fixed optical density of 0.31. In contrast, the density of both the new templates varies with age. For the second source of pre-retinal absorption, the macular pigment, the template proposed

by Walraven[85] (Eq. (5.3), page 56) seems a reasonable description (*c.f.*, Fig. 5.1A, page 57). It has the advantage that it is available as an equation. Finally, the absorption in water enters the model for wavelengths above 700 nm. Van de Kraats *et al.*[3] refered to the data by Smith and Baker[151] and fixed the path length to 24 mm. Recently, van de Berg and Spekreijse analyzed the contribution of water to the spectral absorption of the eye media in the infrared. They tabulated Smith and Baker's data[151] below 800 nm, and provided additional data above this wavelength.[152] They proposed a path length of 22 mm.[152]

7.2.4   Receptor Layer

Light reaching the receptor layer has four possible fates.[3] First, it can be absorbed in the visual pigments. Second, it can be reflected at the stack of disks in the outer segments of the photoreceptors. This produces the directional component of reflectance from the retina. Third, it can traverse the entire outer segment without being reflected. And fourth, it can leak out of the outer segment. Van de Kraats *et al.*'s model elaborates on the absorption in the visual pigments and the three pathways in terms of geometrical optics.[3] An example of a model calculation of light interaction with a photoreceptor in terms of Maxwell's equations, was given by Piket-May *et al.*[104] Unfortunately, such complicated models require too much time to evaluate for on-line analysis of spectral measurements. It is desirable to have a simple model that can be readily evaluated analytically. Van de Kraats *et al.*'s model[3] probably still holds as a reasonable approximation.

In Chapters 4 and 5, the directional reflectance from the disks was studied extensively. At each wavelength, the directional reflectance could be fitted with a Gaussian. The scattering theory by Marcos *et al.*[22] and Marcos and Burns[23] predicts this Gaussian shape, and states that its directionality ρ is the sum of two components. The first is ρ_{wg}, which results from the waveguide properties of the photoreceptors. In our analysis in Chapter 4 this component was assumed to be independent from wavelength, which was a reasonable first order approximation. The second component $\rho_{scatt}(\lambda)$ accounts for the scattering of light from the photoreceptor mosaic. It is proportional to one over wavelength squared, and is related to the row-to-row cone spacing. In Chapter 5 it was shown that reflectance from the photoreceptors is spectrally neutral. This property was already contained in van de Kraats *et al.*'s model.[3]

Currently, with the visual pigments bleached, the directional properties of van de Kraats *et al.*'s model[3] are governed by the spectrally neutral parameter SC. The model does not specify how this parameter SC depends on pupil position x quantitatively, and it does not incorporate Marcos *et al.*'s scattering theory.[22,23] We suggest

to incorporate our new findings in the model. The modified model should explicitly produce a Gaussian shaped distribution in the pupil plane. At the level of the photoreceptors, the amplitude of this Gaussian should be spectrally neutral. Marcos *et al.*'s scattering theory[22, 23] enters the new model via the directionality ρ of the Gaussian distribution.

An unsolved problem is that van de Kraats *et al.*'s model assumes that the entrance and exit pupil move in tandem.[3] In the new instrument the entrance pupil is aligned with the maximum of the directional reflectance, and spectra are obtained for a range of exit pupils. A test can be placed on this aspect of the model by scanning the pupil plane with the configuration of the entrance pupil and the bar shaped exit pupil. Marcos and Burns performed this type of experiments to study the waveguide directionality of the photoreceptors, but their analysis was limited to two wavelengths.[23] With the new instrument, the experiment could be repeated for a continuous range of wavelengths. Finally, as was suggested in the previous Section, it could be attempted to obtain measurements with dark-adapted visual pigments. This would put an additional test on the description of the interaction of light with the photoreceptor layer.

7.2.5 Post-Receptor (Deeper) Layers

In Chapter 5, we assumed that the only source of directional reflectance resides in the outer segments of the photoreceptors. This greatly simplified the model analysis of parameter A versus wavelength. The non-directional or diffuse background B originates from a large number of reflecting layers. In Section 7.2.3 on the pre-receptor layers, we already introduced the reflectance of light from the cornea, the surfaces of the lens, the inner limiting membrane, and the nerve fiber layer, and the back scatter of light from the cornea, the lens, and the vitreous humor. The receptor layer, in addition to acting as a directional reflector, cannot be excluded as a source of diffuse reflectance as well. However, the main source of the diffuse reflectance is believed to reside in layers behind the receptor layer, also referred to as the deeper layers.[3] Here, light is reflected or scattered from the retinal pigment epithelium, Bruch's membrane, the choroid, and the sclera. In van de Kraats *et al.*'s reflectance model[3] the reflectance of the deeper layers is described by:

$$R_{\text{deep}}(\lambda) = R_{\text{sclera}}(\lambda) 10^{-2[D_{\text{mela}}(\lambda)+D_{\text{blood}}(\lambda)+D_{\text{scat}}]} \qquad (7.2)$$

with $R_{\text{deep}}(\lambda)$ the reflectance from the deeper layers, $R_{\text{sclera}}(\lambda)$ the reflectance of the sclera given by $0.5 \exp[-0.00261(\lambda - 675)]$,[2, 3] $D_{\text{mela}}(\lambda)$ the optical density of melanin, $D_{\text{blood}}(\lambda)$ the optical density of a layer of blood with thickness Th_{blood}, and
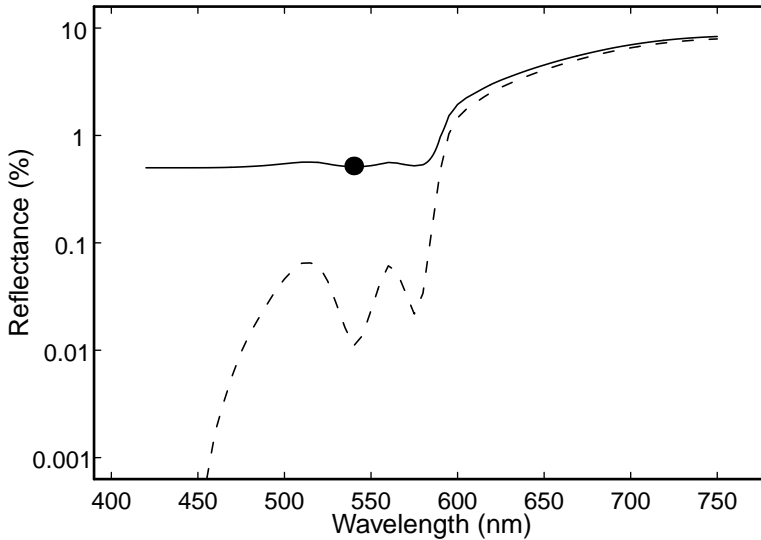
Figure 7.1: The single dot at 540 nm represents the typical value of 0.52% for the diffuse non-directional background at this wavelength. The dashed curve depicts the reflectance from the deeper layers R_{deep} calculated with Eq. (7.2). Typical values for D_{mela}, Th_{blood}, and D_{scat} were used. The predicted reflectance below 600 nm clearly is too low. The required level of non-directional reflectance can be produced by placing an additional reflector in front of the blood rich layers. As an example, the solid curve depicts a model produced by adding a spectrally neutral reflectance of 0.5%.

D_{scat} a parameter accounting for spectrally neutral losses, for instance due to light scattering laterally in the choroid, outside the measurement field.

We have reasons to believe that the model Eq. (7.2) is incorrect. The physical assumption in Eq. (7.2) is that light reflects at the sclera and passes the choroid twice. This may hold at wavelengths above 600 nm, where blood is transparent. In this wavelength region, Eq. (7.2) probably holds as a reasonable approximation. However, at shorter wavelengths, the total optical density strongly increases. The choroid is virtually opaque and light never reaches the sclera. The dashed model curve in Fig. 7.1, calculated according to Eq. (7.2), illustrates this problem. Typical values for $D_{\text{mela}}(\lambda)$, $\text{Th}_{\text{blood}}(\lambda)$, and D_{scat} were taken from Table 3.2 on page 30. Below 600 nm, Eq. (7.2) predicts the reflectance to drop below 0.1%. For the profiles depicted in Fig. 3.5, page 32, the non-directional background is clearly higher than 0.1%. In Fig. 7.1, the typical value for the non-directional background (0.52%, also
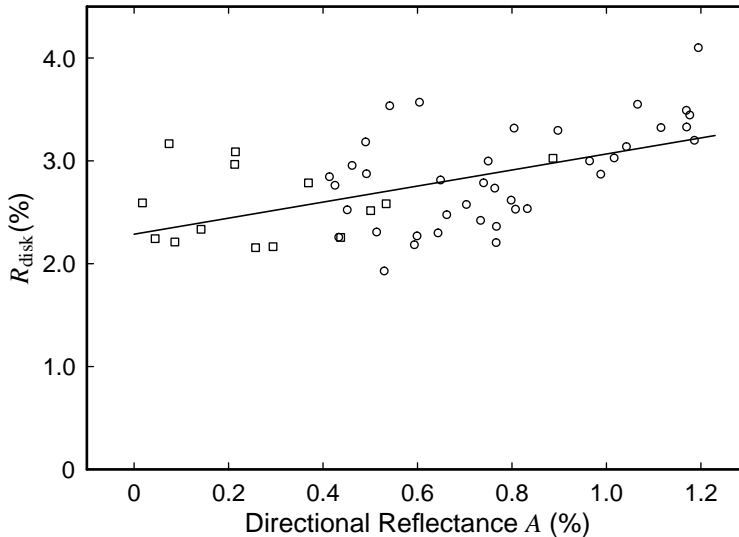
Figure 7.2: Van de Kraats *et al.*'s model parameter[3] R_{disk} versus the amplitude of the directional reflectance A for 39 healthy eyes (circles) and 14 diabetic eyes (squares). The solid curve depicts a linear regression line. The intercept was $(2.3 \pm 0.13)\%$. The correlation between R_{disk} and A was 0.5. Apparently, sources other than the directional reflectance contribute to R_{disk}.

taken from Table 3.2) is indicated with a single dot at 540 nm. Apparently, Eq. (7.2) predicts too low values for the diffuse component.

The solid curve in Fig. 7.1 illustrates how the model "solves" the problem of R_{deep} producing a too low non-directional component. It was already noted in the Discussion in Chapter 3 that the receptor disk reflectance cannot be discerned from a reflecting layer at the level of the retinal pigment epithelium (page 34). That is, R_{disk} not only contains the reflectance of the receptor layer, but is contaminated with a source of diffuse reflectance from deeper layers. Because this light originates from behind the macular pigment, the parameters R_{ilm} and R_{cornea} are not capable of accounting for the additional diffuse reflectance. The solid curve in Fig. 7.1 was calculated with Eq. (7.2) with the same parameters as were used to calculate the dashed curve, but an anterior reflector of 0.5% was added to the model. This brought the resulting curve in agreement with the expected level of diffuse reflectance.

As it seems, the model counteracts the problem of $R_{deep}(\lambda)$ being too low by increasing the parameter R_{disk}. We can put another test on this assumption. The

parameter R_{disk} stands for reflectance from the disks in the outer segments of the cones, in other words, the directional reflectance. It should be closely related to the amplitude of the directional reflectance A. We tested this hypothesis on data obtained from the 39 eyes that were included in the study presented in Chapter 5, and data obtained from the 14 diabetic eyes that were presented in Chapter 6. The parameter R_{disk} was assessed from single spectra at the location where the directional reflectance had a maximum with van de Kraats *et al.*'s fundus reflectance model (*c.f.*, Section 3.4.2, page 27; Section 6.2.4, page 82).[3] The amplitude of the directional reflectance A was assessed from profiles at 540 nm with Eq. (6.1), with the method that was described in Section 6.2.4 on page 82 ff. The relationship between R_{disk} and A can be inferred from the scatter plot depicted in Fig. 7.2. While A approached zero in some of the diabetics, R_{disk} remained at a level of 2.3%. Furthermore, the correlation between R_{disk} and A had the modest value of 0.5. It is concluded that R_{disk} partly represents another source of reflectance, presumably light reflected from the photoreceptor layer itself, the retinal pigment epithelium, or the superficial layers of the choroid. Because the correlation with A is low, it cannot serve as a predictor of photoreceptor integrity.

Our conclusion that the model for $R_{\text{deep}}(\lambda)$ is incorrect is corroborated by a Monte Carlo simulation for light scattering in the choroid by Preece and Claridge, which showed no difference between a spectrum with or without the sclera backing the choroid.[5] They concluded that most of the light originating from the choroid represents light backscattered from within the fundus. Because scattering is involved, a physically correct model capable of replacing Eq. (7.2) is probably complicated.[153] As was already stated above, it is desirable to have a simple model that can be readily evaluated analytically. As a first order approximation, a spectrally neutral reflector could be placed at the level of the photoreceptors. As such, it is located behind the macular pigment, but in front of the blood rich layers. This neutral reflector would take over the role that is presently fulfilled by R_{disk}. To distinguish this diffuse reflectance from the directional R_{disk}, originating from the same level, it is crucial to have a two-dimensional model for fitting the spectral and the directional reflectance simultaneously. Possibly, this would also solve the problem mentioned in Section 6.4, page 88 ff., namely the instability of Gaussian fits to profiles without a directional component.

7.3 Prospects

7.3.1 Ocular Pigments

One of the main applications of the new instrument is assessment of the optical density of ocular pigments. The discussion below will focus on the optical density of the macular pigment and the eye lens. A discussion of other ocular pigments, *e.g.*, the visual pigments and melanin, is outside the scope of the present thesis, for a review see Liem *et al.*[55] and Berendschot *et al.*[45]

Optical Density of the Macular Pigment

Macular pigment was first suggested to improve visual performance by suppressing chromatic aberration in the blue part of the visual spectrum,[154] but recent calculations no longer support this idea.[155] Macular pigment possibly protects the retina as a filter for blue light, or as an antioxidant quenching free radicals. As was stated several times in this thesis, it has been suggested to reduce the risk for age-related macular degeneration (AMD).[9–11] Macular pigment cannot be synthesized *de novo*, it has to be derived from the diet.[156,157] The macular pigment optical density has been demonstrated to increase after dietary supplementation of lutein,[12,13] and with consumption of foods rich in lutein such as spinach or corn.[14] This suggests that individuals with low levels of macular pigment could benefit from dietary supplementation. The "protection" and "intervention" hypotheses have been the incentive for a large number of recent publications on macular pigment, including the present thesis. However, demonstration of the efficacy of macular pigment awaits further supplementation studies, more extensive epidemiological research, and randomized intervention studies.

Regarding the increase of the optical density of macular pigment with supplementation of lutein and zeaxanthin, at least three studies have been published. Landrum *et al.* supplemented lutein to two male subjects and observed a considerable increase in both subjects.[12] Hammond *et al.* added spinach and corn to the diet of eleven subjects (Four male, nine female).[14] Eight of these subjects had an increase of at least 13% in macular pigment density. Finally, Berendschot *et al.* supplemented lutein to eight male subjects and observed an increase in all subjects.[13] Although the conclusion can be drawn that intervention is possible, a number of questions remain unanswered. It is unclear whether supplementation is effective in all individuals. All three studies involved small populations, lacked a control group, and in two cases included only men. It seems necessary to conduct a larger study on both males and females. It should be a randomized double blind study, with the control group receiv-

ing a placebo. Assuming for the moment that dietary supplementation will increase the optical density of macular pigment, will it prevent or reduce the risk for the development of AMD? In a large cross-sectional study, Berendschot *et al.*[158] divided subjects in two groups according to their level of age-related maculopathy[159] (ARM), indicative for the risk to develop AMD. The macular pigment optical density (MPOD) was similar in eyes without any sign of ARM ($n = 289$, MPOD $= 0.33 \pm 0.15$) and in eyes at any stage of ARM ($n = 146$, MPOD $= 0.33 \pm 0.16$) These results seem to disprove a relation between MPOD and ARM. Direct proof of the protection and intervention hypotheses requires an intervention study in a population of elderly with repeated follow up studies.

On the premise that the protection hypothesis holds, a screening tool of the general population might become useful. Such an instrument should be cheap and easy to operate. Preferably, it should rely on a method that does not involve dilation of the pupil with mydriatics. The precision of the outcome is of lesser concern; it suffices to have an indication of the macular pigment level. The new instrument seems too costly, too complicated, and requires dilation of the pupil. On the other hand, fundamental research should rely on objective and precise methods. For this type of research, the new instrument would be an excellent choice.

In the past years, a large number of techniques for measurement of macular pigment has been developed.[2, 3, 13, 31, 65, 160–167] A complete review of currently existing techniques is outside the scope of the present discussion. Good starting points for an overview of techniques are the paper by Delori *et al.*,[65] and the review by Berendschot *et al.*[45] All methods have their pros and cons, and all methods have potential pitfalls. In order to keep track of the results obtained with the different methods, the relation between the different techniques has to be established in the immediate future; A start in this direction has been made.[13, 65, 167] In Chapter 5, we have demonstrated the capability of the new instrument to precisely reproduce the optical density spectrum of macular pigment *in vivo* (*c.f.*, Fig. 5.2, page 59). More extensive research with this new method and with other existing techniques in pseudophakic subjects could lead to an improvement of our understanding of the various techniques for measuring the optical density of macular pigment.

Optical Density of the Eye Lens

Absorption of light in the eye lens has been studied extensively before; reviews were given by Weale,[168] and by Pierscionek and Weale.[169] The absorption has a profound influence on the spectral sensitivity of the photoreceptors in the blue wavelength region. Separation of changes in the contribution of pre-receptor absorption and re-

ceptor sensitivity is of interest for fundamental and clinical studies.[107, 170–172] An example of the latter is the study of color discrimination in diabetic patients.[171, 172] For this type of study, "lens-matched" controls are desired. Moreland[171] and Hardy *et al.*[172] proposed a model to calculate the age of control subjects given the age of the diabetic subjects and the duration of their diabetic condition. Unfortunately, this model cannot account for the large variation between individuals, does not account for individual variations in macular pigment density, and probably leads to a poor match. Direct measurement of the absorption in the lens and the macular pigment could improve this situation.

Possibly, the optical density of the lens provides an indication for the risk of development of cataract in certain patient groups. In Chapter 6, we found an increased optical density in diabetic patients, who are known to have a higher risk to develop cataract. A follow up study design is required to test this hypothesis. It would also be of interest to separate the influence of age, and of the duration of the disease on the lens optical density. Because in our study the sample size was too small, this relation could not be quantified.

7.3.2 Photoreceptor Integrity

Diagnostic tests on the structural integrity of the cone photoreceptors in the fovea are sparse. In our clinic, the method of choice has been the measurement of the visual pigment density, called densitometry. The assets of clinical densitometry have been reviewed by Liem *et al.*[55] The method relies on measuring the difference in reflectance between a fully dark adapted and a completely bleached retina. The main drawback is that full dark adaptation takes considerable time. An alternative test is the psychophysical assessment of the directional sensitivity of the receptors,[76] *i.e.*, the psychophysical Stiles–Crawford effect.[38] As an historical sidemark, an earlier Utrecht University thesis was published on the clinical importance of the Stiles-Crawford effect by Dunnewold in 1964.[173] Potentially, it is a useful clinical test of foveal integrity.[76] In practice, the procedure is also too time consuming, and too demanding for the subject. Assessment of the directional reflectance, *c.f.*, the optical Stiles–Crawford effect, provides comparable information but can be performed in much less time than the other two tests. With the use of a chin-rest the discomfort for the patient is minimal. The only task is central fixation; usually this is possible even with reduced visual acuity. In general, it can be concluded that the new instrument meets the criteria for a clinical test on photoreceptor integrity.[76]

In Chapter 3, it was suggested that the new instrument could provide differential diagnosis of patients with visual acuity loss of unknown origin. The hypothesis is

that in a small subgroup of these undiagnosed cases the reduced visual acuity could be due to an alteration of the photoreceptors, while the media are clear and the fovea appears otherwise normal with an opthalmoscope or on a fundus photograph.[56, 174] We have measured 18 patients with undiagnosed loss of visual acuity. In one case, with reduced visual acuity in one eye and normal acuity in the other, the directional reflectance was absent in the former eye and normal in the latter. Both eyes had an intra ocular lens. The media were clear and the retina was judged normal by an ophthalmologist of our department. We have repeated the measurements twice, after 181 and 293 days, and found consistent results. Apart from this single case, evidence for the hypothesis could not be produced. Further research is required to demonstrate the usefulness of the new instrument for this particular application.

The new instrument opens the road to future clinical studies on common retinal diseases. First, research on patients with diabetes mellitus (Chapter 6) could be continued. It would be of interest to relate the photoreceptor integrity to clinical parameters such as visual acuity, grade of edema, or duration of the disease. Again, because our sample size was too small, this relation could not be addressed in the present thesis. Second, it is hypothesized that the instrument is capable of detecting changes in the photoreceptor integrity in the early phase of age-related macular degeneration. Third, a study by Nork *et al.* on retinal sections suggested that glaucoma induces swelling of the photoreceptors.[175] Possibly, this swelling also occurs in the fovea. In that case, it could be expected to induce changes in the directional reflectance.

A number of less common retinal diseases are known to involve a pathological condition of the photoreceptors. The first example, macula pucker, is characterized by "wrinkling" of the retina.[176] The condition is treated with surgical removal of the vitreous. In most, but not all patients, there is a gradual improvement of visual acuity. It would be worthwhile to have a predictor for the outcome of the visual acuity after the surgery. Possibly, the photoreceptor integrity could fulfill this role. In addition, it is of interest to monitor the integrity after the surgery, and to relate it to the improvement in visual acuity. A second example is a macular hole.[176] This condition is also treated with surgical removal of the vitreous. Again, it is of interest to relate the photoreceptor integrity to the improvement in visual acuity after the surgery. A third example is central serous retinopathy.[176] This idiopathic disease involves the accumulation of subretinal fluid. The fluid resolves spontaneously within 1–6 months in 80% of the patients, in 20% it resolves within 6–12 months. The visual acuity returns to normal or near normal. We expect to be able to demonstrate an improvement of the photoreceptor integrity as well.

Chapter 8

Summary and Conclusion

The main achievement of this investigation was the development of a new instrument for measurement of light reflected from the retina in a living human eye. The instrument measures both the spectral and the directional properties of the reflected light. Model analysis of the spectral reflection yields the optical densities of ocular absorbers, *e.g.*, the eye lens, melanin, and the macular pigment. The directional properties of the retinal reflectance provide information on the integrity of the foveal cone photoreceptors. The applications of the instrument concentrate on the fovea: the region of the retina specialized for acute vision. Therefore, the apparatus was coined the "Foveal Reflection Analyzer".

The first part of this thesis is on the development of the new instrument. The key element is an imaging spectrograph, with its slit placed conjugate to the pupil of the eye. The analysis of existing instruments in Chapter 2 demonstrates the novelty of this concept. The instrument was realized as an experimental setup on an optical bench. In Chapter 3, the optics of the instrument are described in detail. The spectrograph's spectral range is 420–790 nm. It samples a 1.9 deg spot on the retina in one second, and measures the spectral reflectance along a horizontal bar across the dilated pupil. Video observation of the retina and the pupil facilitates proper alignment. The first results obtained on a group of healthy subjects were in agreement with the literature.

Unfortunately, the model[3] available for analysis of the spectral and directional reflectance developed a few years earlier in our group could not be applied to entire spectrograph images. Therefore, the second aim of this thesis was to improve our understanding of this type of spectral reflectance data, which should eventually lead to an improved spectral reflectance model capable of fitting the entire two-dimensional data set simultaneously. This problem was split in several parts. At each wavelength,

single profiles exhibiting the directional reflectance could be described with a Gaussian on top of a background. This way, spectra for the directionality, the amplitude and the background of the Gaussian were produced. Analysis of these spectra allowed us to demonstrate several new aspects of the retinal reflectance.

This is first shown in Chapter 4, where we elaborate on spectra for the directionality described with parameter ρ; a measure for the peakedness of the distribution in the pupil plane. The scattering theory by Marcos *et al.*[22] and Marcos and Burns[23] predicts that ρ versus wavelength can be described by the sum of the waveguide directionality ρ_{wg}, independent from wavelength, and a contribution proportional to one over wavelength squared, attributed to scattering. The contribution of the latter component gives a measure for the row-to-row cone spacing. Our data for ρ as a function of wavelength corroborated the scattering theory. The estimations for cone spacing and the waveguide directionality were in agreement with the literature.

In Chapter 5, we elaborate on the amplitude of the directional reflectance as a function of the wavelength, the second new type of spectra we have introduced. This type of spectra could be described with a simple model. The directional reflectance was supposed to originate from the outer segments of the photoreceptors. This was the single layer contributing to the reflectance. Only two absorbers were considered of significance: the crystalline lens and the macular pigment. In the first part of Chapter 5, model analysis of spectra obtained from five pseudophakic eyes demonstrates that the source of directional reflectance is spectrally neutral. The second part of Chapter 5 includes data obtained on 39 normal eyes aged 18–64 years. This data allowed us to study the absorption in the natural crystalline lens as function of age. Hitherto, the generally accepted description for these changes was Pokorny *et al.*'s model[64] for the optical density of the lens as a function of age. In a first attempt to describe our data with a model incorporating Pokorny *et al.*'s theory, we found small but systematic differences between the model and our data. These discrepancies warranted a search for an improvement of the model for the age-related changes in the spectral absorption of the eye lens. Our newly proposed model comprises a combination of two templates: a "young" template representing the pigment O-β-glucoside of 3-hydroxykynurenine (3-HKG), and an "aged" template representing the pigments accumulating in the lens with age. The final model for the amplitude of the directional reflectance comprises four factors: The optical density of the young and aged template, the optical density of the macular pigment, and the reflectivity of the photoreceptor layer. This model was applied to spectra obtained from individual eyes. As expected, the density of the young template decreased with age. Concomitantly, the density of the aged template increased with age. The total optical density of the eye at 420 nm slightly increased with age. Precise individual estimates for the

macular pigment density were obtained. In comparison with models also including diffuse reflectance from the deeper layers, the model analysis of the isolated directional component was simpler and contained fewer assumptions. This improved the interpretation of the estimates of the optical density of the lens and the macular pigment. Finally, we observed a decrease of the photoreceptor reflectivity with age, possibly reflecting a degradation of the photoreceptors.

In the final part of this thesis, the first application of the new instrument in a clinical setting is presented. This study included a group of patients with diabetes mellitus. The aim was to assess the integrity of the photoreceptors in the fovea, and to measure the optical density of the macular pigment and the eye lens. The results were compared with those of a group of healthy subjects. We found a strong reduction of the amplitude of the directional reflection in the diabetics group. This indicates changes in the integrity of the foveal cone-photoreceptors. The directionality of the cones was not reduced. Macular pigment was not significantly different in diabetics. Lens density increased at a substantially higher rate in diabetics, compared with the normal age-related increase in the controls. The instrument proved to be a fast and practical test on photoreceptor integrity. Macular pigment could be assessed efficiently and accurately in patients, their reduced visual acuity presented no problem for the method.

In conclusion, we have devised a novel type of instrument. The measured spectra and pupil profiles exhibiting the directional reflectance were in accordance with separate measurements of these aspects with earlier instruments. This validated the functionality of the new instrument. Simultaneous measurement of both aspects allowed us to study several new phenomena. First, we have corroborated the scattering theory of Marcos *et al.* Second, it was demonstrated that the cone photoreceptors act as spectrally neutral reflectors. Third, we have proposed a new model for the optical density spectrum of the lens as a function of age. Although significant progress has been made, a major task remains to be done: A satisfactory model for the diffuse non-directional background is lacking. The first pilot study on a group of diabetic subjects warrants the initiation of further clinical studies on a larger scale. For this purpose, our group has recently developed a table-top version of the instrument.

References

1. D. van Norren and L.F. Tiemeijer, "Spectral reflectance of the human eye", Vision Res. **26** (1986), 313–320.
2. F.C. Delori and K.P. Pflibsen, "Spectral reflectance of the human ocular fundus", Appl. Opt. **28** (1989), 1061–1077.
3. J. van de Kraats, T.T.J.M. Berendschot, and D. van Norren, "The pathways of light measured in fundus reflectometry", Vision Res. **36** (1996), 2229–2247.
4. M. Hammer and D. Schweitzer, "Quantitative reflection spectroscopy at the human ocular fundus", Phys. Med. Biol. **47** (2002), 179–191.
5. S.J. Preece and E. Claridge, "Monte Carlo modelling of the spectral reflectance of the human eye", Phys. Med. Biol. **47** (2002), 2863–2877.
6. P.J. DeLint, T.T.J.M. Berendschot, and D. van Norren, "A comparison of the optical Stiles–Crawford effect and retinal densitometry in a clinical setting", Invest. Ophthalmol. Vis. Sci. **39** (1998), 1519–1523.
7. C.W.T.A. Lardenoye, K. Probst, P.J. DeLint, and A. Rothova, "Photoreceptor function in eyes with macular edema", Invest. Ophthalmol. Vis. Sci. **41** (2000), 4048–4053.
8. R.A. Bone, J.T. Landrum, and S.L. Tarsis, "Preliminary identification of the human macular pigment", Vision Res. **25** (1985), 1531–1535.
9. D.M. Snodderly, "Evidence for protection against age-related macular degeneration by carotenoids and antioxidant vitamins", Am. J. Clin. Nutr. **62** (1995), 1448S–1461S.
10. J.T. Landrum, R.A. Bone, and M.D. Kilburn, "The macular pigment: a possible role in protection from age-related macular degeneration", Adv. Pharmacol. **38** (1997), 537–556.
11. S. Beatty, M.E. Boulton, D. Henson, H.-H. Koh, and I.J. Murray, "Macular pigment and age related macular degeneration", Br. J. Ophthalmol. **83** (1999), 867–877.
12. J.T. Landrum, R.A. Bone, H. Joa, M.D. Kilburn, L.L. Moore, and K.E. Sprague, "A one year study of the macular pigment: the effect of 140 days of a lutein supplement", Exp. Eye Res. **65** (1997), 57–62.
13. T.T.J.M. Berendschot, R.A. Goldbohm, W.A.A. Klöpping, J. van de Kraats, J. van Norel, and D. van Norren, "Influence of lutein supplementation on macular pigment, assessed with two objective techniques", Invest. Ophthalmol. Vis. Sci. **41** (2000), 3322–3326.
14. B.R. Hammond Jr., E.J. Johnson, R.M. Russell, N.I. Krinsky, K.J. Yeum, R.B. Edwards, and D.M. Snodderly, "Dietary modification of human macular pigment density", Invest.

Ophthalmol. Vis. Sci. **38** (1997), 1795–1801.

15. J. Krauskopf, "Some experiments with a photoelectric ophthalmoscope", Performance of the Eye at Low Luminances (M.A. Bouman and J.J. Vos, eds.), Delft, 1966, pp. 171–181.

16. G.J. van Blokland and D. van Norren, "Intensity and polarization of light scattered at small angles from the human fovea", Vision Res. **26** (1986), 485–494.

17. G.J. van Blokland, "Directionality and alignment of the foveal receptors, assessed with light scattered from the human fundus in vivo", Vision Res. **26** (1986), 495–500.

18. J.-M. Gorrand and F.C. Delori, "A reflectometric technique for assessing photoreceptor alignment", Vision Res. **35** (1995), 999–1010.

19. S.A. Burns, S. Wu, F.C. Delori, and A.E. Elsner, "Direct measurement of human-cone-photoreceptor alignment", J. Opt. Soc. Am. A **12** (1995), 2329–2338.

20. P.J. DeLint, T.T.J.M. Berendschot, and D. van Norren, "Local photoreceptor alignment measured with a scanning laser ophthalmoscope", Vision Res. **37** (1997), 243–248.

21. J.C. He, S. Marcos, and S.A. Burns, "Comparison of cone directionality determined by psychophysical and reflectometric techniques", J. Opt. Soc. Am. A **16** (1999), 2363–2369.

22. S. Marcos, S.A. Burns, and J.C. He, "Model for cone directionality reflectometric measurements based on scattering", J. Opt. Soc. Am. A **15** (1998), 2012–2022.

23. S. Marcos and S.A. Burns, "Cone spacing and waveguide properties from cone directionality measurements", J. Opt. Soc. Am. A **16** (1999), 995–1004.

24. A.M. Laties, P.A. Liebman, and C.E.M. Campbell, "Photoreceptor orientation in the primate eye", Nature **218** (1968), 172–173.

25. G. Wyszecki and W.S. Stiles, "*Color Science: Concepts and Methods, Quantitative Data and Formulae*", 2nd ed., Wiley, New York, 1982.

26. W. Bloom and D.W. Fawcett, "*A textbook of histology*", Saunders, Philadelphia, 1986.

27. D.A. Atchison and G. Smith, "*Optics of the human eye*", Butterworth–Heinemann, Oxford, 2000.

28. R.L. Gregory, "*Eye and Brain*", Oxford University Press, Oxford, 1998.

29. D.M. Snodderly, P.K. Brown, F.C. Delori, and J.D. Auran, "The macular pigment. I. Absorbance spectra, localization, and discrimination from other yellow pigments in primate retinas", Invest. Ophthalmol. Vis. Sci. **25** (1984), 660–673.

30. D.M. Snodderly, J.D. Auran, and F.C. Delori, "The macular pigment. II. Spatial distribution in primate retinas", Invest. Ophthalmol. Vis. Sci. **25** (1984), 674–685.

31. P.E. Kilbride, K.R. Alexander, M. Fishman, and G.A. Fishman, "Human macular pigment assessed by imaging fundus reflectometry", Vision Res. **29** (1989), 663–674.

32. B.R. Hammond Jr., B.R. Wooten, and D.M. Snodderly, "Individual variations in the spatial profile of human macular pigment", J. Opt. Soc. Am. A **14** (1997), 1187–1196.

33. A.E. Jalkh and J.M. Celorio, "*Atlas of fluorescein angiography*", Saunders, Philadelphia, 1993.

34. C.A. Curcio, K.R. Sloan, R.E. Kalina, and A.E. Hendrickson, "Human photoreceptor topography", J. Comp. Neurol. **292** (1990), 497–523.

35. F.S. Sjöstrand, "Electron microscopy of the retina", The Structure of the Eye (G.K.

Smelser, ed.), Academic, New York, 1961, pp. 1–28.

36. J.M. Enoch and F.L. Tobey Jr. (eds.), "*Vertebrate Photoreceptor Optics*", Springer-Verlag, Berlin, 1981.

37. F.C. Delori and K.P. Pflibsen, "Reflectance properties of the optic disc", Noninvasive assessment of the visual system, OSA technical digest series, Optical Society of America, 1989, pp. 154–157.

38. W.S. Stiles and B.H. Crawford, "The luminous efficiency of rays entering the eye pupil at different points", Proc. R. Soc. Lond. [Biol]. **112** (1933), 428–450.

39. J. Dillon, L. Zheng, J.C. Merriam, and E.R. Gaillard, "The optical properties of the anterior segment of the eye: implications for cortical cataract", Exp. Eye Res. **68** (1999), 785–795.

40. E.R. Gaillard, L. Zheng, J.C. Merriam, and J. Dillon, "Age-related changes in the absorption characteristics of the primate lens", Invest. Ophthalmol. Vis. Sci. **41** (2000), 1454–1459.

41. R.A. Weale, "The lenticular nucleus, light, and the retina", Exp. Eye Res. **53** (1991), 213–218.

42. P.J. DeLint, T.T.J.M. Berendschot, J. van de Kraats, and D. van Norren, "Slow optical changes in human photoreceptors induced by light", Invest. Ophthalmol. Vis. Sci. **41** (2000), 282–289.

43. H. Helmholtz, "*Beschreibung eines Augenspiegels zur Untersuchung der Netzhaut im lebenden Auge*", Förstner, Berlin, 1851.

44. P.E. Kilbride and H. Ripps, "Fundus reflectometry", pp. 479–498, Spinger–Verlag, New York, 1990.

45. T.T.J.M. Berendschot, P.J. DeLint, and D. van Norren, "Fundus reflectance —historical and present ideas", Prog. Retin. Eye Res. **22** (2003), 171–200.

46. R.W. Knighton, "Quantitative reflectometry of the ocular fundus", IEEE engineering in medicine and biology **14** (1995), 43–54.

47. D. van Norren and J. van de Kraats, "Retinal densitometer with the size of a fundus camera", Vision Res. **29** (1989), 369–374.

48. F.C. Delori, "Fluorophotometer for noninvasive measurement of RPE lipofuscin", Noninvasive assessment of the visual system, OSA technical digest series, Optical Society of America, 1992, pp. 164–167.

49. F.C. Delori, "Spectrophotometer for noninvasive measurement of intrinsic fluorescence and reflectance of the ocular fundus", Appl. Opt. **33** (1994), 7439–7452.

50. M. Hammer, D. Schweitzer, L. Leistritz, M. Scibor, K.-H. Donnerhacke, and J. Strobel, "Imaging spectroscopy of the human ocular fundus in vivo", Journal of Biomedical Optics **2** (1997), 418–425.

51. R.H. Webb, G.W. Hughes, and O. Pomerantzeff, "Flying spot TV ophthalmoscope", Appl. Opt. **19** (1980), 2991–2997.

52. R.H. Webb, G.W. Hughes, and F.C. Delori, "Confocal scanning laser ophthalmoscope", Appl. Opt. **26** (1987), 1492–1499.

53. D. van Norren and J. van de Kraats, "Imaging retinal densitometry with a confocal scanning laser ophthalmoscope", Vision Res. **29** (1989), 1825–1830.

54. D. van Norren, "Towards improved instrumentation for retinal densitometry", Advances in the biosciences. Research in retinitis pigmentosa, vol. 62, 1987, pp. 177–179.

55. A.T.A. Liem, J.E.E. Keunen, and D. van Norren, "Clinical applications of fundus reflection densitometry", Surv. Ophthalmol. **41** (1996), 37–50.

56. P.J. DeLint, J.E.E. Keunen, A.T.A. Liem, and D. van Norren, "Scanning laser densitometry in visual acuity loss of unknown origin", Br. J. Ophthalmol. **80** (1996), 1051–1054.

57. D. van Norren and J. van de Kraats, "A continuously recording retinal densitometer", Vision Res. **21** (1981), 897–905.

58. P.E. Kilbride, J.S. Read, G.A. Fishman, and M. Fishman, "Determination of human cone pigment density difference spectra in spatially resolved regions of the fovea", Vision Res. **23** (1983), 1341–1350.

59. J.-M. Gorrand, "Directional effects of the retina appearing in the aerial image", J. Optics **16** (1985), 279–287.

60. D.R. Lide (ed.), "*CRC Handbook of Chemistry and Physics*", CRC Press, 1996.

61. G.S. Brindley and E.N. Willmer, "The reflexion of light from the macular and peripheral fundus oculi in man", J. Physiol. **116** (1952), 350–356.

62. W.H. Press, B.P. Flannery, S.A. Teukolsky, and W.T. Vetterling, "*Numerical Recipes in Pascal*", Cambridge University Press, Cambridge, 1989.

63. S. Chinn, "The assessment of methods of measurement", Stat. Med. **9** (1990), 351–362.

64. J. Pokorny, V.C. Smith, and M. Lutze, "Aging of the human lens", Appl. Opt. **26** (1987), 1437–1440.

65. F.C. Delori, D.G. Goger, B.R. Hammond, D.M. Snodderly, and S.A. Burns, "Macular pigment density measured by autofluorescence spectrometry: comparison with reflectometry and heterochromatic flicker photometry", J. Opt. Soc. Am. A **18** (2001), 1212–1230.

66. T.T.J.M. Berendschot, J. van de Kraats, and D. van Norren, "Wavelength dependence of the Stiles–Crawford effect explained by perception of backscattered light from the choroid", J. Opt. Soc. Am. A **18** (2001), 1445–1451.

67. G. Toraldo di Francia, "Retina cones as dielectric antennas", J. Opt. Soc. Am. **39** (1949), 324–324.

68. J.M. Enoch, "Nature of the transmission of energy in the retinal receptors", J. Opt. Soc. Am. **51** (1961), 1122–1127.

69. A.W. Snyder and C. Pask, "The Stiles–Crawford effect—explanation and consequences", Vision Res. **13** (1973), 1115–1137.

70. P.L. Walraven and M.A. Bouman, "Relation between directional sensitivity and spectral response curves in human cone vision", J. Opt. Soc. Am. **50** (1960), 780–784.

71. J.-M. Gorrand and F.C. Delori, "A model for assessment of cone directionality", J. Mod. Opt. **44** (1997), 473–491.

72. N.P.A. Zagers, J. van de Kraats, T.T.J.M. Berendschot, and D. van Norren, "Simultaneous measurement of foveal spectral reflectance and cone-photoreceptor directionality", Appl. Opt. **41** (2002), 4686–4696.

73. J.J. Vos and F.L. van Os, "The effect of lens density on the Stiles–Crawford effect", Vision Res. **15** (1975), 749–751.

74. R.A. Weale, "On the problem of retinal directional sensitivity", Proc. R. Soc. Lond. [Biol]. **212** (1981), 113–130.

75. D. van Norren and J.J. Vos, "Spectral transmission of the human ocular media", Vision Res. **14** (1974), 1237–1244.

76. R.A. Applegate and V. Lakshminarayanan, "Parametric representation of Stiles–Crawford functions: normal variation of peak location and directionality", J. Opt. Soc. Am. A **10** (1993), 1611–1623.

77. D.R. Williams, "Topography of the foveal cone mosaic in the living human eye", Vision Res. **28** (1988), 433–454.

78. P. Artal and R. Navarro, "High-resolution imaging of the living human fovea: measurement of the intercenter cone distance by speckle interferometry", Opt. Lett. **14** (1989), 1098–1100.

79. S. Marcos, R. Navarro, and P. Artal, "Coherent imaging of the cone mosaic in the living human eye", J. Opt. Soc. Am. A **13** (1996), 897–905.

80. D.T. Miller, D.R. Williams, G.M. Morris, and J. Liang, "Images of cone photoreceptors in the living human eye", Vision Res. **36** (1996), 1067–1079.

81. J. Liang, D.R. Williams, and D.T. Miller, "Supernormal vision and high-resolution retinal imaging through adaptive optics", J. Opt. Soc. Am. A **14** (1997), 2884–2892.

82. N.P.A. Zagers, T.T.J.M. Berendschot, and D. van Norren, "Wavelength dependence of reflectometric cone photoreceptor directionality", J. Opt. Soc. Am. A **20** (2003), 18–23.

83. J.J. Vos, "*Literature review of human macular absorption in the visible and its consequences for the cone receptor primaries*", National organization for applied scientific research in The Netherlands, Institute for perception RVO-TNO, Soesterberg, The Netherlands, 1972.

84. A. Stockman, L.T. Sharpe, and C. Fach, "The spectral sensitivity of the human short-wavelength sensitive cones derived from thresholds and color matches", Vision Res. **39** (1999), 2901–2927.

85. P.L. Walraven, "CIE report TC 1-36, Draft 7", (Personal Communication), 2003.

86. Alcon Nederland BV, "Product information booklet", Alcon Laboratories, Inc. (Personal Communication), 2002.

87. E.A. Boettner and J.R. Wolter, "Transmission of the ocular media", Invest. Ophthalmol. **1** (1962), 776–783.

88. E.A. Boettner, "*Spectral transmission of the eye*", Report of the University of Michigan, Contract AF41(609)-2966, 1967.

89. T.J.T.P. van den Berg and K.E.W.P. Tan, "Light transmittance of the human cornea from 320 to 700 nm for different ages", Vision Res. **34** (1994), 1453–1456.

90. Y. Murata, "Light absorption characteristics of the lens capsule", Ophthalmic. Res. **19** (1987), 107–112.

91. J. Dillon, "Photolytic changes in lens proteins", Curr. Eye Res. **3** (1984), 145–150.

92. J. Dillon, R.-H. Wang, and S.J. Atherton, "Photochemical and photophysical studies on human lens constituents", Photochem. Photobiol. **52** (1990), 849–854.

93. R.C. Heckathorn, J. Dillon, and E.R. Gaillard, "Synthesis and purification of 3-Hydroxykynurenine-O-β-glucoside, a primate lens ultraviolet filter, and its application

in a two-step assay for β-glucosidase activity", Anal. Biochem. **299** (2001), 78–83.

94. G.M. Stutchbury and R.J.W. Truscott, "The modification of proteins by 3-hydroxykynurenine", Exp. Eye Res. **57** (1993), 149–155.

95. J. Dillon, "The photophysics and photobiology of the eye", J. Photochem. Photobiol. B **10** (1991), 23–40.

96. R.A. Weale, "Age and the transmittance of the human crystalline lens", J. Physiol. **395** (1988), 577–587.

97. G.L. Savage, G. Haegerstrom-Portnoy, A.J. Adams, and S.E. Hewlett, "Age changes in the optical density of human ocular media", Clin. Vision. Sci **8** (1993), 97–108.

98. R. van Heyningen, "Fluorescent glucoside in the human lens", Nature **230** (1971), 393–394.

99. M. Bando, A. Nakajima, and K. Satoh, "Spectrophotometric estimation of 3-OH L-Kynurenine O-β-Glucoside in the human lens", J. Biochem. **89** (1981), 103–109.

100. A.M. Wood and R.J.W. Truscott, "UV Filters in human lenses: tryptophan catabolism", Exp. Eye Res. **56** (1993), 317–325.

101. L.M. Bova, M.H.J. Sweeney, J.F. Jamie, and R.J.W. Truscott, "Major changes in human ocular UV protection with age", Invest. Ophthalmol. Vis. Sci. **42** (2001), 200–205.

102. S. Zigman, "Eye lens color: formation and function", Science **171** (1971), 807–809.

103. S.A. Burns, J.C. He, and F.C. Delori, "Do the cones see light scattered from the deep retinal layers?", Vision science and its applications, OSA technical digest series, Optical Society of America, 1997.

104. M.J. Piket-May, A. Taflove, and J.B. Troy, "Electrodynamics of visible-light interactions with the vertebrate retinal rod", Opt. Lett. **18** (1993), 568–570.

105. A. Roorda and D.R. Williams, "Optical fiber properties of individual human cones", Journal of Vision **2** (2002), 404–412.

106. C.A. Johnson, D.L. Howard, D. Marshall, and H. Shu, "A noninvasive video-based method of measuring lens transmission properties of the human eye", Optom. Vis. Sci. **70** (1993), 944–955.

107. G.L. Savage, C.A. Johnson, and D.L. Howard, "A comparison of noninvasive objective and subjective measurements of the optical density of human ocular media", Optom. Vis. Sci. **78** (2001), 386–395.

108. F.S. Said and R.A. Weale, "The variation with age of the spectral transmissivity of the living human crystalline lens", Gerontologia **3** (1959), 213–131.

109. F.C. Delori and S.A. Burns, "Fundus reflectance and the measurement of crystalline lens density", J. Opt. Soc. Am. A **13** (1996), 215–226.

110. J. Xu, J. Pokorny, and V.C. Smith, "Optical density of the human lens", J. Opt. Soc. Am. A **14** (1997), 953–960.

111. J. Mellerio, "Light absorption and scatter in the human lens", Vision Res. **11** (1971), 129–141.

112. G.F. Cooper and J.G. Robson, "The yellow colour of the lens of man and other primates", J. Physiol. **203** (1969), 411–417.

113. K.E.W.P. Tan, "Vision in the ultraviolet", Ph.D. thesis, Universiteit Utrecht, Utrecht, The Netherlands, 1971.

114. T.J.T.P. van den Berg and J. Felius, "Relationship between spectral transmittance and slit lamp color of human lenses", Invest. Ophthalmol. Vis. Sci. **36** (1995), 322–329.

115. S. Coren and J.S. Girgus, "Density of human lens pigmentation: in vivo measures over an extended age range", Vision Res. **12** (1972), 343–346.

116. P.A. Sample, F.D. Esterson, R.N. Weinreb, and R.M. Boynton, "The aging lens: in vivo assessment of light absorption in 84 human eyes", Invest. Ophthalmol. Vis. Sci. **29** (1988), 1306–1311.

117. G. Wyszecki and W.S. Stiles, "*Color Science: Concepts and Methods, Quantitative Data and Formulae*", 1th ed., Wiley, New York, 1967.

118. E. Ludvigh and E.F. McCarthy, "Absorption of visible light by the refractive media of the human eye", Arch. Ophthalmol. **20** (1938), 37–51.

119. R.A. Weale, "Light absorption by the lens of the human eye", Optica Acta **1** (1954), 107–110.

120. W.S. Stiles and J.M. Burch, "N.P.L. colour-matching investigation: Final report (1958)", Optica Acta **6** (1959), 1–26.

121. J.S. Werner, S.K. Donnelly, and R. Kliegl, "Aging and human macular pigment density. Appended with translations from the work of Max Schultze and Ewald Hering", Vision Res. **27** (1987), 257–268.

122. R.A. Bone, J.T. Landrum, L. Fernandez, and S.L. Tarsis, "Analysis of the macular pigment by HPLC: retinal distribution and age study", Invest. Ophthalmol. Vis. Sci. **29** (1988), 843–849.

123. T.A. Ciulla, J. Curran-Celantano, D.A. Cooper, B.R. Hammond Jr., R.P. Danis, L.M. Pratt, K.A. Riccardi, and T.G. Filloon, "Macular pigment optical density in a Midwestern sample", Ophthalmology **108** (2001), 730–737.

124. W.M.R. Broekmans, T.T.J.M. Berendschot, I.A.A. Klöpping-Ketelaars, A.J. de Vries, R.A. Goldbohm, L.B.M. Tijburg, A.F.M. Kardinaal, and G. van Poppel, "Macular pigment density in relation to serum and adipose tissue concentrations of lutein and serum concentrations of zeaxanthin", Am. J. Clin. Nutr. **76** (2002), 595–603.

125. B.R. Hammond Jr. and M. Caruso-Avery, "Macular pigment optical density in a Southwestern sample", Invest. Ophthalmol. Vis. Sci. **41** (2000), 1492–1497.

126. S. Beatty, I.J. Murray, D.B. Henson, D. Carden, H.-H. Koh, and M.E. Boulton, "Macular pigment and risk for age-related macular degeneration in subjects from a Northern European population", Invest. Ophthalmol. Vis. Sci. **42** (2001), 439–446.

127. B.R. Wooten and G.A. Geri, "Psychophysical determination of intraocular light scatter as a function of wavelength", Vision Res. **27** (1987), 1291–1298.

128. D. Whitaker, R. Steen, and D.B. Elliott, "Light scatter in the normal young, elderly, and cataractous eye demonstrates little wavelength dependency", Optom. Vis. Sci. **70** (1993), 963–968.

129. T.J.T.P. van den Berg and J.K. IJspeert, "Light scattering in donor lenses", Vision Res. **35** (1995), 169–177.

130. C.A. Curcio, C.L. Millican, K.A. Allen, and R.E. Kalina, "Aging of the human photoreceptor mosaic: evidence for selective vulnerability of rods in central retina", Invest. Ophthalmol. Vis. Sci. **34** (1993), 3278–3296.

131. J. Marshall, "Ageing changes in human cones", International congress series (K. Shimizu and J.A. Oosterhuis, eds.), Excerpta Medica, 1979, pp. 375–378.

132. P. Zimmet, K.G.M.M. Alberti, and J. Shaw, "Global and societal implications of the diabetes epidemic", Nature **414** (2001), 782–787.

133. H. King, R.E. Aubert, and W.H. Herman, "Global burden of diabetes, 1995–2025", Diabetes Care **21** (1998), 1414–1431.

134. R.D.G. Leslie, "Metabolic changes in diabetes", Eye **7** (1993), 205–208.

135. R.V. North, "Early ocular and non-ocular indications of diabetes mellitus", Ophthalmic. Physiol. Opt. **18** (1998), 167–172.

136. R. Klein, B.E.K. Klein, and S.E. Moss, "Visual impairment in diabetes", Ophthalmology **91** (1984), 1–9.

137. J. Haut, J.Y. Redor, E. Abboud, G. van Effenterre, and F. Moulin, "Classification of diabetic retinopathy", Ophthalmologica **195** (1987), 145–155.

138. C. Strøm, B. Sander, N. Larsen, M. Larsen, and H. Lund-Andersen, "Diabetic macular edema assessed with optical coherence tomography and stereo fundus photography", Invest. Ophthalmol. Vis. Sci. **43** (2002), 241–245.

139. N.P. Davies and A.B. Morland, "Color matching in diabetes: optical density of the crystalline lens and macular pigments", Invest. Ophthalmol. Vis. Sci. **43** (2002), 281–289.

140. J.J. Harding, M. Egerton, R. van Heyningen, and R.S. Harding, "Diabetes, glaucoma, sex, and cataract: analysis of combined data from two case control studies", Br. J. Ophthalmol. **77** (1993), 2–6.

141. A.J. Bron, J. Sparrow, N.A.P. Brown, J.J. Harding, and R. Blakytny, "The lens in diabetes", Eye **7** (1993), 260–275.

142. R.C. Zeimer and J.M. Noth, "A new method of measuring in vivo the lens transmittance, and study of lens scatter, fluorescence and transmittance.", Ophthalmic. Res. **16** (1984), 246–255.

143. J.A. van Best, E.W.S.J. Tjin A Tsoi, J.P. Boot, and J.A. Oosterhuis, "In vivo assessment of lens transmission for blue-green light by autofluorescence measurement", Ophthalmic. Res. **17** (1985), 90–95.

144. J.A. van Best, L. Vrij, and J.A. Oosterhuis, "Lens transmission of blue-green light in diabetic patients as measured by autofluorophotometry", Invest. Ophthalmol. Vis. Sci. **26** (1985), 532–536.

145. M.A. Mosier, J.R. Occhipinti, and N.L. Burstein, "Autofluorescence of the crystalline lens in diabetes", Arch. Ophthalmol. **104** (1986), 1340–1343.

146. M. Lutze and G.H. Bresnick, "Lenses of diabetic patients "yellow" at an accelerated rate similar to older normals", Invest. Ophthalmol. Vis. Sci. **32** (1991), 194–199.

147. A.E. Elsner, S.A. Burns, L.A. Lobes Jr., and B.H. Doft, "Cone photopigment bleaching abnormalities in diabetes", Invest. Ophthalmol. Vis. Sci. **28** (1987), 718–724.

148. A. Weiner, V.A. Christopoulos, C.H. Gussler, D.H. Adams, S.R. Kaufman, H.D. Kohn, and D.T. Weidenthal, "Foveal cone function in nonproliferative diabetic retinopathy and macular edema", Invest. Ophthalmol. Vis. Sci. **38** (1997), 1443–1449.

149. J.M. Gorrand and F.C. Delori, "Reflectance and curvature of the inner limiting membrane at the foveola", J. Opt. Soc. Am. A **16** (1999), 1229–1237.

150. R.W. Knighton, S.G. Jacobson, and C.M. Kemp, "The spectral reflectance of the nerve fiber layer of the macaque retina", Invest. Ophthalmol. Vis. Sci. **30** (1989), 2392–2402.

151. R.C. Smith and K.S. Baker, "Optical properties of the clearest natural waters", Appl. Opt. **20** (1981), 177–184.

152. T.J.T.P. van den Berg and H. Spekreijse, "Near infrared light absorption in the human eye media", Vision Res. **37** (1997), 249–253.

153. G.B Rybicki and A.P. Lightman, "*Radiative Processes in Astrophysics*", Wiley, New York, 1979.

154. V.M. Reading and R.A. Weale, "Macular pigment and chromatic aberration", J. Opt. Soc. Am. **64** (1974), 231–234.

155. J.S. McLellan, S. Marcos, P.M. Prieto, and S.A. Burns, "Imperfect optics may be the eye's defence against chromatic blur", Nature **417** (2002), 174–176.

156. M.R. Malinow, B.L. Feeney, L.H. Peterson, M.L. Klein, and M. Neuringer, "Diet-related macular anomalies in monkeys", Invest. Ophthalmol. Vis. Sci. **19** (1980), 857–863.

157. O. Sommerburg, J.E.E. Keunen, A.C. Bird, and F.J.G.M. van Kuijk, "Fruits and vegetables that are sources for lutein and zeaxanthin: the macular pigment in human eyes", Br. J. Ophthalmol. **82** (1998), 907–910.

158. T.T.J.M. Berendschot, J.J.M. Willemse-Assink, M. Bastiaanse, P.T.V.M. de Jong, and D. van Norren, "Macular pigment and melanin in age-related maculopathy in a general population", Invest. Ophthalmol. Vis. Sci. **43** (2002), 1928–1932.

159. C.C. Klaver, J.J. Assink, R. van Leeuwen, R.C. Wolfs, J.R. Vingerling, T. Stijnen, A. Hofman, and P.T.V.M. de Jong, "Incidence and progression rates of age-related maculopathy. The Rotterdam Study", Invest. Ophthalmol. Vis. Sci. **42** (2001), 2237–2241.

160. B.R. Wooten, B.R. Hammond Jr., R.I. Land, and D.M. Snodderly, "A practical method for measuring macular pigment optical density", Invest. Ophthalmol. Vis. Sci. **40** (1999), 2481–2489.

161. S. Beatty, H.H. Koh, D. Carden, and I.J. Murray, "Macular pigment optical density measurement: a novel compact instrument", Ophthalmic. Physiol. Opt. **20** (2000), 105–111.

162. S.-F. Chen, Y. Chang, and J.-C. Wu, "The spatial distribution of macular pigment in humans", Curr. Eye Res. **23** (2001), 422–434.

163. I.V. Ermakov, R.W. McClane, W. Gellermann, and P.S. Bernstein, "Resonant Raman detection of macular pigment levels in the living human retina", Opt. Lett. **26** (2001), 202–204.

164. W. Gellermann, I.V. Ermakov, R.W. McClane, and P.S. Bernstein, "Raman imaging of human macular pigments", Opt. Lett. **27** (2002), 833–835.

165. W. Gellermann, I.V. Ermakov, M.R. Ermakova, R.W. McClane, D.-Y. Zhao, and P.S. Bernstein, "In vivo resonant Raman measurements of macular carotenoid pigments in the young and the aging human retina", J. Opt. Soc. Am. A **19** (2002), 1172–1186.

166. H. Wüstemeyer, C. Jahn, A. Nestler, T. Barth, and S. Wolf, "A new instrument for the quantification of macular pigment density: first results in patients with AMD and healthy subjects", Graefe's Arch. Clin. Exp. Ophthalmol. **240** (2002), 666–671.

167. A.G. Robson, J.D. Moreland, D. Pauleikhoff, T. Morrissey, G.E. Holder, F.W. Fitzke,

A.C. Bird, and F.J.G.M. van Kuijk, "Macular pigment density and distribution: comparison of fundus autofluorescence with minimum motion photometry", Vision Res. **43** (2003), 1765–1775.

168. R.A. Weale, "*The senescence of human vision*", Oxford University Press, New York, 1992.

169. B.K. Pierscionek and R.A. Weale, "The optics of the eye-lens and lenticular senescence", Doc. Ophthalmol. **89** (1995), 321–335.

170. P.A. Sample, F.D. Esterson, and R.N. Weinreb, "A practical method for obtaining an index of lens density with an automated perimeter", Invest. Ophthalmol. Vis. Sci. **30** (1989), 786–787.

171. J.D. Moreland, "Lens-equivalent age controls for diabetics", Invest. Ophthalmol. Vis. Sci. **34** (1993), 281–282.

172. K.J. Hardy, J.H.B. Scarpello, D.H. Foster, and J.D. Moreland, "Effect of diabetes associated increase in lens optical density on colour discrimination in insulin dependent diabetes", Br. J. Ophthalmol. **78** (1994), 754–756.

173. C.J.W. Dunnewold, "On the Campbell and Stiles–Crawford effects and their clinical importance", Ph.D. thesis, Universiteit Utrecht, Utrecht, The Netherlands, 1964.

174. J.M. Enoch, "The retina as a fiber optics bundle", Appendix B in Kapany, N.S., "*Fiber Optics*", Academic, New York, 1967, pp. 372–396.

175. T.M. Nork, J.N. Ver Hoeve, G.L. Poulsen, R.W. Nickells, M.D. Davis, A.J. Weber, Vaegan, S.H. Sarks, H.L. Lemley, and L.L. Millecchia, "Swelling and loss of photoreceptors in chronic human and experimental glaucomas", Arch. Ophthalmol. **118** (2000), 235–245.

176. J.J. Kanski, "*Clinical Ophthalmology*", Butterworth–Heinemann, Oxford, 1999.

Samenvatting

Dit proefschrift beschrijft de ontwikkeling van een nieuw optisch instrument voor onderzoek van het levende menselijk oog. Het instrument projecteert een lichtbundel in het oog. Een klein gedeelte van het licht reflecteert terug uit het oog. Met het nieuwe instrument kunnen voor het eerst gelijktijdig de spectrale en de richtingsafhankelijke eigenschappen van de oogreflectie gemeten worden. Het instrument heeft twee belangrijke toepassingen. De eerste toepassing is het bepalen van de hoeveelheid van een aantal pigmenten in de lens en in het netvlies. Voorbeelden van pigmenten in het netvlies zijn de visuele pigmenten, die licht opvangen in de kegeltjes, en verder het macula pigment, melanine, en het hemoglobine in bloed. De hoeveelheid van de pigmenten volgt uit een analyse van de spectrale reflectie met een fysisch model. De tweede toepassing is het bepalen van de integriteit van de kegeltjes. Gezonde kegeltjes produceren een bepaalde karakteristieke richtingsafhankelijke reflectie. Afwijkingen in deze eigenschap geven een indicatie dat de kegeltjes aangedaan zijn. De twee toepassingen van het instrument hebben beiden betrekking op de fovea, het deel van het netvlies dat is gespecialiseerd voor scherp zien.

Het door ons gebruikte fysisch model voor de spectrale reflectie is gebaseerd op de aanname dat licht enerzijds wordt gereflecteerd door een beperkt aantal lagen in het oog, en anderzijds wordt geabsorbeerd in een beperkt aantal pigmenten. De verschillende pigmenten in het oog hebben elk een uniek absorptiespectrum. Hoe hoger de hoeveelheid van een bepaald pigment, hoe hoger de absorptie bij de voor het pigment karakteristieke golflengten, en hoe lager de gemeten reflectie. De mate van absorptie wordt uitgedrukt als een optische dichtheid (*optical density*, OD). Door in het model de optische dichtheid van de verschillende pigmenten en de reflectie van de reflecterende lagen te variëren, wordt gezocht naar die combinatie van parameters welke de spectrale reflectie het beste beschrijft. De op deze manier verkregen optische dichtheden geven de gewenste maat voor de hoeveelheid van de verschillende pigmenten in het oog.

Met name het gele macula pigment heeft de afgelopen jaren veel belangstelling gekregen. Dit pigment bevindt zich voornamelijk in de fovea, die daarom ook wel de gele vlek wordt genoemd. Het macula pigment is een samenstelling van de carotenoïden luteine en zeaxanthine. Sommige onderzoekers verwachten dat macula pigment het risico verlaagt voor het krijgen van een belangrijke ouderdomsziekte van het netvlies: leeftijd gebonden macula degeneratie. Het is aangetoond dat de optische dichtheid van macula pigment kan worden verhoogd door het toevoegen van luteine aan het dieet, of door het eten van voeding die rijk is aan luteine, zoals spinazie of maïs. De suggestie dat macula pigment beschermend werkt, en de bevinding dat verhogen van de optische dichtheid ervan mogelijk lijkt, hebben de laatste jaren geleid tot veel onderzoek op dit gebied. Een aantal vragen zijn nog onvoldoende beantwoord. Ten eerste is verder onderzoek nodig aan het effect van toevoegen van luteine en zeaxanthine aan het dieet, en tevens is verder epidemiologisch onderzoek gewenst. Voor het direct aantonen van de werkzaamheid van luteine is een gerandomiseerde interventie studie nodig. Uiteindelijk, op voorwaarde dat de beschermende werking van macula pigment kan worden aangetoond, kan het wenselijk zijn een groot bevolkingsonderzoek te doen. Het nieuwe instrument kan in alle genoemde voorbeelden van onderzoek aan macula pigment een rol spelen.

Het tweede aspect van de reflectie, de richtingsafhankelijkheid, wordt bestudeerd door de verdeling van het gereflecteerde licht te meten in de pupil van het oog. Voor dit doel wordt de pupil met oogdruppels verwijd tot ongeveer 8 mm. De druppels verlammen de spier in de iris, zodat deze niet meer samenknijpt wanneer de felle meetbundel in het oog schijnt. In de meeste gezonde ogen is de reflectie het sterkst nabij het centrum van de pupil, en zwakker aan de rand. Dit verschijnsel wordt het optisch Stiles–Crawford effect genoemd. De richtingsafhankelijke reflectie heeft zijn oorsprong in de kegeltjes. De kegeltjes hebben een langwerpige cilindrische vorm. In een gezond oog zijn alle kegeltjes nauwkeurig gericht naar een gemeenschappelijke locatie in de pupil. Wanneer een smalle lichtbundel op deze plaats van de pupil in het oog geschenen wordt, werken de kegeltjes als een "zaklamp" in omgekeerde richting: ze reflecteren voornamelijk in de richting van gemeenschappelijke uitlijning in de pupil. Als gevolg hiervan treedt een duidelijk maximum op in de reflectie in de pupil. Zowel de amplitude van de richtingsafhankelijke reflectie, als de breedte van de verdeling in de pupil verschaffen informatie over de gezondheid van de kegeltjes. Objectieve informatie over de integriteit van de kegeltjes in de fovea is vrijwel niet te verkrijgen met bestaande klinische tests.

Het eerste deel van dit proefschrift gaat over de ontwikkeling van het nieuwe instrument. Het belangrijkste onderdeel is een afbeeldende spectrograaf. De pupil van het gemeten oog wordt door het instrument afgebeeld op een horizontale spleet in de

spectrograaf. Omgekeerd, de horizontale spleet kan men zien als een horizontale balk in de pupil van het gemeten oog. Alleen het licht afkomstig uit deze balk passeert de spleet, en wordt gemeten door de spectrograaf. Voor een groot aantal punten binnen de horizontale balk wordt een afzonderlijk spectrum opgenomen. Het overzicht van de bestaande apparaten in hoofdstuk 2 toont aan dat dit principe nog niet eerder werd toegepast.

Hoofdstuk 3 beschrijft de optiek van het instrument in detail. Het nieuwe instrument werd opgebouwd op een optische tafel. Figuur 1.6 op pagina 9 toont een foto van de opstelling. De lichtbundel van het instrument wordt geproduceerd door een halogeen lamp. Deze bundel verlicht een enkele vlek op het netvlies, ongeveer ter grootte van de fovea. De spectrale reflectie wordt gemeten in het golflengtegebied van 420 nm (blauw licht) tot 790 nm (rood licht). De afmetingen van de horizontale balk in de pupil van het oog zijn 0.8×12 mm. De verdeling binnen deze balk geeft de richtingsafhankelijkheid van de reflectie. De meettijd is slechts 1 seconde. Voor het uitlijnen en scherpstellen van het instrument kan met een video camera zowel de pupil als het netvlies bekeken worden. Hoofdstuk 3 beschrijft tevens de eerste metingen met het nieuwe instrument, die werden verkregen van 21 gezonde proefpersonen. Zowel de spectrale, als de richtingsafhankelijke eigenschappen van de reflectie waren in overeenstemming met eerdere resultaten uit de literatuur.

Het model dat beschikbaar was voor de analyse van de spectrale reflectie werd enkele jaren geleden in onze groep ontwikkeld. [Van de Kraats *et al.*, Vision Res. **36** 2229–2247 (1996)] Helaas kan dit model niet worden toegepast op alle spectra die het nieuwe instrument in één enkele meting oplevert. De analyse in Hoofdstuk 3 was om die reden beperkt tot één enkel spectrum, verkregen op de locatie in het pupil-vlak waar de richtingsafhankelijke reflectie maximaal was. Om deze reden werd als tweede doel in dit proefschrift nagestreefd om ons inzicht in de samenhang tussen de spectrale en de richtingsafhankelijke reflectie te verbeteren. Het uiteindelijke doel is een model dat beide aspecten gelijktijdig kan beschrijven. Dit probleem werd opgesplitst in meerdere delen. Voor elke golflengte kan de reflectie worden beschreven met hetzelfde wiskundig model: een klokvormige Gauss-functie op een vlakke achtergrond. Een dergelijke Gauss-functie wordt beschreven door vier parameters: de positie van het maximum in de reflectie, de amplitude van de richtingsafhankelijke component A, de achtergrond B, en een maat voor de gerichtheid van de reflectie ρ. Deze laatste parameter is omgekeerd evenredig met het kwadraat van de breedte op halve hoogte van de Gauss-functie.

Hoofdstuk 4 beschrijft een analyse van de mate van gerichtheid van de reflectie ρ als functie van de golflengte. Het voornaamste doel was de metingen te vergelijken met de theorie van Marcos *et al.* [J. Opt. Soc. Am. A **15** 2012–2022 (1998)] en

Marcos en Burns. [J. Opt. Soc. Am. A **16** 995–1004 (1999)] Deze theorie voorspelt dat ρ als functie van de golflengte kan worden beschreven met de som van twee componenten. De eerste wordt bepaald door de golfgeleider-eigenschappen en wordt aangegeven met ρ_{wg} (van: *waveguide directionality*). Deze component is in eerste orde onafhankelijk van de golflengte. De tweede component is gerelateerd aan de verstrooiing van licht aan de mozaïek van kegeltjes en geeft een maat voor de afstand van de ene rij kegeltjes tot de andere rij. Deze component is omgekeerd evenredig met de golflengte in het kwadraat. Onze gegevens voor de gerichtheid als functie van de golflengte bevestigden de theorie van Marcos *et al.* De schatting voor de afstand tussen de kegeltjes was in overeenstemming met de anatomische literatuur.

Hoofdstuk 5 beschrijft een analyse van de amplitude van de richtingsafhankelij-ke reflectie als functie van de golflengte. Dit is het tweede aspect dat kon worden bestudeerd door analyse van de reflectie bij verschillende golflengten met een Gauss-functie. Dit type spectrale reflectiemetingen kon worden beschreven met een simpel model. De richtingsafhankelijke reflectie werd verondersteld afkomstig te zijn uit de achtersegmenten van de kegeltjes. De kegeltjes vormden de enige reflecterende laag. Slechts twee absorberende pigmenten werden belangrijk verondersteld: de ooglens en het macula pigment. In het eerste deel van hoofdstuk 5 worden metingen van vijf ogen met een plastic kunstlens uitgewerkt. De absorptie in een dergelijke plastic lens kan vrijwel verwaarloosd worden, alleen voor golflengten korter dan ongeveer 450 nm werd een kleine correctie toegepast. In deze ogen speelt alleen absorptie in macula pigment een rol. De absorptie-eigenschappen van macula pigment zijn bekend. Als enige onbekende factor in de analyse rest dan nog de reflectie van de kegeltjes als functie van de golflengte. Het bleek dat de reflectie van de kegeltjes even sterk is voor iedere golflengte tussen 420 en 650 nm.

Het tweede deel van hoofdstuk 5 beschrijft de metingen aan 39 normale ogen met een leeftijd van 18 tot 64 jaar. Aan de hand van deze gegevens werd de absorptie in de ooglens als functie van de leeftijd bestudeerd. Tot dusver werd voor een be-schrijving hiervan gebruik gemaakt van de theorie van Pokorny *et al.* [Appl. Opt. **26** 1437–1440 (1987)] In een eerste poging om onze metingen te beschrijven met een model gebaseerd op deze theorie vonden wij kleine, maar systematische verschillen tussen het model en onze gegevens. Deze onvolkomenheden van het model waren de aanleiding voor het zoeken naar een verbeterde theorie voor de beschrijving van de absorptie van licht in de ooglens, en de veranderingen hierin met de leeftijd. De voor-gestelde nieuwe theorie bevat twee componenten. De eerste component staat voor een "jong" pigment, het pigment O-β-glucoside van 3-hydroxykynurenine (3-HKG). Dit pigment domineert de absorptie in jonge lenzen, en verdwijnt op oudere leeftijd. De tweede component staat voor één of een groep "oude" pigmenten, die zich langzaam

in de lens verzamelen. De absorptie in de oude pigmenten neemt het geleidelijk over van de absorptie in de jonge pigmenten.

Het uiteindelijke model voor de amplitude van de richtingsafhankelijke reflectie bevat vier factoren: de optische dichtheid van het jonge pigment, de oude pigmenten, het macula pigment en de reflectie van de kegeltjes. Dit model werd toegepast op individuele metingen. Zoals verwacht, nam de hoeveelheid jong pigment af met de leeftijd. Gelijktijdig namen wij een sterke toename van de oude pigmenten waar. De totale optische dichtheid in de lens, de som van de optische dichtheid van de twee componenten, nam licht toe met de leeftijd. Met het model werden precieze individuele metingen van de optische dichtheid van het macula pigment verkregen. Het voordeel van de analyse van alleen de richtingsafhankelijke reflectie, in plaats van de totale reflectie, is dat het model aanmerkelijk eenvoudiger kan zijn dan de modellen die gebruikt worden voor analyse van de totale reflectie. De reden hiervoor is dat de totale reflectie ook een component bevat die is gereflecteerd in de dieper gelegen lagen van het netvlies. Hier speelt de verstrooiing van licht een hoofdrol, en het is moeilijk om dit proces met een model te beschrijven. Het hier gebruikte model voor de analyse van de richtingsafhankelijke component levert metingen van het macula pigment op die beter te interpreteren zijn dan waarden die volgen uit een analyse van de totale reflectie. Tot slot namen wij een afname van de reflectie van de kegeltjes met de leeftijd waar. Waarschijnlijk wijst dit op een aftakeling van de kegeltjes.

In het laatste deel van dit proefschrift, hoofdstuk 6, laten wij een toepassing zien van het apparaat in de kliniek. Dit hoofdstuk beschrijft het onderzoek aan een groep patiënten met diabetes mellitus. Het doel was het bepalen van de gezondheid van de kegeltjes in de fovea, en het meten van de optische dichtheid van het macula pigment en de ooglens. Ter vergelijking werd een groep gezonde proefpersonen gemeten. Wij vonden een sterk verminderde amplitude van de richtingsafhankelijke reflectie in de diabetes groep. Dit wijst op een verandering in de kegeltjes. De mate van gerichtheid was niet verminderd. Macula pigment was niet significant verschillend tussen de normale proefpersonen en de diabetes patiënten. De optische dichtheid van de lens nam sneller toe met de leeftijd vergeleken met de normale leeftijdsgebonden toename in de gezonde ogen. De ervaringen opgedaan met dit onderzoek geven aan dat het instrument een snelle en praktische test is voor de gezondheid van de kegeltjes. Ook in de groep patiënten kon het macula pigment efficiënt en nauwkeurig gemeten worden. De verminderde gezichtsscherpte in een aantal van de patiënten vormde geen probleem voor de methode.

Samengevat: wij hebben een nieuw type instrument ontwikkeld. De metingen van de spectrale en richtingsafhankelijke reflectie zijn vergelijkbaar met eerdere metingen van deze twee aspecten afzonderlijk. Het nieuwe element van het instrument is dat beide aspecten gelijktijdig gemeten kunnen worden. Dit nieuw type metingen gaf aanleiding tot een aantal nieuwe inzichten. Ten eerste hebben wij krachtig bewijs verzameld voor de theorie van Marcos *et al.* over de verstrooiing van licht aan het mozaïek van kegeltjes. Ten tweede hebben wij laten zien dat de kegeltjes licht van iedere golflengte even sterk reflecteren. Ten derde, met dit gegeven bekend, werd een nieuw model voor de absorptie van licht in de ooglens en de veranderingen met de leeftijd afgeleid. Het belangrijkste dat nog moet gebeuren is het ontwikkelen van een model voor de niet richtingsafhankelijke reflectie. Zoals al eerder werd aangeven, bestaat deze component van de reflectie uit licht dat is verstrooid in het netvlies, en is het opstellen van een model hiervoor lastig. Parallel aan het fundamentele werk is een start gemaakt met onderzoek in de kliniek. De resultaten van het onderzoek aan patiënten met diabetes mellitus rechtvaardigen het opstarten van verder onderzoek in de kliniek. Voor dit doel werd recent een handzame versie van het apparaat ontwikkeld.

Curriculum Vitae

De auteur van dit proefschrift werd geboren op 16 september 1976 te Zundert. Van 1988 tot 1994 volgde hij het voorbereidend wetenschappelijk onderwijs aan het Mencia de Mendoza Lyceum te Breda. Het diploma werd behaald op 14 juni 1994. In hetzelfde jaar begon hij aan de studies natuurkunde en sterrenkunde aan de Universiteit Utrecht. Het diploma van beide studies werd op 31 augustus 1999 cum laude behaald. Van 1 september 1999 tot en met 31 december 2003 was de auteur als assistent in opleiding verbonden aan het Universitair Medisch Centrum Utrecht. Het promotieonderzoek werd uitgevoerd bij de groep Oogheelkundige Fysica, onder begeleiding van Prof. dr. D. van Norren.

Dankwoord

In dit dankwoord wil ik alle collega's, vrienden en familie bedanken voor de prettige samenwerking, de geboden hulp en de morele ondersteuning. Tevens wil ik op deze plaats iedereen bedanken die aan de metingen heeft meegedaan. Een aantal mensen wil ik graag persoonlijk noemen.

Dick van Norren, jouw inbreng was bij het tot stand komen van dit proefschrift van onschatbare waarde. Het samen schrijven was steeds een plezierige en zeer leerzame ervaring. Bij het bepalen van de juiste prioriteiten speelde je vaak een belangrijke rol. Ik bewaar ook goede herinneringen aan de twee ARVO conferenties die wij samen bezochten.

Jan van de Kraats, bij het ontwerp en bouwen van het apparaat kon ik steeds gebruik maken van jouw uitgebreide ervaring. Een groot deel van "de C^{++} software" voor het uitlezen van de CCD en de analyse van de metingen kwam van jouw hand. Bovendien was je later erg behulpzaam bij het verwerken van de resultaten. Maar dat is nog niet alles. Ook in de privésfeer bestaan er banden; min of meer dankzij je zoon Roel heb ik destijds voor het project gesolliciteerd.

Tos Berendschot, jouw begeleiding heeft het project goed op gang geholpen. Bij het inlezen en vooral op het gebied van klinische studies en macula pigment was je een goede vraagbaak. De latere versies van "de C^{++} software" kregen door jouw programmeerwerk steeds op tijd de nodige aanpassingen.

Pieter van den Biesen, Mary van Schooneveld, Marja Breedijk, Gerard van Meel, de andere oogartsen, de arts-assistenten, de medewerkers van de polikliniek, en de collega's van de afdeling functieonderzoek wil ik bedanken voor de hulp met het onderzoek aan patiënten. Birgit Wilms, ook jou wil ik bedanken voor je hulp. Gerard de Graaf, bedankt voor het maken van de foto's van de opstelling. Annette Ossewaarde-van Norel, in de begintijd was je een fijne collega-promovendus. Later, tijdens je opleiding tot oogarts, was je erg behulpzaam met het werven van patiënten. Hans Vos, jouw deskundige advies, met name bij "het lensverhaal", was zeer welkom en kwam zeker van pas. Maartje Pot en Michiel van Werkum, bedankt voor de plezierige

samenwerking tijdens jullie stage bij onze groep.

René de Bruijn, het bijna wekelijks uitwisselen van onze ervaringen heeft me erg geholpen. Wouter Bergmann Tiest, bedankt voor de LaTeX tips. Roel van de Kraats en Martijn West, bedankt dat jullie mijn paranimfen willen zijn.

Lieve zus Sietske, niet iedere stagiaire maakt direct kennis met de hoogste baas bij TNO Technische Menskunde. Je had dan ook "connecties". Bedankt voor je hulp met het ontwerp van de kaft. Lieve ouders, zonder jullie hulp was ik nooit zo ver gekomen. Jullie hebben steeds het beste met mij voor gehad en jullie hebben altijd alles gedaan om mij te helpen. Bedankt voor jullie levenslange toewijding en steun.

Lieve Jessica, dat wij elkaar gevonden hebben is uniek! Van jouw ervaringen met promoveren heb ik veel kunnen opsteken, maar het belangrijkste is dat we het samen zo goed kunnen vinden. Ik hoop dat we samen nog veel mooie en onvergetelijke momenten mogen beleven.